2022

GEOPHYSICAL MODELLING OF MAGNETIC ANOMALIES OVER THE BALLANTRAE OPHIOLITE COMPLEX AND SOUTHERN UPLANDS FAULT SYSTEM, SW SCOTLAND

Can, Arzum Cansu

http://hdl.handle.net/10026.1/20064

http://dx.doi.org/10.24382/617
University of Plymouth

UNIVERSITY OF
PLYMOUTH

GEOPHYSICAL MODELLING OF MAGNETIC ANOMALIES OVER THE BALLANTRAE OPHIOLITE COMPLEX AND SOUTHERN UPLANDS FAULT SYSTEM, SW SCOTLAND

by

ARZUM CANSU CAN

A thesis submitted to the University of Plymouth

in partial fulfilment for the degree of

RESEARCH MASTERS

School of Geography, Earth, and Environmental Sciences

October 2022

Copyright Statement

ACKNOWLEDGEMENTS

I would first like to thank my supervisors Professor Antony Morris, Professor Mark Anderson, and Dr Michelle Harris for their endless support and patience throughout my research and writing-up period. They have always been helpful and tried to create time for conversations about my project. I would also like to thank James Hepworth, PhD research student, for all his help during the fieldwork. Particularly, I am thankful and grateful for everything new I have learnt in terms of geology and geophysics at the University of Plymouth. Besides my supervisors, I would like to thank the Ministry of National Education of the Republic of Turkey for the scholarship and for covering all the expenses. Also, apart from the financial issues, I appreciate that authorized personnel in London working for the Ministry always tried to help with other concerns too.

I am also grateful to have had a chance to meet some staff from the Student Wellbeing Services at the University of Plymouth. I have a special thanks to them for supporting me.

Lastly, my biggest thanks to my family for all the support you have shown me through this research, especially my mother and my fiancé who is one of the gifts that came with this journey. I would also like to thank my friends who supported me when I feel down. Their belief in me has kept my spirits and motivation high during this process.

Author's Declaration

At no time during the registration for the degree of *Research Masters* has the author been registered for any other University award without prior agreement of the Doctoral College Quality Sub-Committee.

This thesis has been proofread by a third party; no factual changes or additions or amendments to the argument were made as a result of this process. A copy of the thesis prior to proofreading will be made available to the examiners upon request.

Work submitted for this research degree at the University of Plymouth has not formed part of any other degree either at the University of Plymouth or at another establishment.

This study was financed with the aid of a studentship from the *Ministry of National Education of the Republic of Turkey*.

A programme of advanced study was undertaken, which included *GEOL5002 MGeol Advanced Fieldwork, and GEOL5003 Advanced Analytical Skills.*

Participation in field trips:

-Girvan-Ballantrae field trip in the scope of this project.

Word count of main body of thesis: 14,577 words

Signed *ACANSU*

Date 30/10/2022

ARZUM CANSU CAN

GEOPHYSICAL MODELLING OF MAGNETIC ANOMALIES OVER THE BALLANTRAE OPHIOLITE COMPLEX AND SOUTHERN UPLANDS FAULT SYSTEM, SW SCOTLAND

Abstract

The Ballantrae Complex is located in the area north of the Southern Uplands Fault and Southern Uplands accretionary complex of southwest Scotland. It consists of a tectonically emplaced ophiolite dominated by two serpentinised peridotite massifs known as the Southern and Northern Serpentinite Belts. It also contains smaller serpentinite bodies, including a concealed body proved in a BGS borehole at Knocklaugh Lodge. The highly magnetic serpentinites are associated with pronounced magnetic anomalies that form the focus of this study. The project aims to improve understanding of the shape, size and distribution of serpentinites in the subsurface, by integrating detailed ground-level magnetic surveying, analysis of the bulk magnetic properties of rocks present in the area, Fourier-based upward continuation, and 2D and 3D magnetic modelling techniques.

3D modelling of the Knocklaugh Lodge anomaly identifies a NE-SW-trending, wedge-shaped, fault-bounded sliver of serpentinite beneath surficial boulder clay. A 2.8 km long ground-level magnetic profile extending to the NW from this locality to beyond the NW margin of the Northern Serpentinite Belt was upward continued to 100 m elevation to suppress short wavelength near-surface signals. 2D modelling of these data reveals presence of a large, concealed serpentinite body to the SE of the Northern Serpentinite Belt, and suggests that the boundaries of the major serpentinite units are all steeply dipping. 3D modelling at the regional-scale using data from the National Aeromagnetic Survey further constrains the complex 3D subsurface geometry of the Northern and Southern Serpentinite Belts. It also suggests that a separate linear magnetic anomaly extending ~25 km further to the NE along the strike of the major fault systems in the region is caused by highly magnetic sedimentary rocks of the Ordovician Traboyack Formation Finally, upward continuation of a ground-level magnetic survey over a raised marine platform near Lendalfoot demonstrates presence of a regional magnetic gradient associated with a deep peridotite source combined with a complex pattern of small-scale, local gradients due to shallow sources that probably reflects variations in the paleotopography of a rocky shoreline beneath the terrace.

Table of Contents

List of Figures

Chapter 1 – Introduction and geological background

1.1. Introduction

This study is an investigation of the subsurface sources of prominent magnetic anomalies that occur over the Ballantrae Ophiolite Complex and Southern Uplands Fault system in southwest Scotland. This study is based on geomagnetic survey data collected during field work in this area and two and three-dimensional numerical modelling of these data, using methods that have been employed in subsurface modelling in a number of different geological contexts.

Magnetic anomalies may arise from contrasts in the magnetic susceptibilities of Earth materials (resulting in induced magnetization contrasts), from differences in the remanent (permanent) magnetizations of rocks in the subsurface, or from a combination of induced and remanent magnetization sources. Igneous rocks and zones of metalliferous mineralisation often produce pronounced magnetic anomalies due to their ferromagnetic mineral content, as these minerals can retain remanent magnetizations over geological time periods and have high magnetic susceptibilities. Magnetite usually dominates ferromagnetic grain assemblages and may be present as a primary phase or as a secondary phase formed during alteration and mineralisation (for instance during serpentinization of ultramafic rocks).

1.2. Aims and objectives

This project aims to use two and three-dimensional modelling of magnetic anomalies to constrain the subsurface geometry of serpentinized peridotite and other highly magnetic bodies associated with the Ballantrae ophiolite and Southern Uplands Fault system. The specific objectives designed to achieve this aim were to:

1. conduct ground-level total magnetic field surveys over several key areas in the Ballantrae region using either 2D profiles or 3D grid surveys. The main targets were: (i) a 3D survey over a suspected, small, fault-bound buried serpentinite body located near Knocklaugh Lodge; (ii) a 2D profile across the Knocklaugh Lodge anomaly but extending to the coast to the NW in order to establish the relationship between it and a much larger magnetic anomaly seen over the exposure of the Northern Serpentinite Belt of the Ballantrae ophiolite; and (iii) a 3D survey over a prominental raised marine terrace at the coast where published geological mapping suggests the bedrock consists of serpentinite containing gabbroic intrusions.
2. collect low field magnetic susceptibility data from key lithologies exposed in the field area using a Bartington susceptibility probe, and additional susceptibility measurements on core specimens drilled from oriented hand samples, to allow determination of likely intensities of induced magnetisations associated with these rocks to inform the magnetic modelling.
3. measure the natural remanent magnetization (NRM) of oriented rock samples to determine the direction and intensity of remanences to inform the magnetic modelling.
4. perform upward continuation of the ground-level magnetic anomaly data to varying elevations above sea-level to filter out shallow, superficial signals and focus on deeper sources.
5. perform two and three-dimensional modelling studies to determine the potential geometry and nature of subsurface structures responsible for the observed anomalies. In addition, 3D modelling was also conducted of regional-scale aeromagnetic anomaly data collected during the National Aeromagnetic Survey (Institute of Geological Sciences, 1972, 1980).

1.3. - Geological background

The Ballantrae Complex is located in southwest Scotland (Figure 1.1), to the north of the Southern Uplands Fault (SUF) and Southern Uplands accretionary complex. The Ballantrae Complex is considered as a tectonically emplaced ophiolite formed in an intra-oceanic context inside the Iapetus Ocean, consisting of a suite of mafic lavas, serpentinite, and other associated basic and ultrabasic rocks (Leggett 1987; Fujisaki et al., 2015).

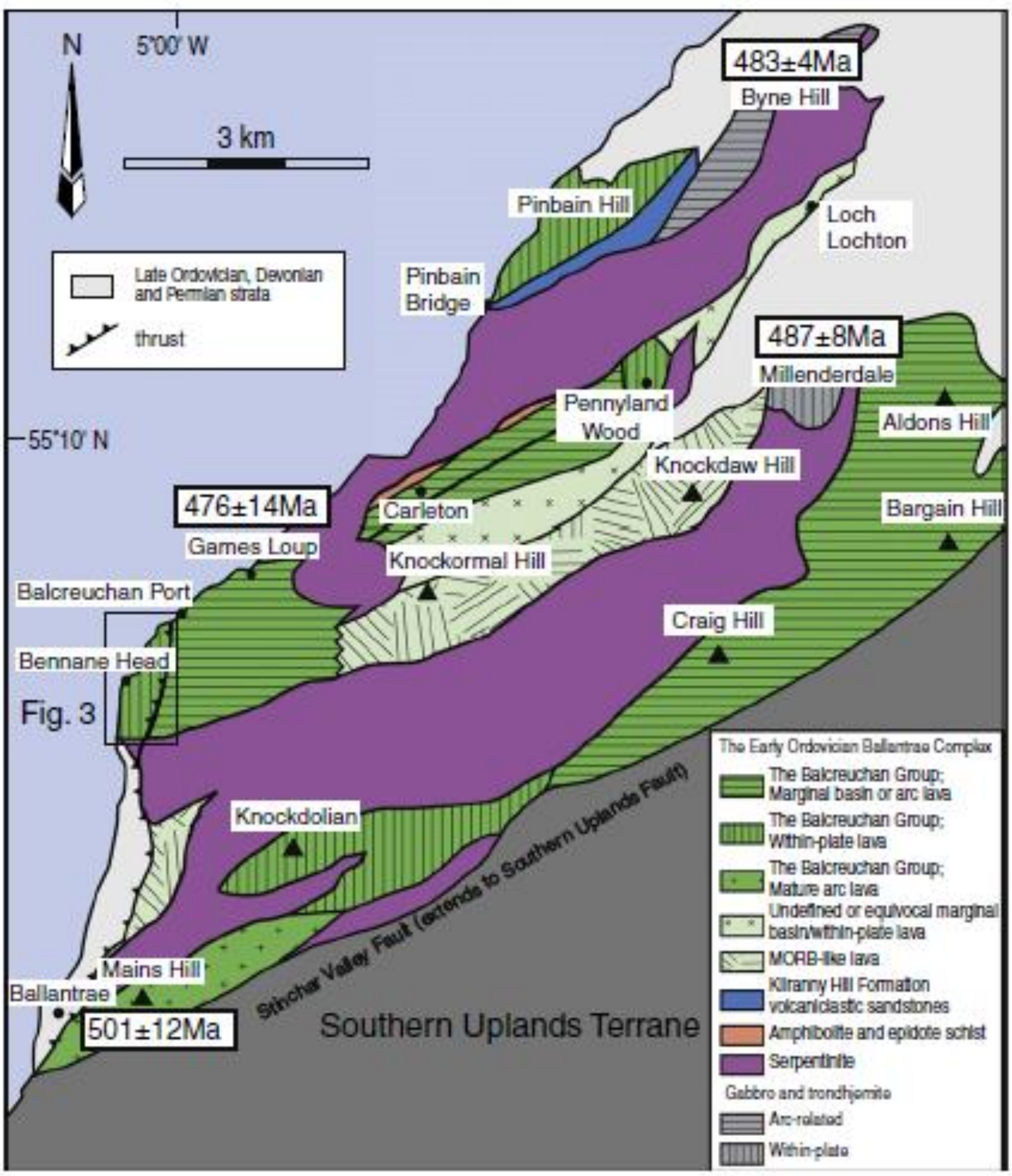

Figure 1.1. A simplified geological map of the early Ordovician Ballantrae Complex. It demonstrates the distribution and inferred geotectonic setting of crustal rocks (from Fujisaki et al., 2015).

The Southern Uplands is interpreted as an accretionary wedge formed by northwards subduction of Iapetus oceanic crust during the Ordovician and Silurian (Leggett *et al.* 1979, 1982; Fujisaki et al., 2015). The Ballantrae ophiolite lies in a critical position at the northern margin of this accretionary terrane (Robertson 1988). The Ballantrae Complex consists of a tectonically emplaced ophiolite that is generally Early and early Middle Ordovician age. Stone and Rushton (2018) considered the age of the Ballantrae Complex to be about 478–464 Ma for the tectonic assembly and ultimate obduction.

The Ballantrae Complex is bounded to the south by a major fault zone along the Stinchar valley (Figure 1.1) that extends to the Southern Uplands Fault system. To the south lies a separate body of mafic pillow lavas and minor pelagic sediments forming the Downan block. Major masses of extrusive rocks within the Complex are split by two zones of ultramafic and mafic rocks (Figure 1.1), termed the Southern and Northern Serpentinite Belts (Peach & Horne, 1899). Bailey and McCallien (1952) argued the two serpentinite belts were the limbs of a major plunging anticline. In contrast, geochemical and petrographic evidence shows that these belts were unlikely to have been originally laterally continuous (Stone et al. 1987).

1.3.1. Lithologies of the Ballantrae Complex

The Ballantrae Complex is an ophiolite made up of serpentinized ultramafic rocks with minor gabbroic intrusions, gabbros, a poorly exposed sheeted dyke complex, volcanic units (consisting of mostly pillow lavas) and sedimentary rocks (Thirlwall & Bluck, 1984). An idealised slice of an ophiolite can be seen in Figure 1.2, and brief descriptions of the main lithologies present in the Ballantrae complex are summarised below.

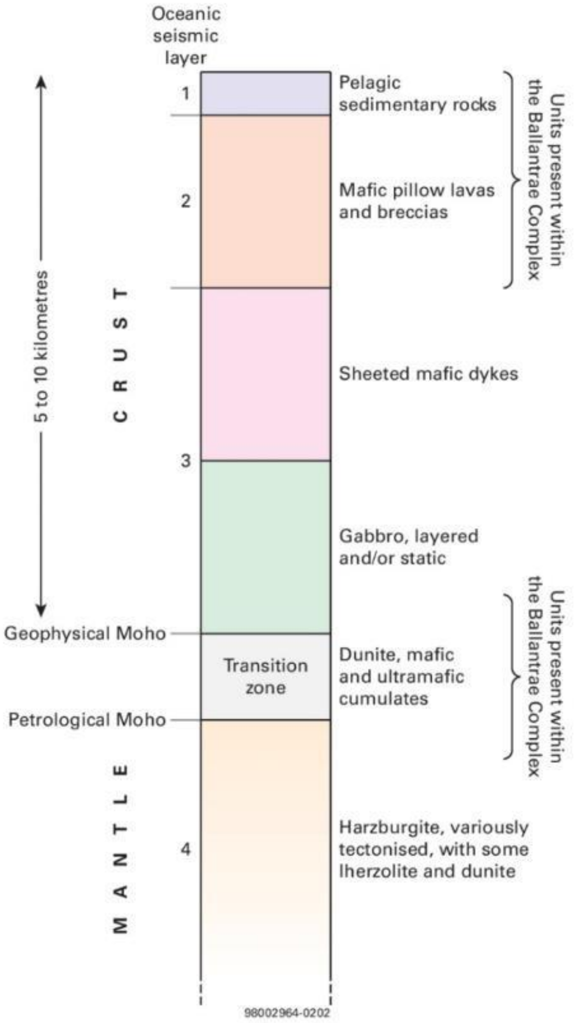

Figure 1.2. Idealised slice of an ophiolite (from Earthwise, 2022).

a) Sedimentary rocks:
These are mainly observed in faulted contact with other ophiolite rocks with the exception of the cherts and associated rocks at Bennane Head (Oliver et al., 2002). They are well-exposed at Bennane Head, Pinbain, and North Ballaird, where a borehole study had conducted (Stone 1982; Stone & Strachan 1981).

b) Lava sequences
In the Ballantrae area, lava sequences consist of three main parts from north to south, Pinbain block, central Bennane Head block, and south block with Mains Hill (Figure 1.1). The lavas consist of pillowed and massive flows (Oliver et al., 2002), with the best exposures of pillow lavas at Downan Point. These geochemistry of the lava sequences

has been important in identifying the origin of the Ballantrae ophiolite (Bluck & Inghan, 1992).

c) Serpentinite

In the Ballantrae complex, there is an altered form of ultramafic rock, in which olivine has been replaced by serpentine (Stone, 2014), exposed in two main outcrops called the Northern and Southern Serpentinite Belts (Figure 1.1). The Northern Serpentinite Belt is more metasomatised than the Southern Belt (Stone, 2014). While the Northern Belt consists of harzburgite with some lherzolite and pyroxenites, the Southern Belt consist of coarser-grained harzburgite with dunite, wehrlite, and troctolite (Stone, 2014). Independent of their various geotectonic settings, the depth of Southern Serpentinite Belt's ultramafic protolith is considerably shallower than the Northern Belt (Stone & Smellie, 1990 in Stone, 2014, p.11).

d) Gabbros

Unfoliated gabbros are observed in three main areas, around Millenderdale, Mains Hill, and between Byne Hill and Grey Hill (Figure 1.2) (Stone, 2014). These gabbros are surrounded by serpentinite against which they exhibit chilled contacts (Bloxam, 1968 in Stone, 2014, p.17). They generally are coarse-grained. The gabbro bodies at Millenderdale are more banded and foliated than other gabbro bodies and doleritic dykes cut these bodies (Stone, 2014). As can be seen in Figure 1.2, gabbro bodies around Mains Hill are intruded into the Southern Serpentinite Belt.

e) Sheeted dykes

Church & Gayer (1973) suggested an array of dykes cutting foliated gabbros at Millenderdale (in Oliver et al., 2002) represent a sheeted dyke complex. Oliver and McAlpine (1998) describe another example where various (sub)parallel dolerite dykes form a large tectonic inclusion in serpentinite on the north side of Knockdolian (in Stone, 2014).

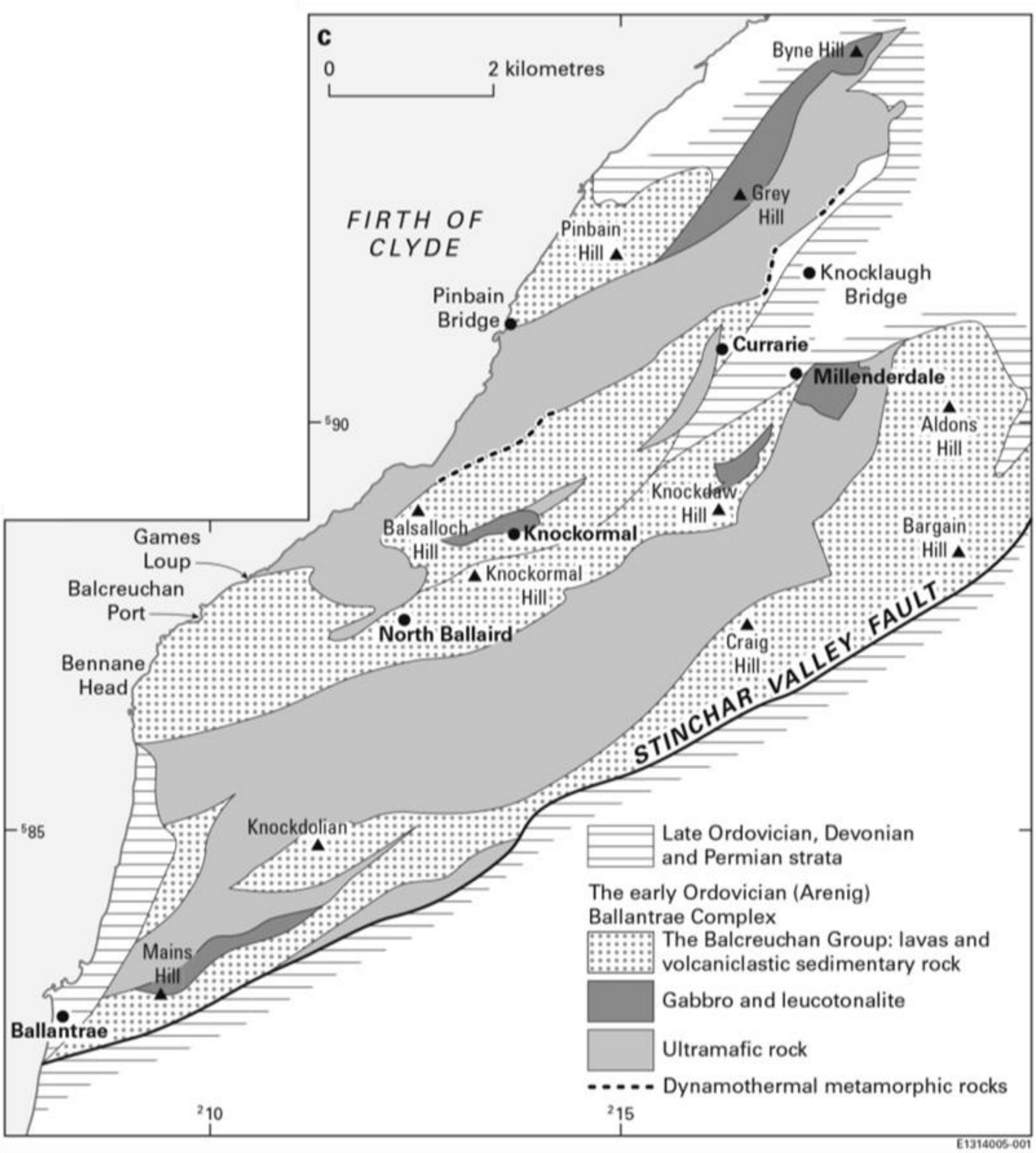

Figure 1.3. The geological map of the area. Three main gabbro areas, around Millenderdale, Mains Hill and Byne Hill, can be seen as solid dark grey (from Stone, 2014).

1.3.2. Other geological units

There are also some non-ophiolitic rocks in the Ballantrae Complex area that are relevant to understanding the source of the magnetic anomalies present in the region. For example, the aeromagnetic map based on the British Geological Survey (BGS) national survey also shows a pronounced anomaly that is not associated with the igneous rocks of the Ballantrae Complex (Figure 1.4). Floyd and Kimbell (1995) argued that the source of the anomaly seems to be the fault-bounded sedimentary unit known as the Traboyack Formation which is in the Tappins Group. The Tappins Group consists of the Downan Point Lava, Traboyack, Dalreoch, Currarie and Corsewall formations (Figure 1.5).

The Downan Point Lava Formation is narrowing to the northeast between two bounding faults (Figure 1.4). These lavas cause a significant magnetic anomaly with a 060° trend near the coast. The Currarie, Dalreoch and Corsewall Formations have low magnetic susceptibility ($0.33\text{-}0.93\text{x}10^{-3}$ SI, $3.95\text{x}10^{-3}$ and $0.43\text{x}10^{-3}$ SI, respectively) and do not make a significant contribution to the observed anomalies (Floyd and Kimbell, 1995). In contrast, the Traboyack Formation (located mainly between the Stinchar Valley Fault-Pyet Thrust and the Dove Cove Fault; Figure 1.5) consists of red-purple greywackes and mudstones up to 1 km thick and has a mean susceptibility of 40.62×10^{-3} SI (Floyd and Kimbell, 1995), representing the highest susceptibility rocks in the Tappins Group. As discussed below, the mean susceptibility of the serpentinite in the Ballantrae Complex is 76×10^{-3} SI (Powell, 1978). Hence the Traboyack Formation and the serpentinites of the Ballantrae Complex are the most magnetic rocks in the Ballantrae area.

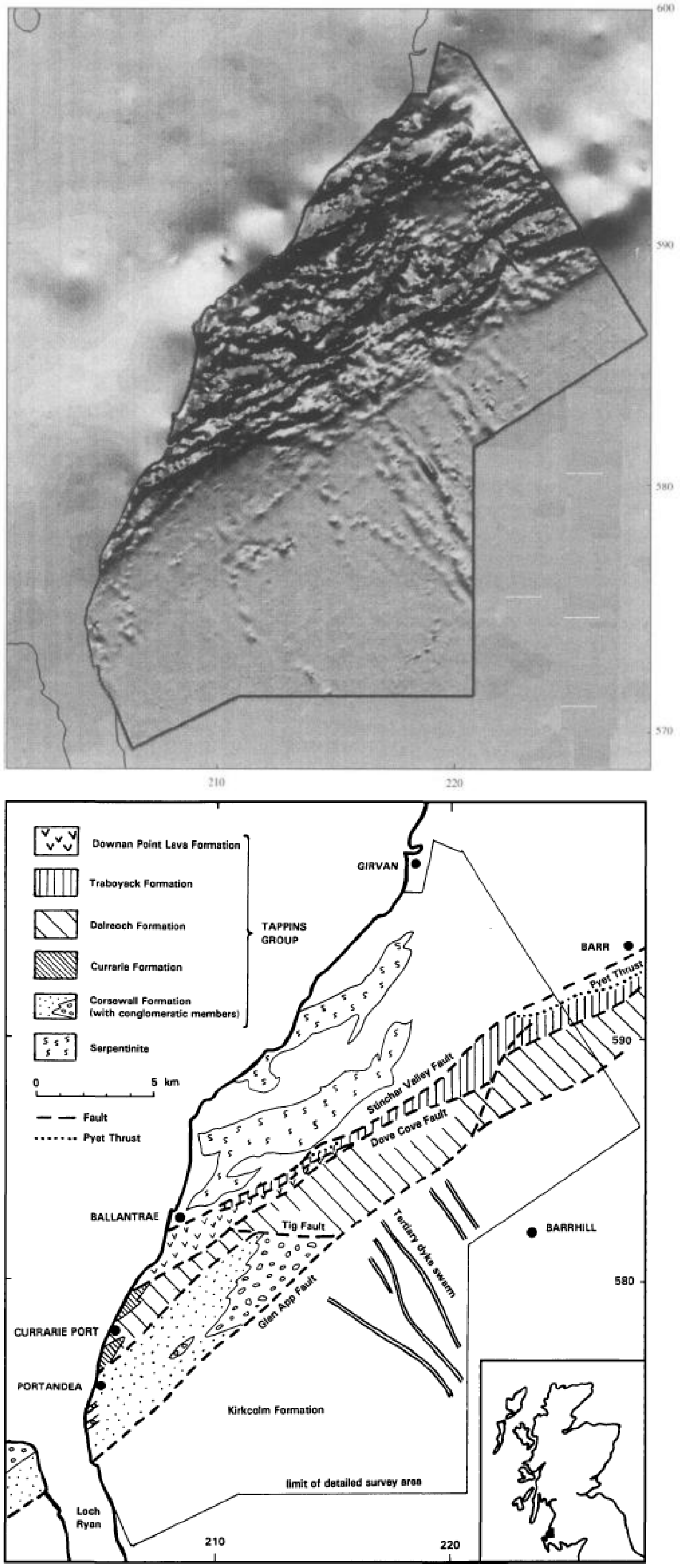

Figure 1.4. top: An aeromagnetic anomaly map showing the total magnetic field data as shaded pseudo-relief illuminated from the north. Bottom: Outline geologic map of showing interpretation of this aeromagnetic image (from Floyd and Kimbell, 1995)

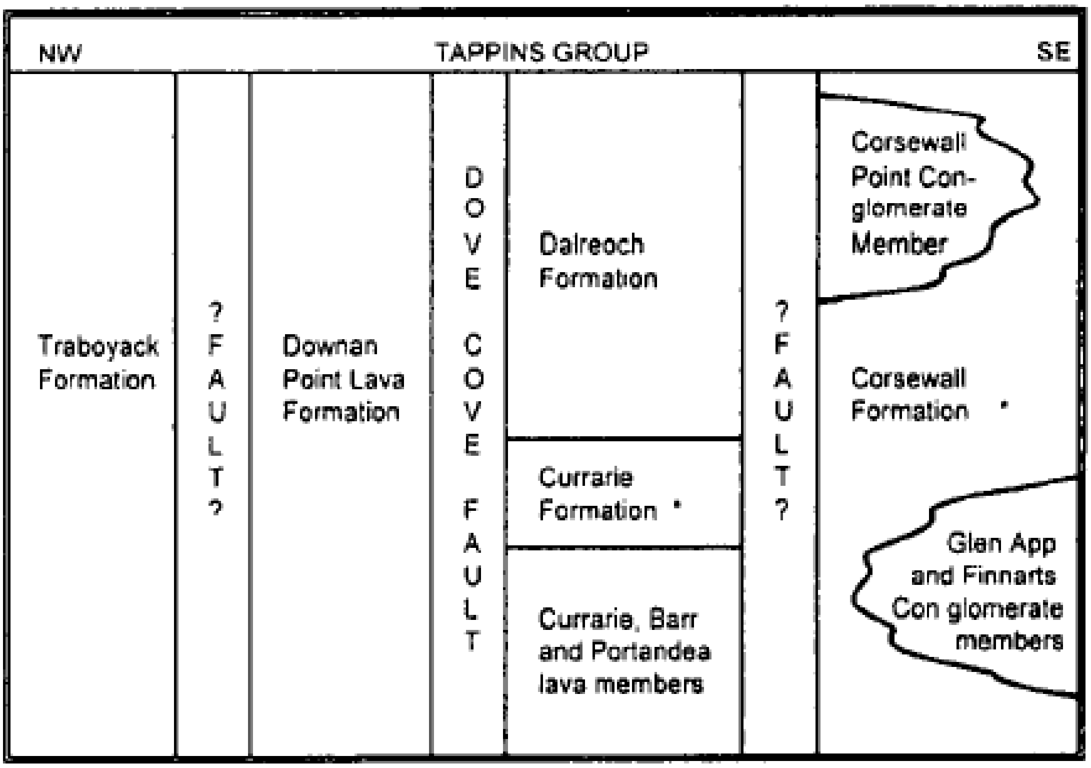

Figure 1.5. The lithostratigraphy for the Tappins Group (from Floyd and Kimbell, 1995).

1.4. Previous modelling of magnetic anomalies in the Ballantrae region and BGS drilling of a concealed serpentinite body

An investigation of the magnetic anomalies associated with the main serpentinite belts of the Ballantrae Complex was carried out by Powell (1978), who presented maps of the ground-level vertical magnetic component and residual Bouguer gravity anomalies (Figure 1.10). Powell (1978) found that the serpentinites are the most magnetic rocks in the area, with a mean magnetic susceptibility of 76 x 10^{-3} SI, compared with mean susceptibilities of approximately 25 x 10^{-3} SI for both volcanic and sedimentary units (1978). Forward modelling along two profiles (Figure 1.9) across the Ballantrae Complex by Powell (1978) suggested that a 1000 nT anomaly over the Northern Serpentinite Belt may be caused by a wedge-shaped serpentinite body extending to a depth of over 3.0 km, whereas the lower amplitude anomaly over the Southern Belt may be attributed to a thinner, folded and faulted serpentinite sheet at about 1.0 km depth.

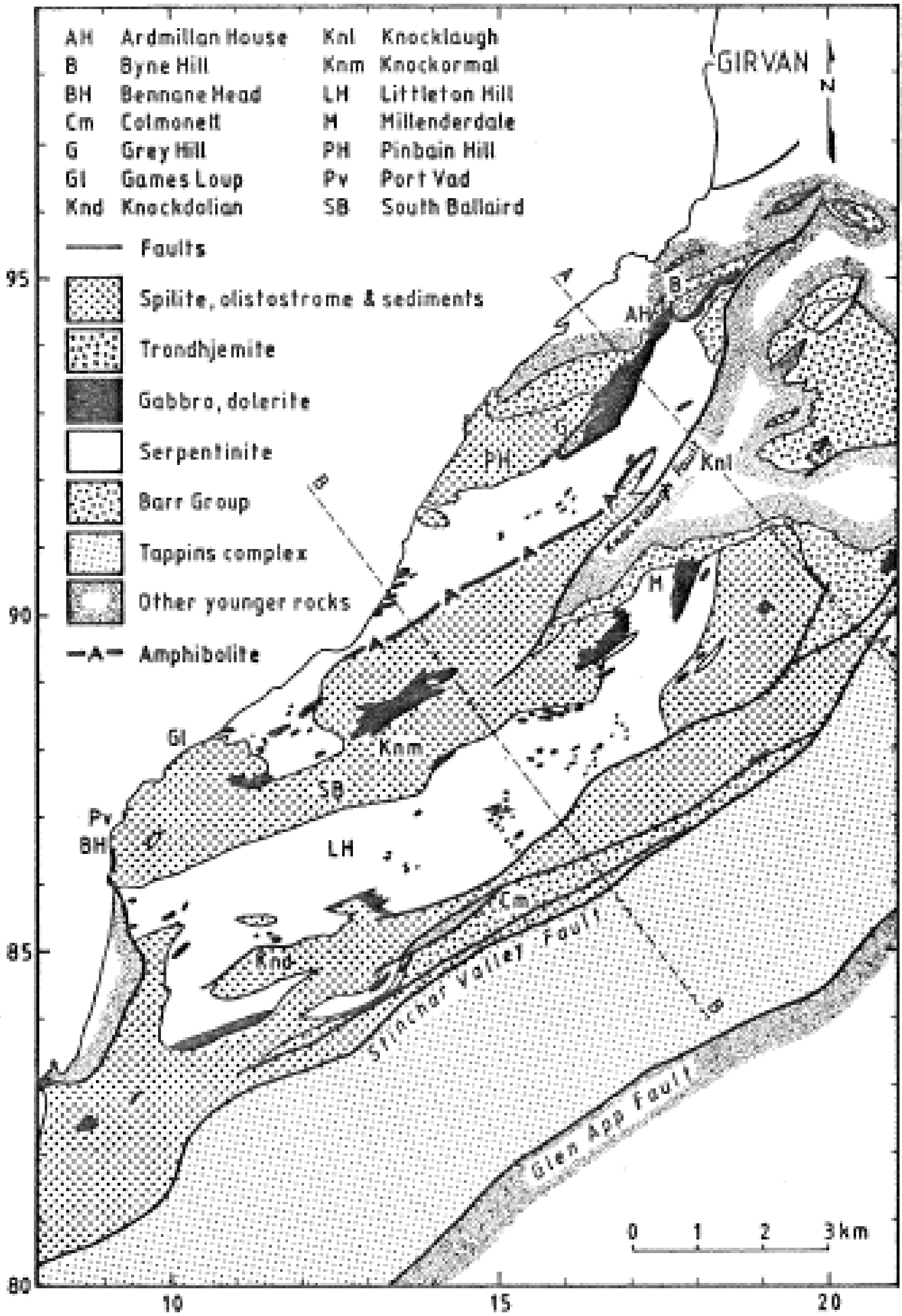

Figure 1.6. A simplified map of the Ballantrae complex showing the profile lines A-A and B-B modelled by Powell (1978).

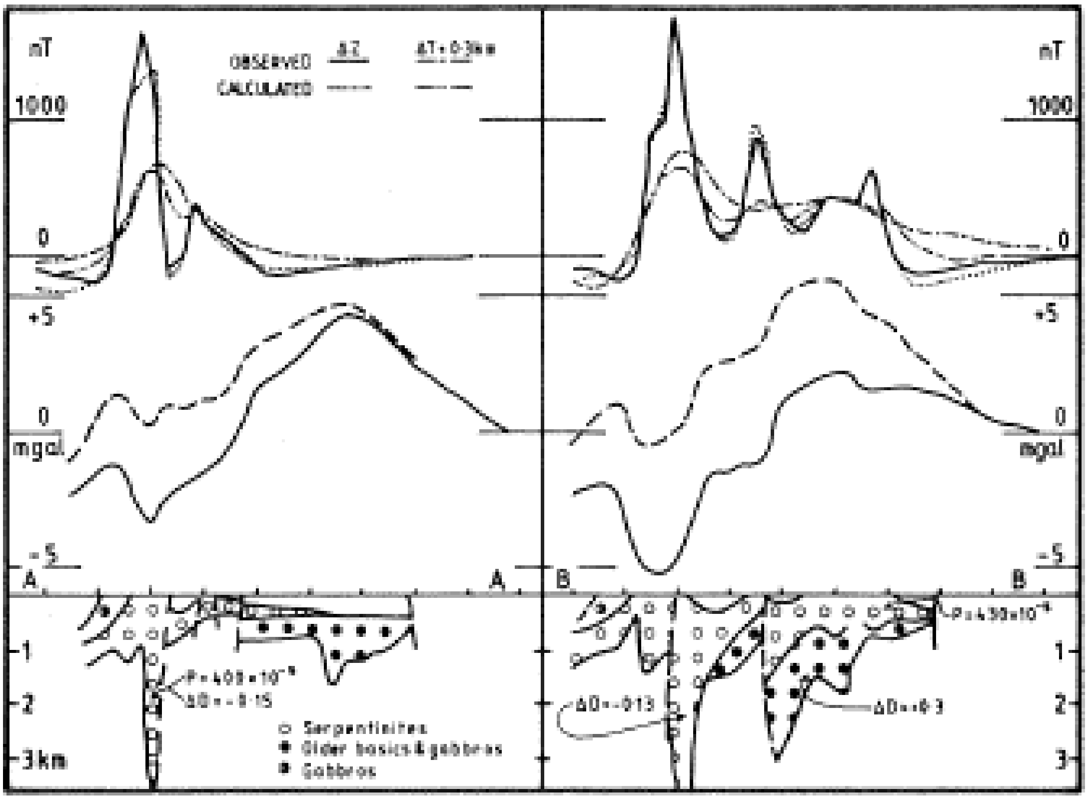

Figure 1.7. Observed and calculated magnetic and gravity anomalies along profiles A-A and B-B (from Powell, 1978). The pseudogravity effect of the serpentinite has been added to the residual gravity profile (solid line) to produce the profile on which the dense body is modelled. P is the polarisation contrast in cgs and D is density in gm/cc. The location of the profile lines A-A and B-B can be seen in Figure 1.6.

Following the pioneering study by Powell (1978), the Institute of Geological Sciences (IGS) conducted further aeromagnetic and ground level surveys as part of a mineral reconnaissance programme for the Department of Industry (Carruthers, 1980). This identified a prominent local anomaly approximately 250 m north of Knocklaugh Lodge (which forms a target for this study). This anomaly occurs over ground covered by glacial boulder clay, but subsequent IGS drilling confirmed that it could be attributed to presence of serpentinite at depth at this location (Figure 1.8) (Stone et al. 1984). Two inclined boreholes both proved serpentinite beneath about 15 m of boulder clay (Figures 1.8 and 1.9; Stone et al. 1984), one of which demonstrated that the serpentinite was fault-bounded to the SE. However, the subsurface relationship of this body to the nearby Northern Serpentinite Belt remained unknown.

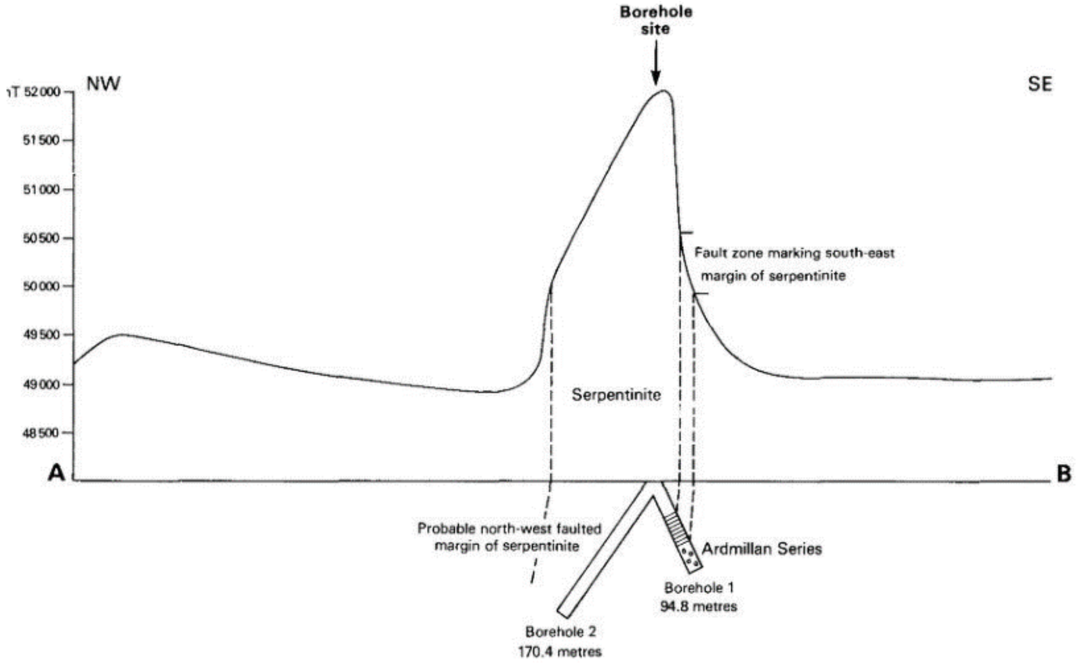

Figure 1.8. A graph showing the magnetic anomaly for the Knocklaugh Lodge area and borehole summary data (from Stone et.al, 1984).

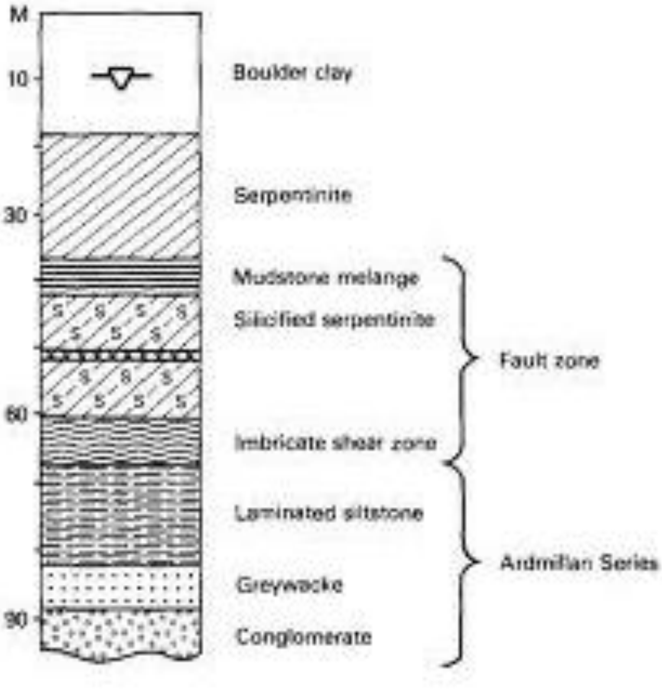

Figure 1.9. A graphic log showing the result of the Knocklaugh Lodge Borehole No. 1 (from Stone et.al, 1984).

Chapter 2 - Theoretical background and magnetic terms

2.1 The Earth’s Magnetism

The main magnetic field of the Earth is generated by a self-exciting dynamo process in the fluid metal of the Earth's outer core (Bullard, 1948) (Figure 2.1). The Earth’s magnetic field at any location can be described by three parameters (Figure 2.2): (i) the total field intensity, F; (iii) the magnetic declination, D, which is the positive clockwise angle from geographic north to magnetic north, ranging from 0° to 360° degrees (Butler, 2004); and (iii) the magnetic inclination, I, which is the angle made with the horizontal by the Earth's magnetic field lines (McElhinny & McFadden, 1999), ranging from 0° to ±90° (Butler,

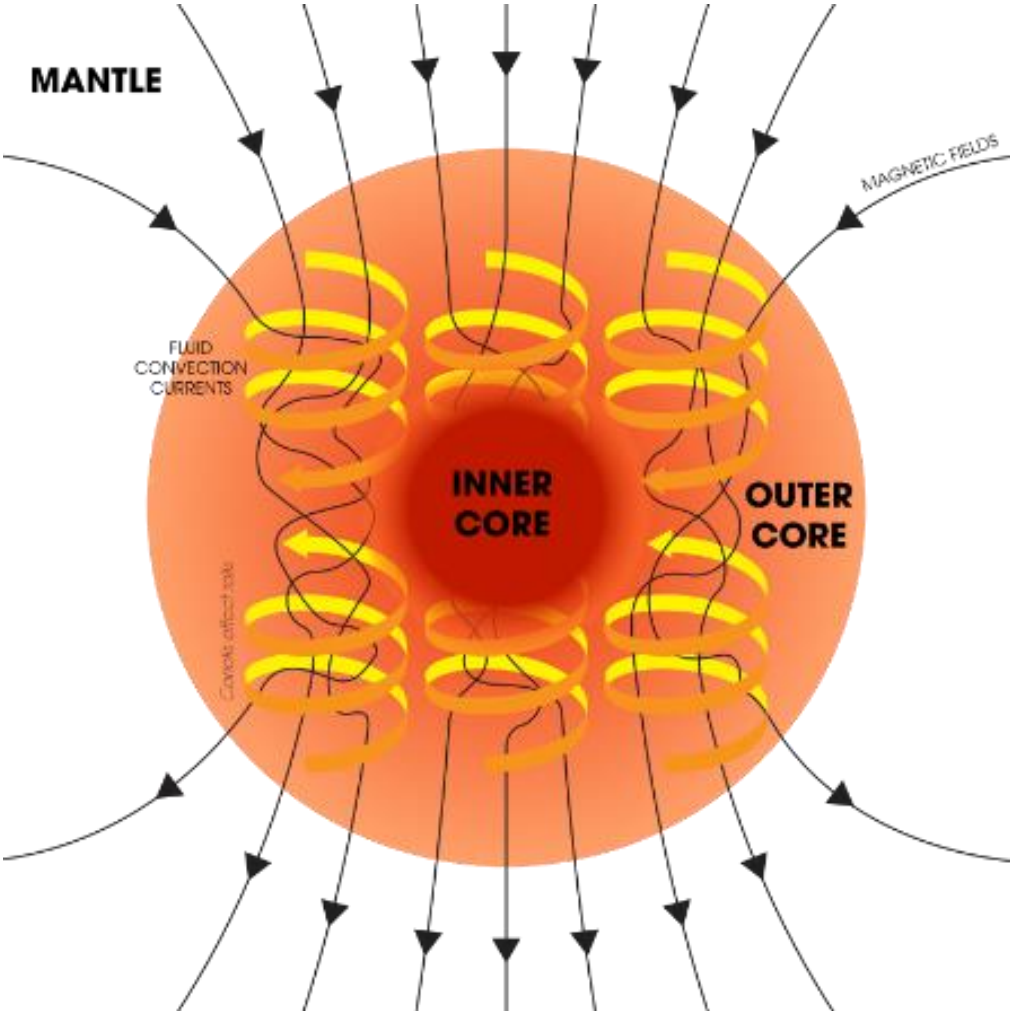

Figure 2.1. Illustration of the dynamo process in the Earth's outer core (from the USGS website).

2004). A positive/negative inclinations indicate downward/upward directed fields, respectively (McElhinny & McFadden, 1999).

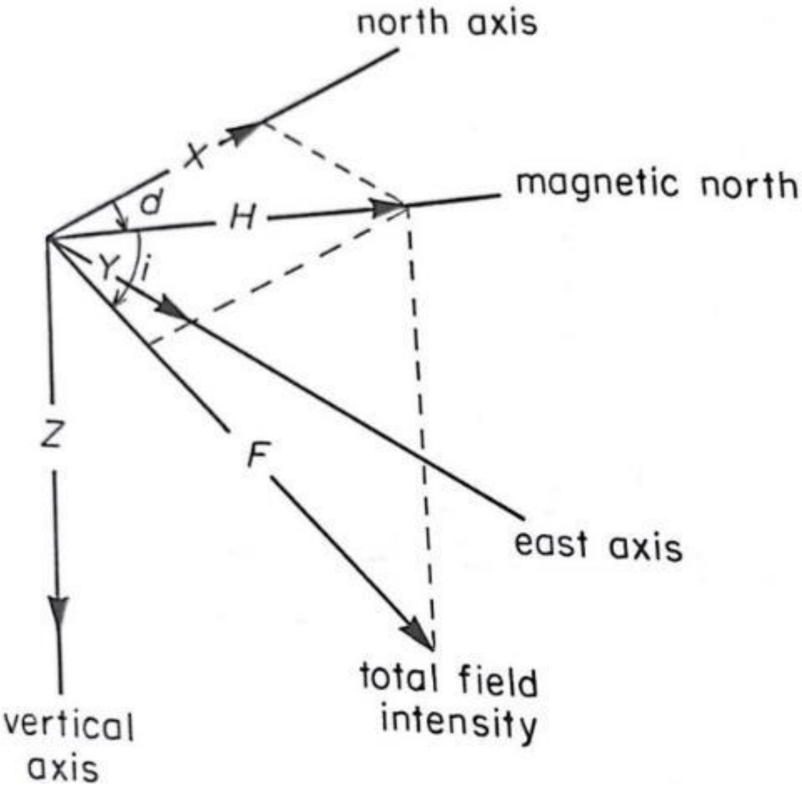

Figure 2.2. Illustration of the magnetic declination, inclination and total field intensity of the geomagnetic field (from Robinson and Çoruh, 1988).

In SI units, the fundamental unit of Earth's magnetic field is Tesla (T) (Butler, 2004). In field studies, magnetic field values are generally measured in nanotesla (1 nT = 10^{-9} T). The intensity of the field varies on the Earth's surface, from 22,000 to 67,000 nT (BGS, 2022).

As can be seen in Figure 2.3, a single dipole in the Earth's centre can account for most of the present geomagnetic field and has a tilt angle of ~11.5° (Butler, 2004). It means the magnetic poles do not intersect with the geographical poles. However, there is a significant contribution from non-dipole field elements.

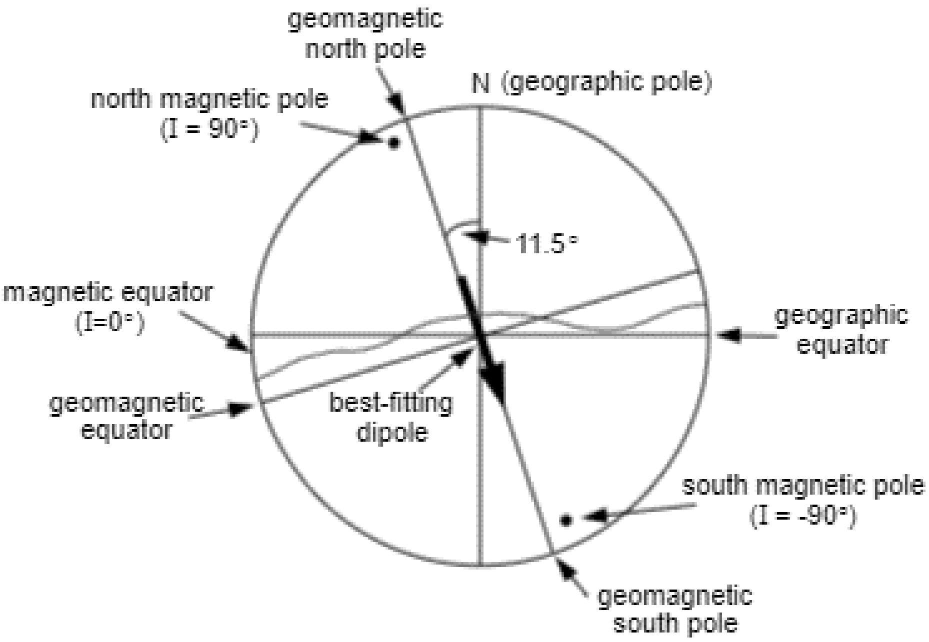

Figure 2.3. An inclined geocentric dipole model (from Butler, 2004).

The International Geomagnetic Reference Field (IGRF) is a reference model for the Earth's magnetic field and is represented in Figures 2.4 – 2.6 by maps showing the variations in declination, inclination and total field intensity (British Geological Survey, 2022).

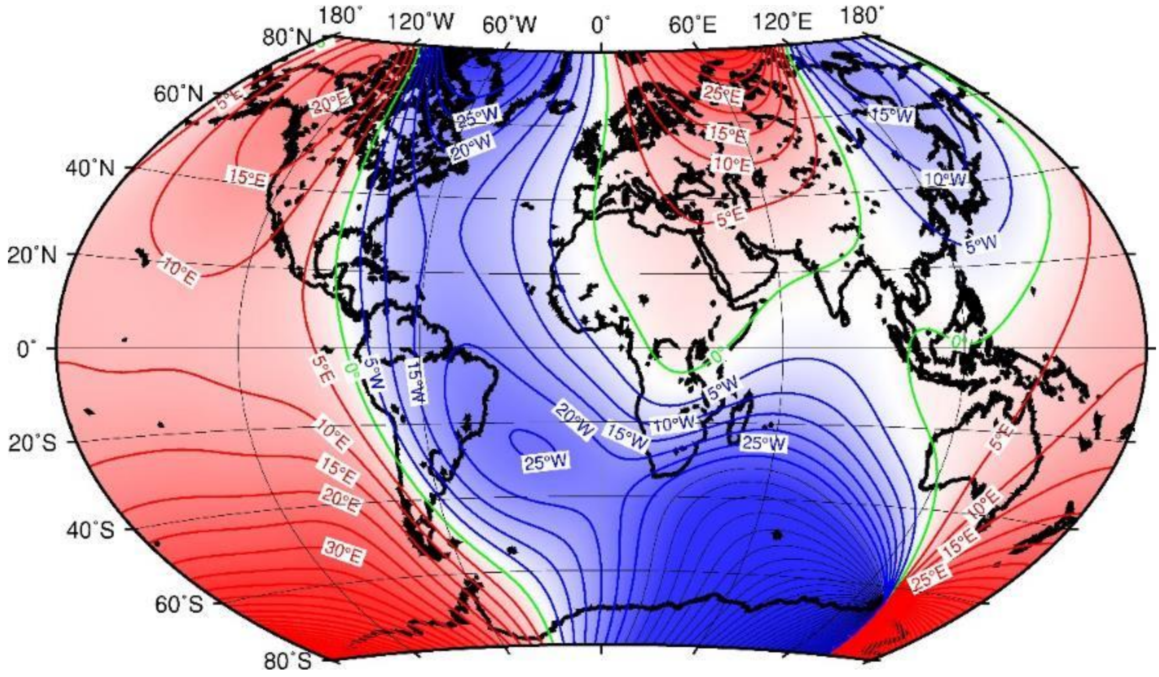

Figure 2.4. A map of declination (from BGS, 2022).

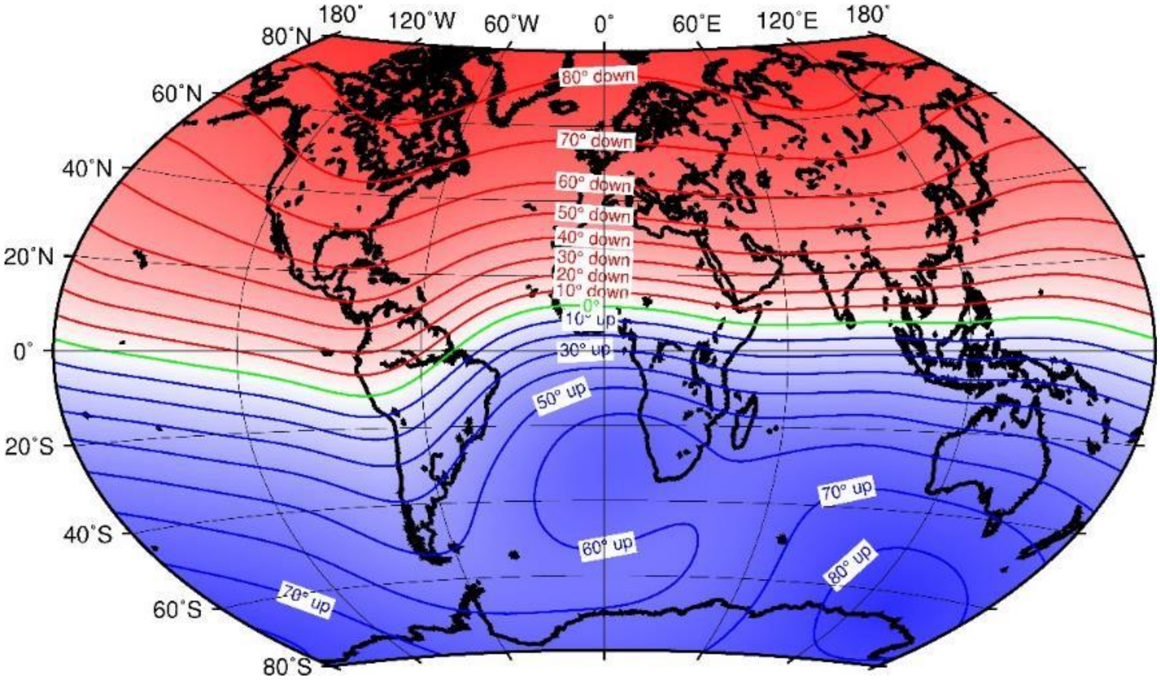

Figure 2.5. Inclination map (from BGS, 2022).

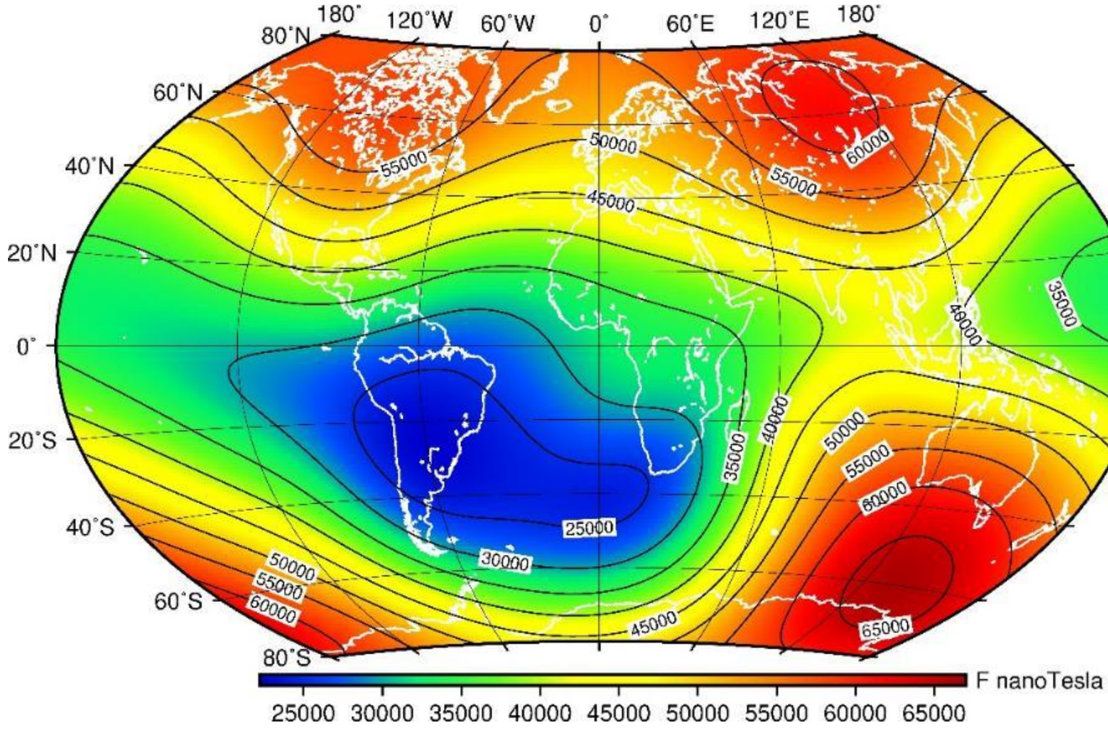

Figure 2.6. A total field intensity map (from BGS, 2022).

2.2 The variations of the geomagnetic field

There are some variations that affect the geomagnetic field, such as diurnal variations, secular variations and reversals. Diurnal variations are daily variations (Figure 2.7). They represent the change over a day in Earth's field, which is determined by measurements made by observatories. This variation seldom reaches 100 nT but it can exceed 1000 nT in the case of a magnetic storm (Musset & Khan, 2000). A magnetic storm is defined by a period with rapid magnetic field variation, caused by ionospheric currents induced by solar UV & X-ray radiation. Figure 2.8 shows the effect of the magnetic storm on field readings. Diurnal variation may be corrected for in geomagnetic surveying by recording field variations using a base station magnetometer and using these data to correct data collected during surveying (Chapter Three).

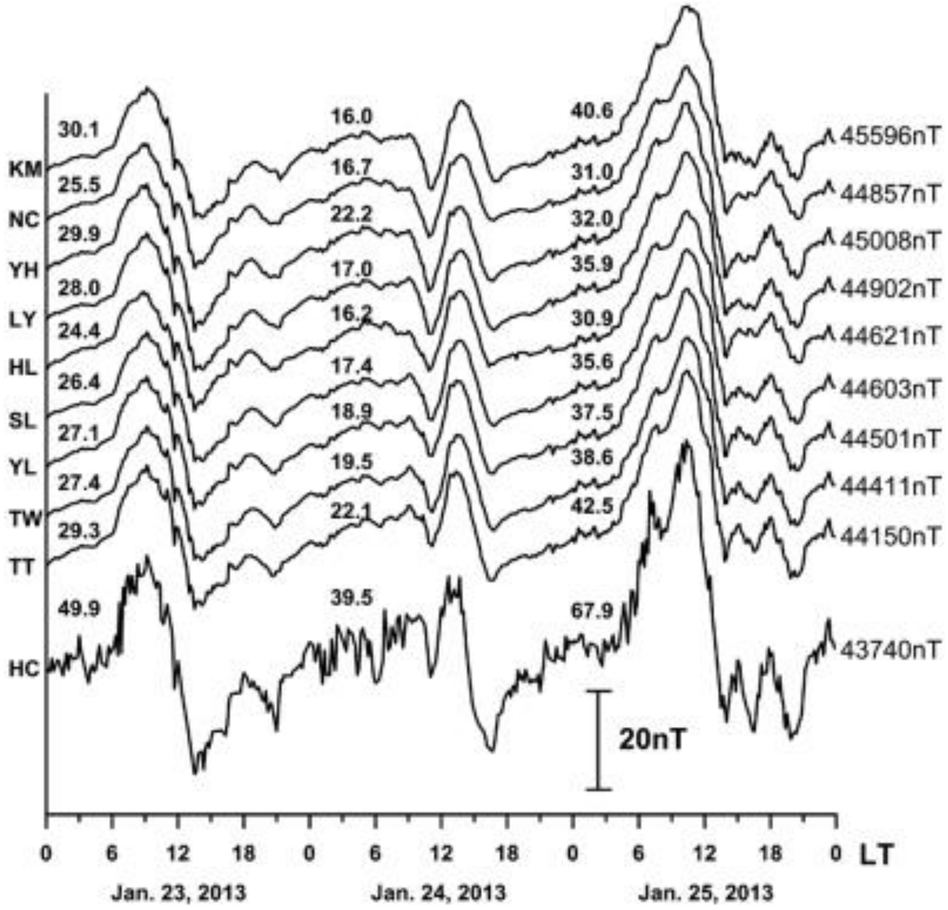

Figure 2.7. A graph showing the geomagnetic field total intensity changes over three days. The numbers represent the diurnal variation sequence at stations for these three days (from Chen, et al., 2015)

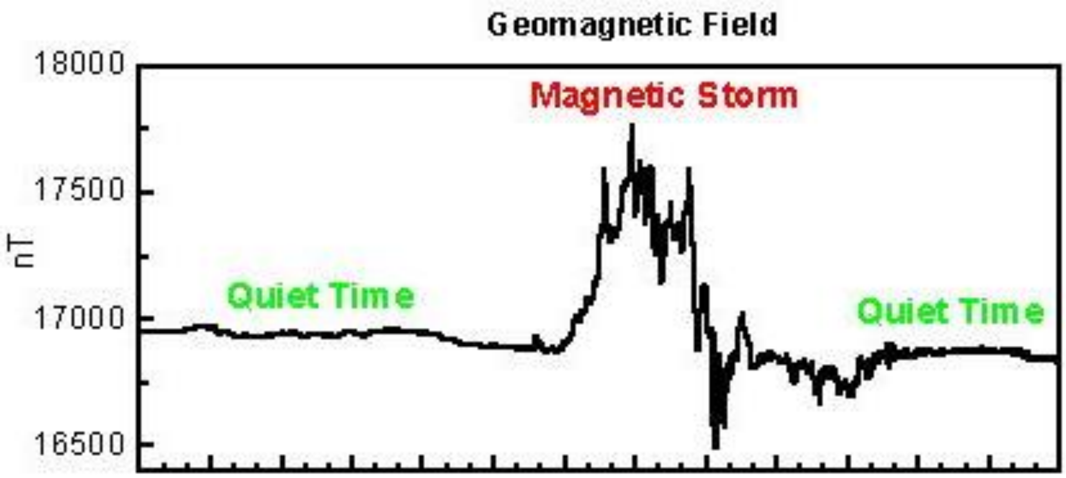

Figure 2.8. A graph showing the effect of a magnetic storm (Adapted from Natural Resources Canada).

Secular variation can be defined as long-term changes in the Earth's magnetic field (Figure 2.9-10). These are slow changes due to changing relative influences of dipole and non-dipole components of the field over periods of decades or centuries.

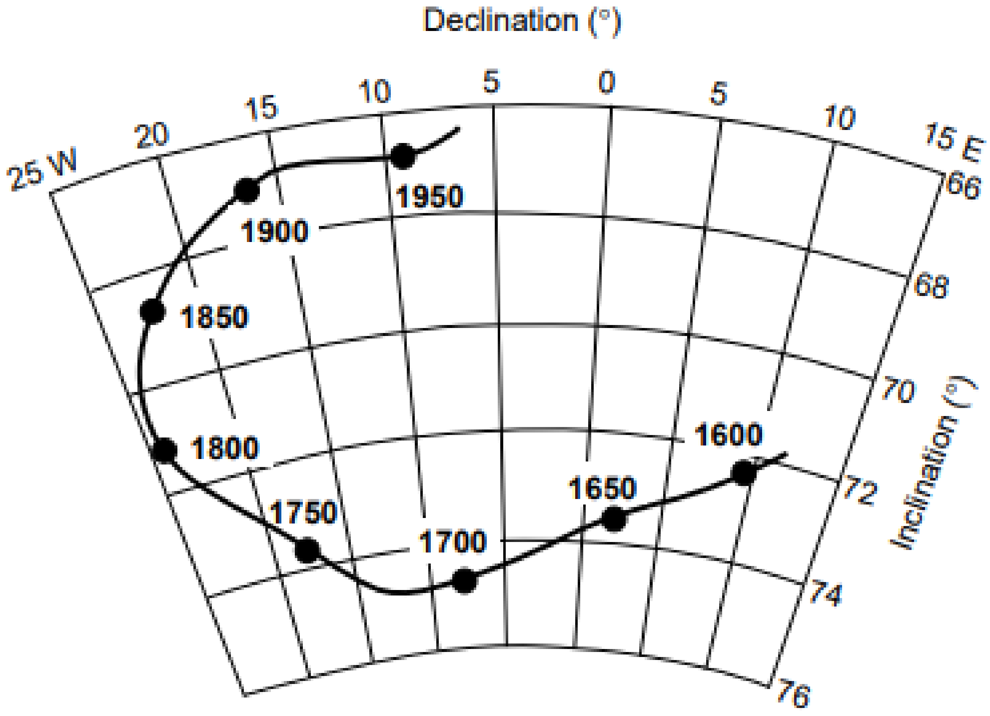

Figure 2.9. Historic secular variations at Greenwich, England (from Butler, 2004).

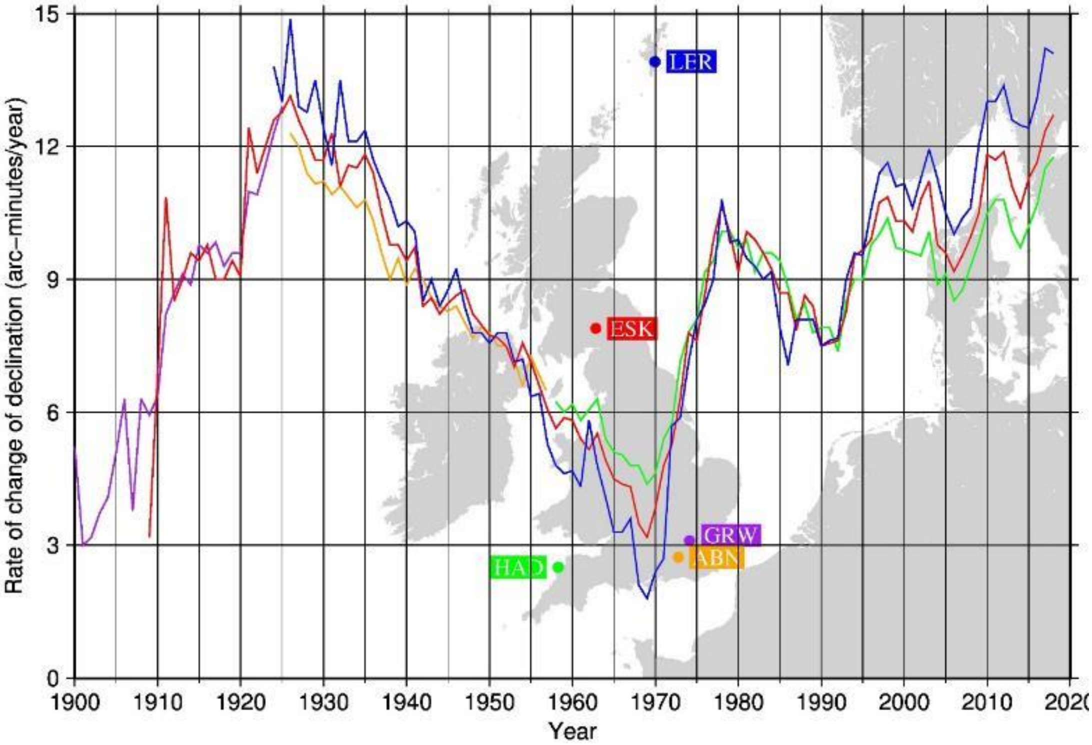

Figure 2.10. A graph showing the rate of change of declination at Greenwich, Abinger, Hartland, Eskdalemuir, and Lerwick observatories (from BGS, 2022).

The displacement of magnetic north and magnetic south in the Earth's magnetic field is called a geomagnetic reversal (Figure 2.11). The normal polarity state has the same direction as the dominant direction of the Earth's field today, while the reverse polarity

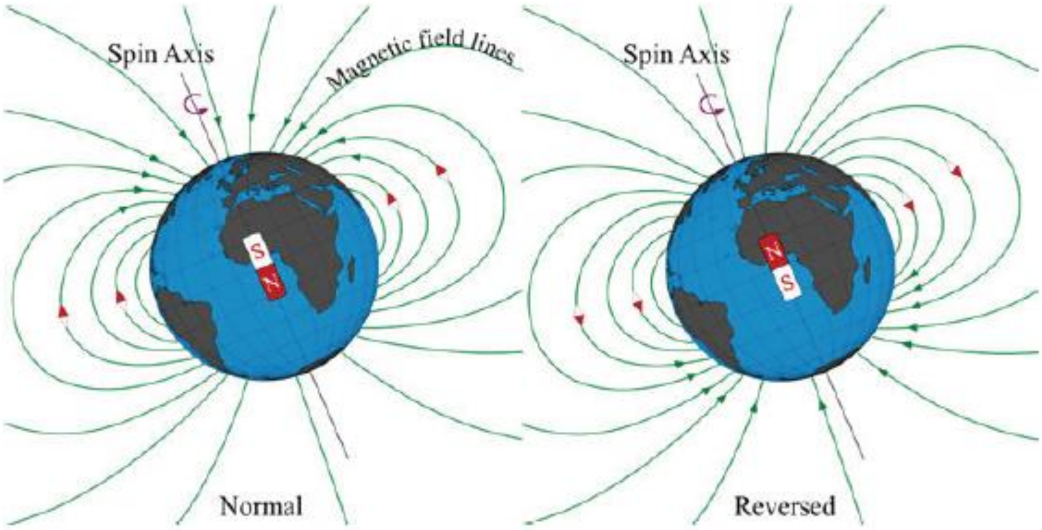

Figure 2.11. Schematic of the Earth's magnetic field for normal and reversed polarity (from Wiers, 2020).

state is the opposite. Studies of geological records of the Earth's magnetic field have shown that reversals have occurred throughout Earth history, but with the frequency of reversals varying through time (BGS, 2022).

Many principles of paleomagnetism are related to the geocentric axial dipole (GAD) concept. This axial dipole model represents the long-term geometry of the Earth's magnetic field by a single magnetic dipole located at the centre of the Earth (Figure 2.12) (Butler, 2004). For this model, the declination of the field is equal to zero (D = 0°) at any point on the Earth's surface, while the inclination is related to latitude by the simple equation:

$$\tan I = 2 \tan \lambda \tag{2.1}$$

Figure 2.12 shows the GAD model. M is the geocentric axial dipole moment. The geographic latitude is shown by λ, varying from –90° at the geographic south pole to +90° at the geographic north pole. The Earth’s radius is shown by r_e (Butler, 2004).

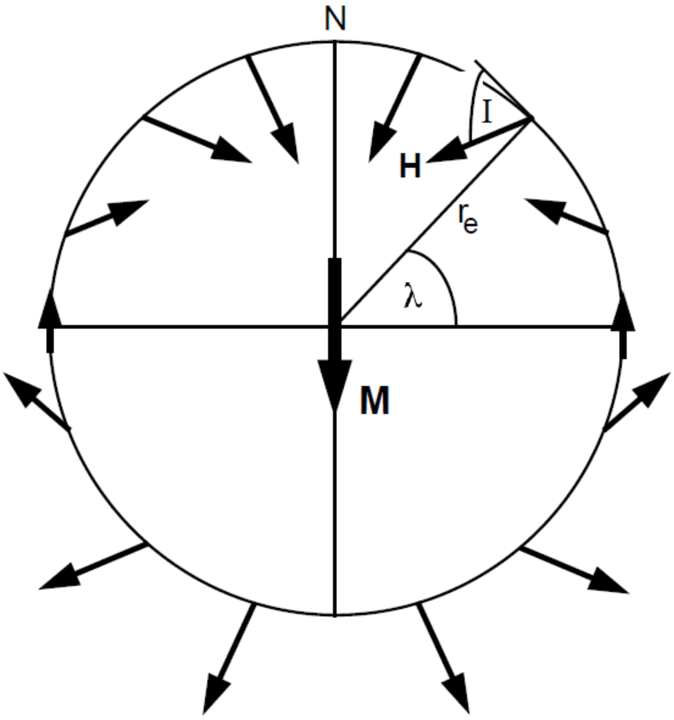

Figure 2.12. A diagram representing the geocentric axial dipole model (from Butler, 2004).

The study of the former pole positions and natural remanent magnetizations (NRMs) in rocks to reconstruct the direction and strength of the geomagnetic field over geological time is called paleomagnetism. The equation between inclination and geographic latitude, the dipole equation, is a key foundation of paleomagnetic studies. As mentioned above, the geomagnetic field switches its polarity in the long term. It means that rocks may acquire different magnetisation components at various times during their geological history. The main aim of palaeomagnetic studies is to identify and isolate these different components of remanent magnetization using palaeomagnetic analyses and demagnetization techniques.

2.3 Magnetization components

Induced and remanent magnetizations are two main components of magnetization. Induced magnetisation can be defined as the magnetization of material that disappears after the magnetic field is removed. The remanent magnetization remains in the material after removing the magnetic field. This remanent magnetization carries the information of past magnetic fields on the material. The total magnetism of rock (M) is equal to the vector sum of induced (M_I) and remanent magnetization (M_R).

$$M = M_I + M_R \tag{2.2}$$

There is a relation between induced magnetism (M_I), magnetic field intensity (H), and magnetic susceptibility (k) (Butler, 2004):

$$M_I = \mathrm{k\ H} \tag{2.3}$$

The ratio of remanent magnetization to induced magnetization is known as the Koenigsberger ratio (Q) (McElhinny and McFadden, 1999). If the ratio is larger than 1.0, it means that the remanent magnetization dominates the rock’s magnetization.

$$Q = \frac{M_R}{M_I} = \frac{M_R}{k\ H} \tag{2.4}$$

The natural remanent magnetization (NRM) is defined as the initial magnetism of rock prior to any laboratory treatment and is determined by the rock type, history, and mineral texture (McElhinny and McFadden, 1993).

2.4 Magnetic behaviour of materials

At the atomic level, all materials have magnetic characteristics, which result from the motion of electrons that spin on their axes and orbit around the atomic nucleus (Lowrie, 2009). These characteristics can be classified on the basis of magnetic susceptibility and how they respond to an external magnetic field. The main three classifications are diamagnetism, paramagnetism, and ferromagnetism. These magnetic properties can be observed with the relation between susceptibility (k or χ), magnetization (M or J), and magnetizing field (H).

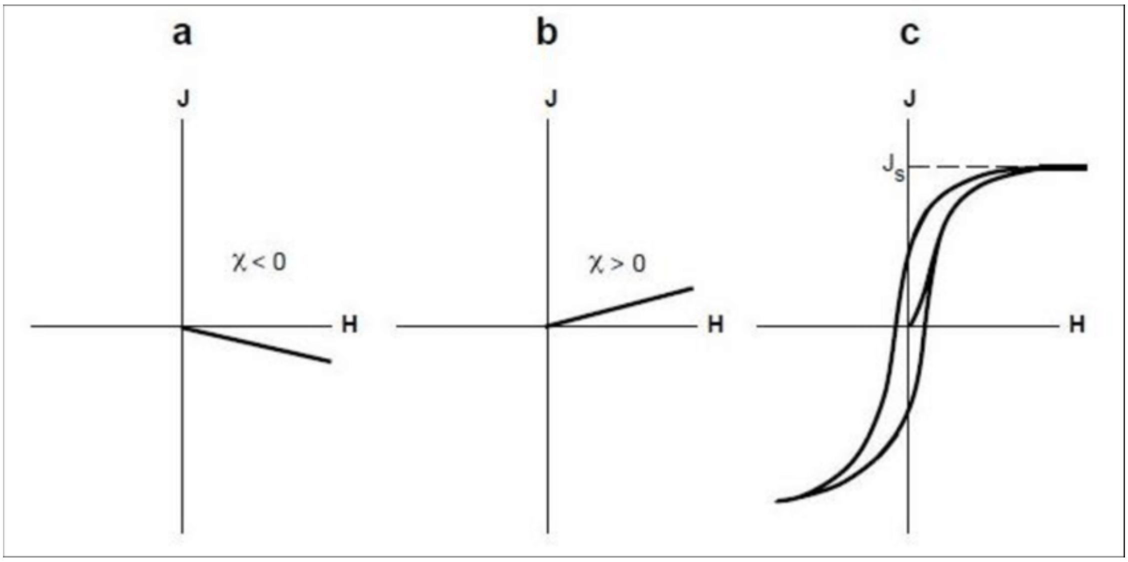

Figure 2.13. Three graphs showing magnetisation (J) against to applied field (H) (from Butler, 2004). a) Negative magnetic susceptibility (χ) (diamagnetic materials), b) Positive susceptibility (paramagnetic materials), c) Non-constant magnetic susceptibility (ferromagnetic minerals).

When a magnetic field is applied to diamagnetic materials, a very weak magnetization is produced with direction opposite to the applied field and this magnetisation vanishes just after removing the external applied magnetic field (Butler, 2004). This induced magnetization has a linear relation to the applied field (Figure 2.13a). The magnetic susceptibility of diamagnetic materials is negative and independent of temperature (Butler, 2004). This magnetisation can be observed in many essential minerals of rock-forming, like quartz and calcite and their susceptibility value is around -10^{-6} SI (Lowrie, 2009).

Paramagnetic materials respond to an applied field by acquiring an induced magnetization parallel to the field direction and it disappears after removing the inducing field (Butler, 2004). They have a positive magnetic susceptibility (Figure 2.13b). Examples of paramagnetic materials include many iron-containing minerals, like fayalite, pyroxene, biotite, olivines, amphiboles, and chlorite and they have low susceptibility values ($\sim 5 \times 10^{-4}$ SI) (Tarling and Hrouda, 1993).

In contrast to paramagnetic materials, ferromagnetic materials produce strong interactions between adjacent atomic moments, so these materials have much stronger magnetic susceptibilities (Butler, 2004). When the magnetic field disappears, magnetization does not return to zero and the material maintains some permanent magnetisation (Lowrie, 2009). As can be seen in Figure 2.13.c, the relationship between magnetization and applied field is not linear, and the magnetic susceptibility is not a simple constant. In the periodic table, iron (Fe), cobalt (Co), and nickel (Ni) elements and their alloys are ferromagnetic elements. For paleomagnetic studies, magnetite (Fe_3O_4), hematite (Fe_2O_3), and pyrrhotite ($Fe_{1-x}S$) are the significant minerals which contain information about the geomagnetic field's direction at their formation time.

There are three types of ferromagnetic behaviour: true ferromagnetism, antiferromagnetic, and ferrimagnetism (Robinson and Çoruh, 1988). True ferromagnetic materials display a parallel alignment of magnetic moments in the same direction (Figure 2.14.a). Iron, nickel, and cobalt are examples of true ferromagnetic elements and can rarely exist in the Earth's crust (Robinson and Çoruh, 1988). Antiferromagnetic materials show an antiparallel alignment of magnetic moments with equal magnitude (Figure 2.14.b). However, there is no net magnetic moment (Tarling and Hrouda, 1993). Hematite is a well-known antiferromagnetic mineral. Ferrimagnetic materials have two opposite directions of magnetic moments with different strengths (Figure 2.14.c). Ferrimagnetic materials retain a remanent magnetization after removing the applied field (Tarling and Hrouda, 1993). The most known examples are magnetite and pyrrhotite.

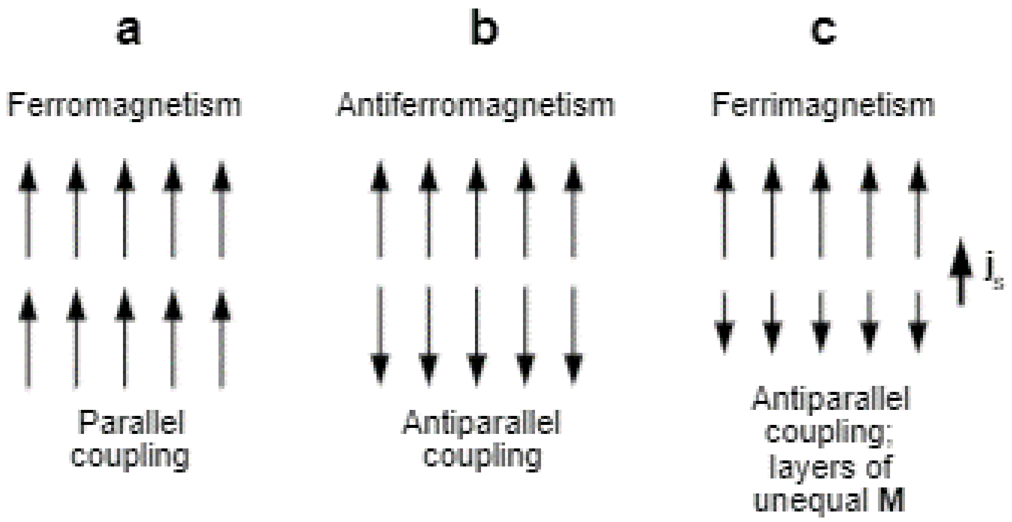

Figure 2.14. Schematic representations of different forms of magnetisation. a)ferromagnetic, b)antiferromagnetic, c) ferrimagnetic materials (from Butler, 2004).

Curie Temperature is a temperature at which certain magnetic materials undergo a dramatic change in their magnetic properties. At this temperature, magnetic moments are no longer able to interact, and magnetization is lost. After this temperature level, ferromagnetic materials behave paramagnetically (Butler, 2004).

2.5 Magnetic Minerals

For paleomagnetic studies, the majority of ferromagnetic minerals have importance because they contain some information about Earth's former magnetic field. The minerals that are responsible for rock magnetism may be described in the ternary oxide diagram with rutile (TiO_2), wustite (FeO), and hematite (Fe_2O_3) at the apexes (Figure 2.15) (Butler, 2004).

These magnetic minerals belong to two solid-solution series that are titanomagnetite and titanohematite series. The first series lies between magnetite (Fe_3O_4) and ulvöspinel (Fe_2TiO_4) and the minerals of this series are opaque and cubic, and crystallize in the spinel structure (Figure 2.15) (Butler, 2004). The second important series of magnetic minerals is the titanohematite series shown in Figure 2.15. These series are between Fe_2O_3 (hematite) and Fe_2TiO_3 (ilmenite) and have opaque minerals that crystallize in the hexagonal system (Butler, 2004). Figure 2.15 also shows that the Curie temperature of intermediate members of both series decreases as the amount of titanium increases.

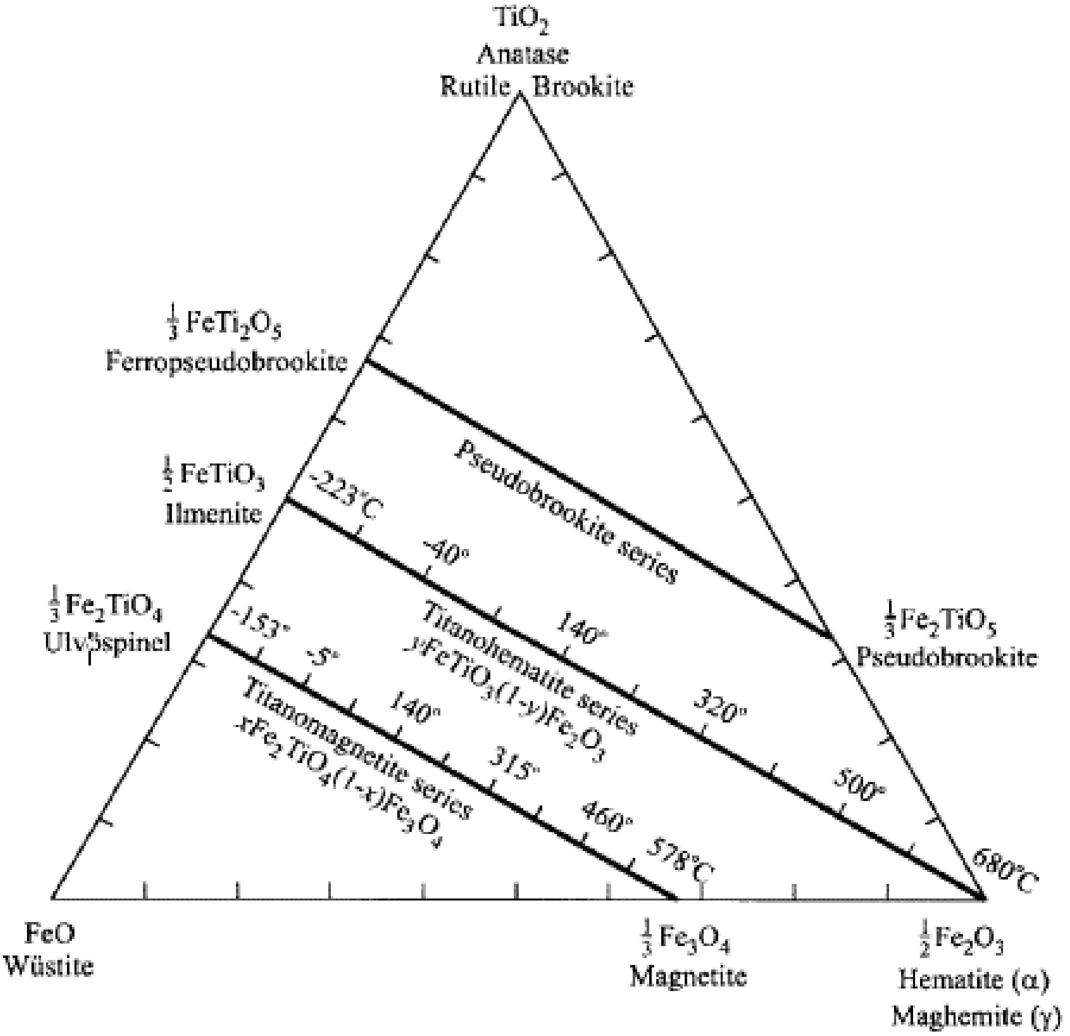

Figure 2.15. The ternary oxide diagram with rutile (TiO_2), wustite (FeO), and hematite (Fe_2O_3) at the apexes (from McElhinny and McFadden, 1999).

Butler (2004) argues that these two series form in the early crystallization of igneous rocks at approximately 1300°C. Also, the cooling rate plays a fundamental role in the grain size distribution of FeTi oxides. While pillow lavas have <1 μm grain sizes because of the rapid cooling, larger grain sizes like 100 μm might be observed on slowly cooled intrusive rocks.

2.6 Magnetic anomalies

Magnetic surveys, one of the geophysical methods, are used to detect anomalies caused by source bodies within the subsurface. This method can be used for archaeological studies, detecting hazardous waste sites, exploring dykes and mapping. Magnetic anomalies are differences in the Earth's magnetic field due to variations in the magnetism of the rocks. As an example of an anomaly, a buried ore body may acquire an induced magnetization in the Earth’s magnetic field, which causes variations in the magnetic field. The body produces an anomaly in the field and the location of the body in the subsurface can be determined. For anomalies caused by induced magnetizations, the direction of magnetization of rocks in the subsurface is parallel to that of the present day field at the location. Alternatively, anomalies can also be due to remanent magnetizations that differ in direction to the present day field.

Magnetometers are used to measure the strength of the field and to detect anomalies. Proton precession and fluxgate magnetometers are the main two main types. While proton precession magnetometers measure the total strength of the magnetic field without its direction, fluxgate magnetometers measure the field component along the sensor's axis (Mussett and Khan, 2000). Figure 2.16 shows a proton and a fluxgate magnetometer in use. Proton magnetometers are preferred for land surveys (and are used here), while detailed gradiometer investigations and borehole studies are conducted by fluxgate magnetometers (Mussett and Khan, 2000).

Figure 2.16. Left: A proton precession magnetometer (from GEOMETRICS, 2014). Right: A Fluxgate magnetometer (from Ernenwein and Hargrave, 2007).

Anomalies vary in shape depending on the magnetic properties, depth and orientation of the bodies that produce them and their location on Earth.

2.6.1 The effect of depth on magnetic anomalies

Depth is one of the important variables that affect magnetic anomalies. When there is a shallower body, it creates a sharp anomaly with a short wavelength. There is a link between the anomaly shape and the magnetization direction (Mussett and Khan, 2000). Positive and negative anomalies are generally observed together, as seen in the anomaly graphs below.

Figure 2.17 shows the relationship between depth and the anomaly shape. Depth is the only variable that was changed in these graphs. The amplitude of the anomaly decreases and its width increases as the depth of the source body increases.

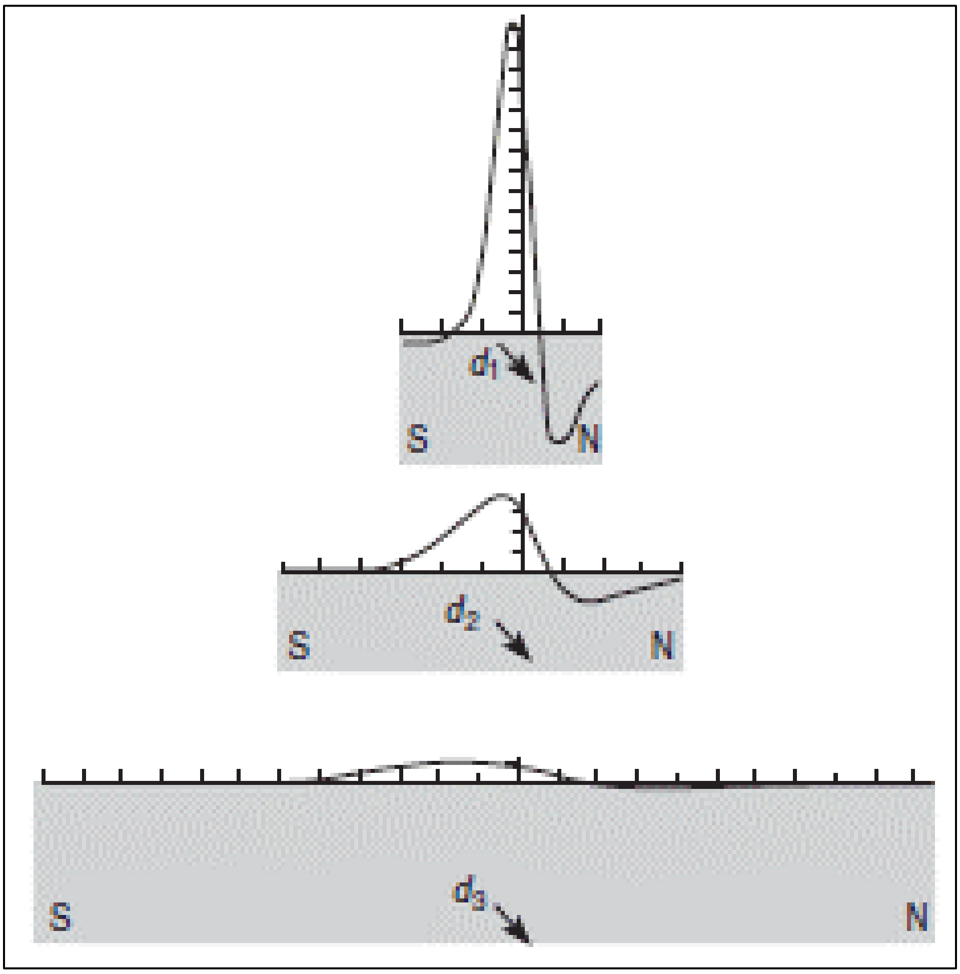

Figure 2.17. Graphs showing dipole anomalies for a different levels of depths (form Mussett and Khan, 2000).

2.6.2 The effect of latitude, shape and orientation

For induced magnetic anomalies, the direction of induced magnetization is aligned in the direction of the Earth's field, but this varies systematically with latitude. Figure 2.18 shows the effect of three different latitudes on an anomaly. These differences have resulted from the Earth's field varying with latitude. A negative inverse anomaly is expected at the equator (Figure 2.18a), and weak positive peak points are observed along the northern and southern edges of the body. Also, the anomaly is symmetrical between the two peak points. At all mid-latitude locations (Figure 2.18b), there is a larger positive anomaly to the south of the body than negative to the north. As can be seen in Figure 2.18c, at magnetic poles, since the magnetic field of an induced dipole will be in the same direction as the Earth's magnetic field, it will strengthen the Earth's magnetic field and produce a large positive anomaly. In summary, the size and shape of the anomaly are significantly affected by latitude.

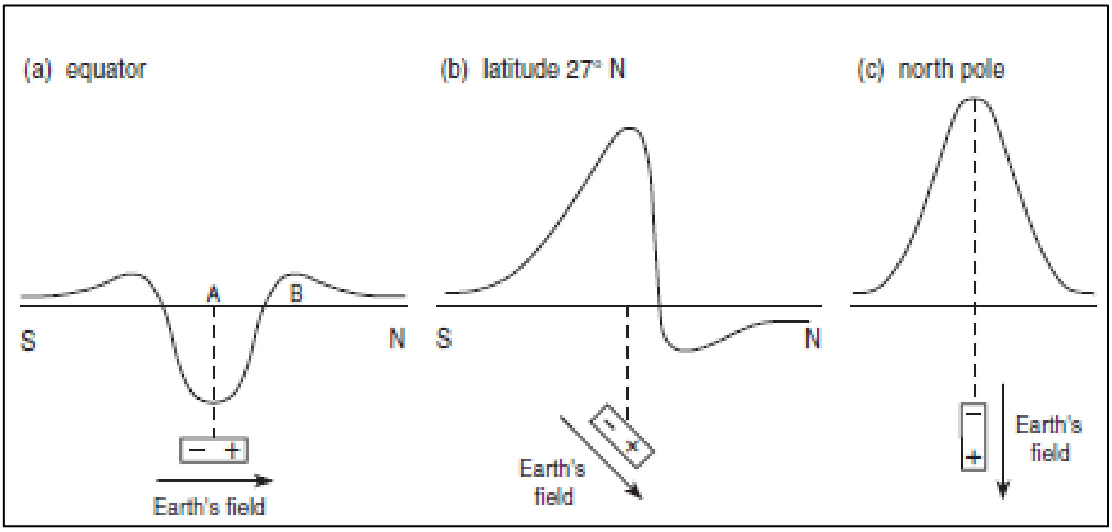

Figure 2.18. Change in the anomaly of a dipole at different latitudes. a) tan I = 2 tan λ, b) at latitude 27° N (45 °) c) downwards (from Mussett and Khan, 2000).

Consideration of induced anomalies due to thin, vertical sheet-like bodies of varying orientations is also informative. (Mussett and Khan, 2000). Figure 2.19a, b and c show anomalies over vertical sheets striking east-west and these are similar in form to those caused by a simple dipole source (Figure 2.18).

In contrast, Figure 2.19d, e and f represent a sheet striking north-south, at three different latitudes (Mussett and Khan, 2000). This situation generates no magnetic anomaly when the body is located at the equator where the field is horizontal, and symmetrical anomalies whose amplitude depends on the inclination of the field and the induced magnetization at other latitudes.

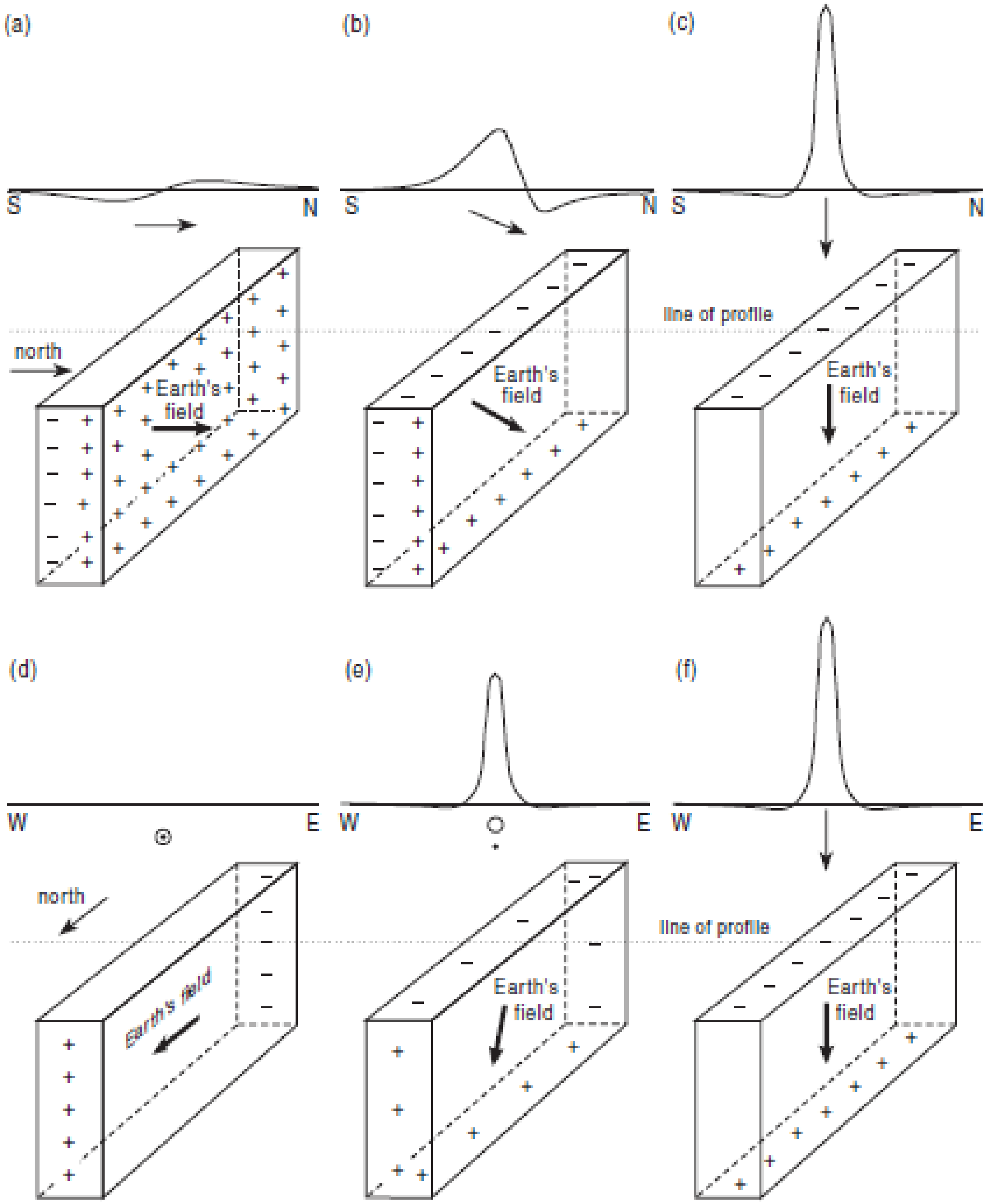

Figure 2.19. Graphs representing the anomaly of poles formed on a thin vertical sheet (from Mussett and Khan, 2000).

2.7 Anisotropy of magnetic susceptibility (AMS)

Anisotropy of magnetic susceptibility (AMS) is a directional variability of magnetic susceptibility produced by the same magnetic fields applied in different directions. The anisotropy of magnetic susceptibility can be visualized using an ellipsoid which has principal axes along three directions of susceptibility (Figure 2.20). These axes belong to maximum (k1), intermediate (k2), and minimum (k3) susceptibility. When these three axes are equal to each other, a spherical ellipsoid is obtained and the sample's magnetic susceptibility is isotropic (Morris, 2003).

As can be seen in Figure 2.20, a prolate ellipsoid is observed when the maximum principal axis of the AMS ellipsoid is significantly larger than the intermediate axis, i.e. $k_1 >> k_2 \geq k_3$. Generally, prolate ellipsoids result from flow during the formation of volcanic and sedimentary rocks, where the maximum axis is parallel to the palaeo-flow direction (Morris, 2003). When $k_1 \geq k_2 >> k_3$, ellipsoids have an oblate shape (Figure 2.20). Sedimentary rocks and highly foliated metamorphic rocks have generally oblate susceptibility ellipsoids where minimum axes are perpendicular to the bedding and foliation, respectively (Morris, 2003). When $k_1 > k_2 > k_3$, this represents a triaxial ellipsoid shape (Figure 2.20).

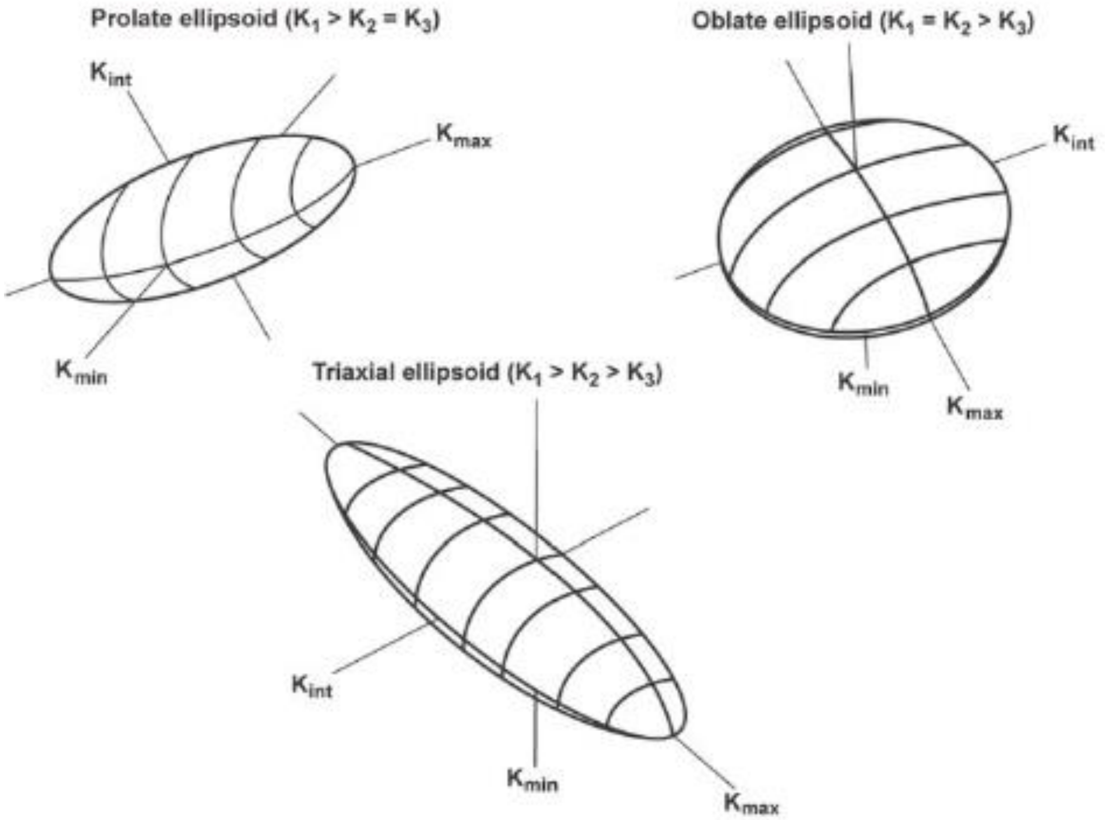

Figure 2.20. Illustration describes the prolate, oblate and triaxial magnetic susceptibility ellipsoids with principal axis relations (from O'Driscoll, 2006).

Although AMS determinations are not normally conducted in association with geomagnetic surveying and modelling, in this study the AMS of oriented samples collected from the Ballantrae region was measured as part of the routine processing of samples and was used to provide bulk susceptibility values that are valuable for modelling purposes.

Chapter 3 - Methodologies

In this section, detailed information about all methodologies is given. The main method of this study is a field study involving collection of geomagnetic field data, field measurement of low field magnetic susceptibility of exposed rocks and the collection of oriented hand samples for laboratory analysis. After applying some data corrections and data processing, two-dimensional and three-dimensional modelling of the resulting magnetic anomaly data can give detailed information about the subsurface geology of the study area.

Figure 3.1. Location of the study area with a Google Earth image.

3.1 Fieldwork

The study area is around Ballantrae in Scotland (Figure 3.1). Three main studies were conducted, which are magnetic field surveying, hand sample collection, and field susceptibility measurements.

In the Ballantrae region and the Southern Uplands, low-field susceptibility data were measured from exposed rocks. Figure 3.2 shows the location of these measurements.

These data sets were used for 2D and 3D modelling and combined with additional measurements of hand samples in the laboratory in order to identify their potential as sources of induced magnetic anomalies.

Figure 3.2. Google Earth image shows the locations of field susceptibility measurements.

The ground-level total magnetic field study was conducted in two main areas (Knocklaugh Lodge and Coastal Area) using a Geometrics G857 proton precession magnetometer, with a second G857 unit installed at the field accommodation to act as a base station magnetometer. The base station was set up at about five kilometres from the 3D survey areas for the duration of fieldwork, and was used to detect potential geomagnetic storms and to record diurnal variation of the field during the day (Figure 3.3). While deciding on the place of the base station, safety, near magnetic sources around, continuity, and distance to the fields were considered. A Geometrics G857 proton precession magnetometer was used for field studies with two sensors with a one-meter distance between them and operated in gradiometer mode.

Figure 3.3. The base station was located away from human-made magnetic sources. The magnetometer of the base station was put into a plastic box to protect it from rain.

The first area is Knocklaugh Lodge where a prominent local magnetic anomaly has been previously observed and where drilling has confirmed serpentinite at depth (Stone et. al., 1984). Previous modelling has not been carried out to determine the subsurface geometry of this body, so a ground-level total field magnetic survey was conducted as a grid survey (1 km x 1 km) over the Knocklaugh Lodge anomaly for modelling (Figures 3.4 and 3.5). The magnetometer readings were collected at approximately ten-pace intervals apart, with roughly fifteen paces between survey lines, with the location of each measurement being automatically recorded using a Garmin GPS unit connected to the magnetometer. Figure 3.6 shows the data points collected for the Knocklaugh Lodge grid study. Also, total magnetic field data were collected on a longer profile across the Knocklaugh Lodge anomaly (Figure 3.5). That profile extended across the exposed outcrop of the Northern Serpentinite Belt of the Ballantrae ophiolite to investigate the subsurface geometry of the Belt and the nature of the associated ground-level magnetic anomaly. Magnetic data readings were collected at fifteen pace intervals as much as possible under field conditions on the profile.

Figure 3.4. Magnetic data collection on Knocklaugh Lodge Profile.

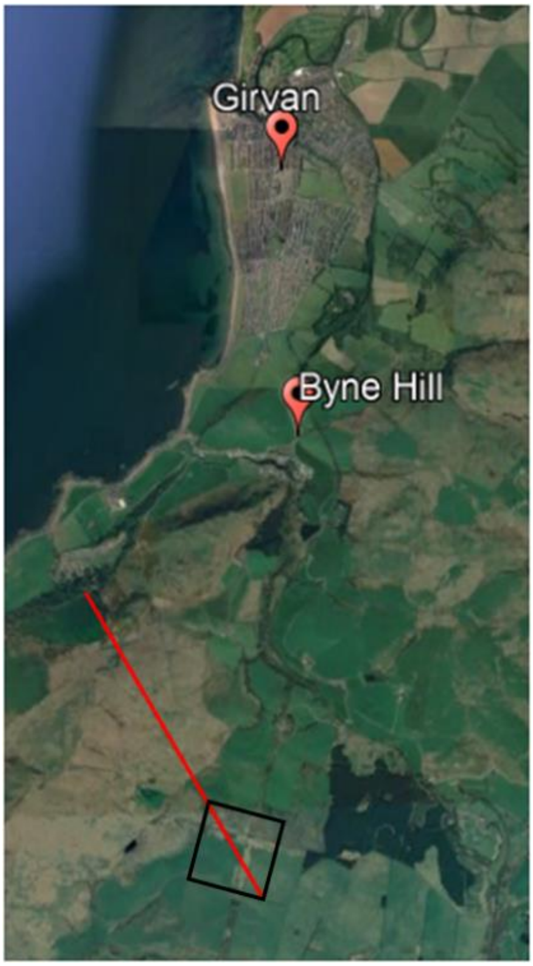

Figure 3.5. Google Earth image of Knocklaugh Lodge Profile that is marked as a red line and grid survey showing by a square.

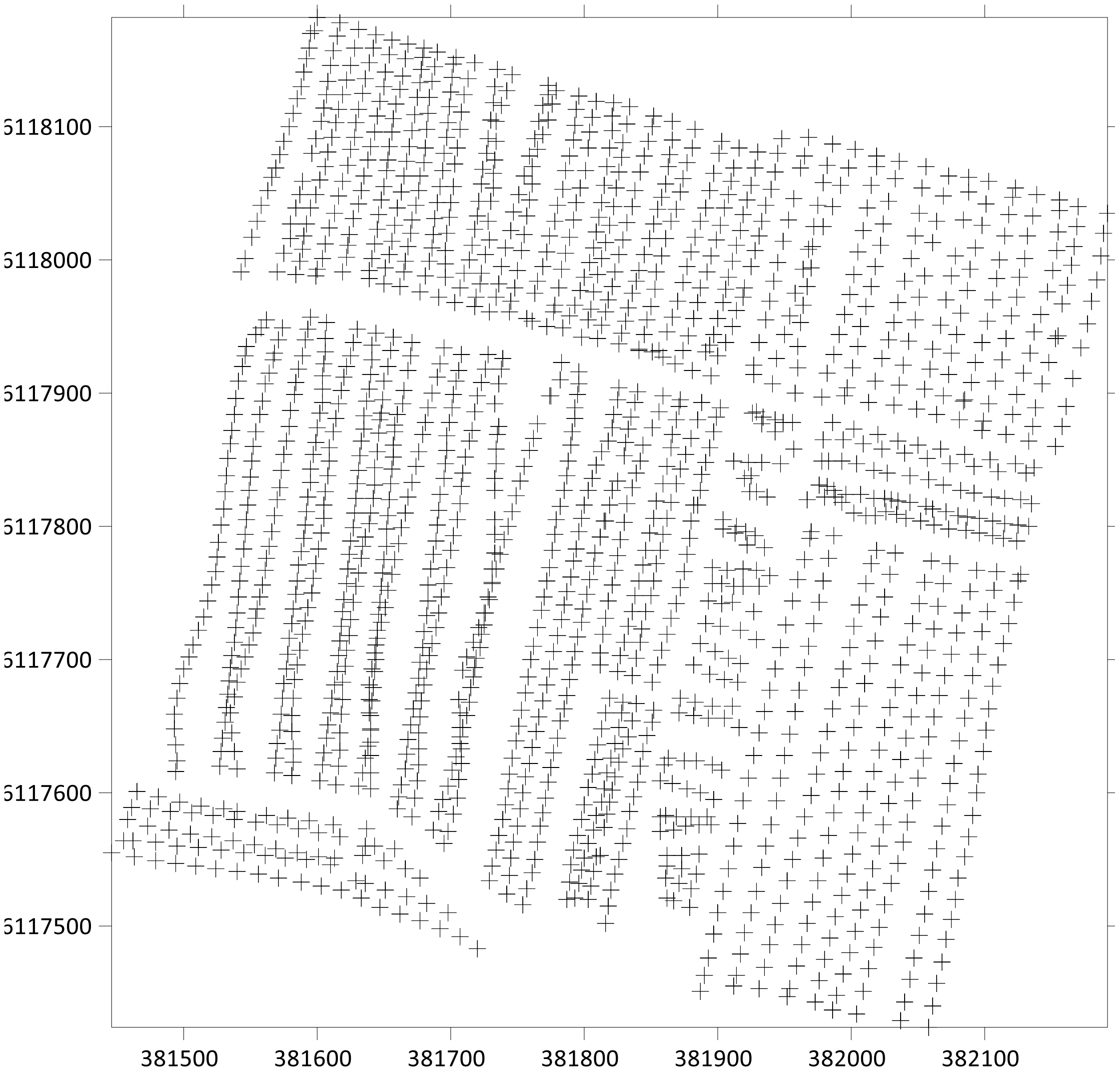

Figure 3.6. Data points of the grid survey are plotted using Surfer®. The axes of the map are in UTM (easting and northing).

The second magnetic field study was conducted in a coastal area where the BGS map shows serpentinite as the bedrock, and where dyke-like bodies of dolerite/gabbro are exposed in fields representing a raised wave-cut platform. This coastal study was conducted to investigate the nature of signals arising from mafic intrusions within serpentinite. Magnetic data were collected at approximately five pace intervals and there was an approximately ten pace distance between the grid lines. Figure 3.8 shows the location of the "Coastal Area" via Google Earth and data collection points that were plotted using Surfer® is in Figure 3.9.

Figure 3.7. An image from Coastal Area with some outcrops. A hand sample was collected from an outcrop which is on the left. Some microgabbro outcrops were observed.

Figure 3.8. Google Earth image of Coastal Area Survey that is marked as a blue rectangle.

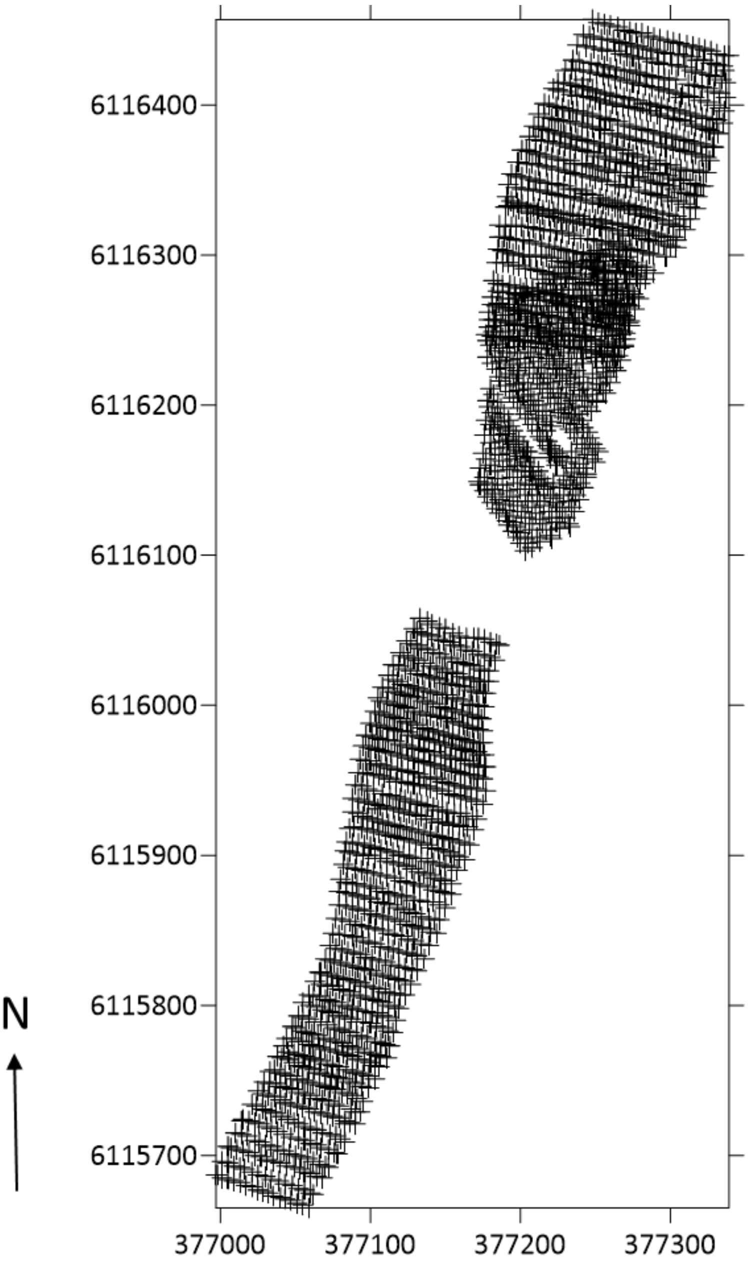

Figure 3.9. The grid survey data points for the Coastal Area plotted using Surfer®. The axes of the map are in UTM (easting and northing).

Twenty-three oriented hand samples were collected from each main rock unit from eight sites and their dip and dip direction measured using a compass-clinometer. The locations of the oriented hand samples can be seen in Figure 3.10. These samples were used to determine Natural Remanent Magnetizations (intensity and directions) and Anisotropy of Magnetic Susceptibility. These data were combined with magnetic susceptibilities to calculate Koenigsberger (Q) ratios, for determining which magnetization dominates magnetic anomalies in this region.

Figure 3.10. Google Earth image of oriented hand samples locations (represented by pink pins).

3.2. Processing of the geomagnetic field data

Before data acquisition, some corrections should be applied to the data sets to get accurate results. For example, daily magnetization fluctuations can affect the results of the study. Also, shallow sources might complicate identifying the deep source. These effects can minimize with corrections.

3.2.1 Diurnal corrections using base station data

As mentioned in Chapter 2.2, some variations affect the geomagnetic field that should removed from collected data sets to get true results. Diurnal correction is used to remove the influence of daily fluctuation and transient disturbance of the geomagnetic field. For diurnal correction, each magnetic field value which was collected from the field was matched with the base station reading taken at the same date and time, and the correction's result which belongs to that match was removed from the magnetic field value. Base station readings occasionally showed noise attributed to environmental changes (e.g. passing of tractors near the base station, so smooth trends through the data were determined by fitting sixth-order polynomials through each day's record. This also allowed accurate interpolation between base station readings to facilitate matching with the times of each field reading collected during surveying.

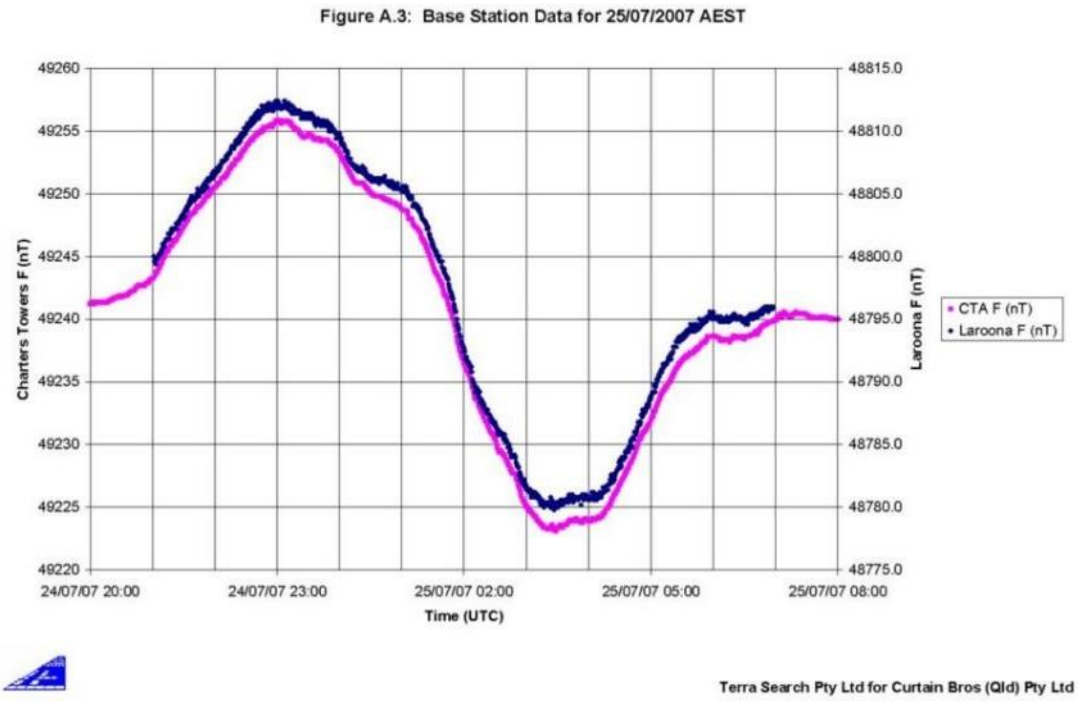
Figure A.3: Base Station Data for 25/07/2007 AEST

Terra Search Pty Ltd for Curtain Bros (Qld) Pty Ltd

Figure 3.11. An example of magnetic diurnal correction (from Beams, 2019).

Total field intensity readings were then converted to magnetic anomalies by subtracting the IGRF value from each reading. To create accurate anomaly profiles from the 2D survey at Knocklaugh Lodge, the GPS coordinates of each field station (measuring point) were used to calculate the distance of each station from the starting point of the profile.

3.2.2 Contour mapping of the magnetic anomalies

Magnetic field station locations were collected as latitude and longitude using GPS in the field. For an accurate contour map, these coordinate values were converted into UTM coordinates using an "Online application to convert Latitude Longitude to UTM" (ESurveying-Softech, 2022). After the coordinate conversion, the anomaly data sets for the Knocklaugh Lodge and the Coastal Area surveys were mapped as contour maps using Surfer® software. This software helps to show the maps on Google Earth too. While plotting, only the values collected in the field were selected. An example of the contour map can be seen in Figure 3.12.

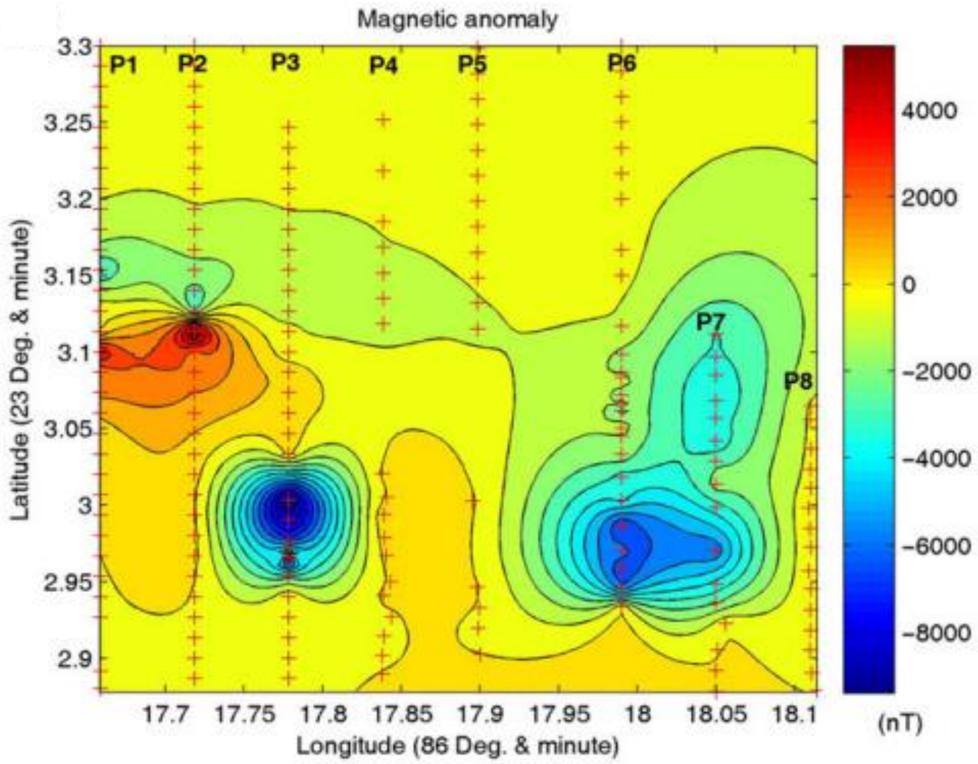

Figure 3.12. A contour map (from Mandal & Sharma, 2015).

In addition to ground-level total magnetic field contour maps, an aeromagnetic anomaly map was plotted using Surfer® software. Data were drawn from the UK National Aeromagnetic Survey (Institute of Geological Sciences, 1972, 1980). From this national dataset, data over the Ballantrae area were isolated for modelling. Locations in this survey were originally specified as the British National Grid (OSGB36) references. These were converted into UTM coordinates using the Grid InQuestII software.

3.2.3 Upward continuation of magnetic anomalies

In magnetic anomaly studies, observed anomalies are typically cause by a combination of shallow and deep sources, with the latter typically producing regional-scale anomalies. The purpose of upward continuation is to suppress short wavelength components originating from shallow sources in order to highlight the contribution of deeper sources. Upward continuation was used in this study to detect anomalies from the regional anomaly sources. Upward continuation of anomaly data collected at ground level can therefore give similar results to an aeromagnetic survey.

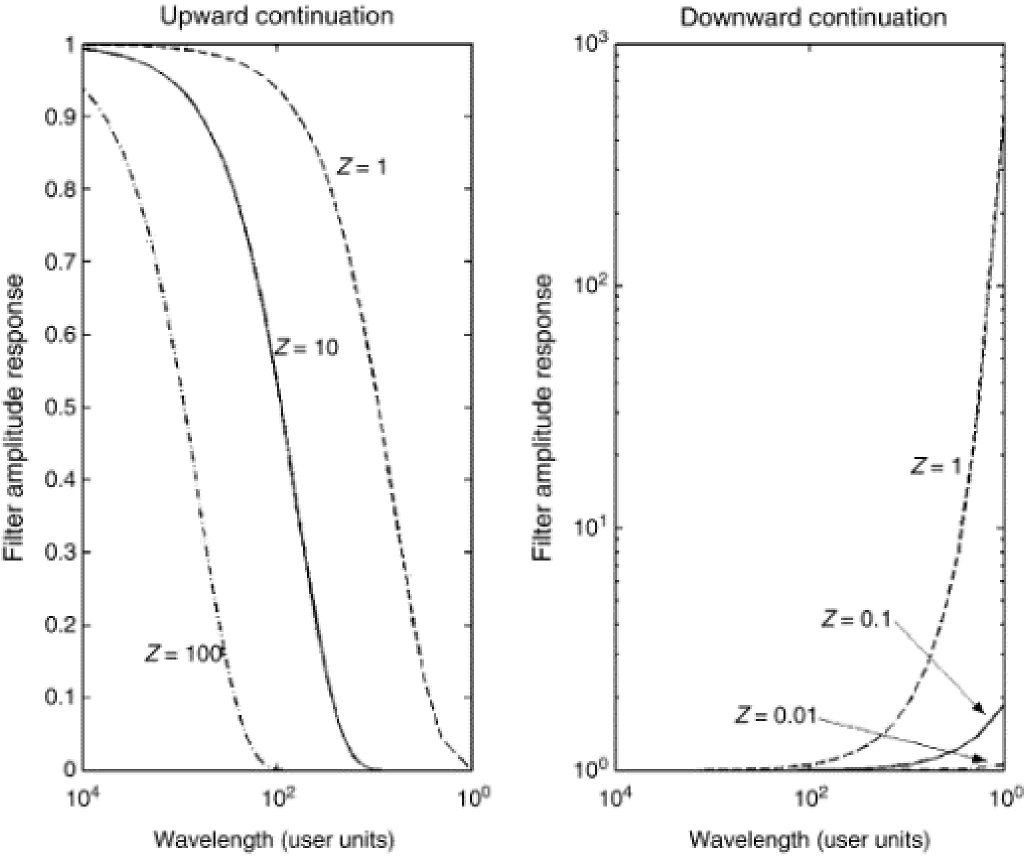

Figure 3.13. The change in amplitudes for different height values (z) using continuation operators (from Ravat, 2007).

As outlined by the Encyclopaedia of Geomagnetism and Paleomagnetism (Ravat, 2007), the continuation operator in the wavenumber domain helps to understand how the upward (and downward) continuation works. This operator can be defined by $e^{\pm|k|z}$, where z is the continuation level, and $|k|$ is the wave number (defined as $|k| = 2\pi\lambda$, where λ =

wavelength). Upward continuation means going away from the sources and is represented by the negative sign the exponent of the operator. A positive sign would indicate going towards the source, and results in downward continuation (Ravat, 2007). Figure 3.13 shows the amplitude changes for different height values using continuation operators. In the process of upward continuation, shorter wavelengths are attenuated and smoothed out (Figure 3.13). However, in the process of downward continuation, it is seen in Figure 3.13 that shorter wavelengths are amplified and sharpened.

In more detail, Laplace's equation underlines the upward and downward continuation of magnetic anomaly data. The following information on Laplace's equation for upward and downward continuation is summarized from Morris (1986). The equation states that the sum of potential gradient rates of change in three directions equals zero. In a Cartesian coordinate system, x and y represent the horizontal axes, while z is the vertical axis and Laplace's equation becomes:

$$\frac{\partial^2 A}{\partial x^2} + \frac{\partial^2 A}{\partial y^2} + \frac{\partial^2 A}{\partial z^2} = 0 \tag{3.1}$$

In this equation, A represents a potential field. In two-dimensions Laplace’s equation in the same coordinate system (with x and z directions) is:

$$\frac{\partial^2 A}{\partial x^2} + \frac{\partial^2 A}{\partial z^2} = 0 \tag{3.2}$$

When assuming A is a function of only x and z directions, this equation can be solved using the technique of variable separation. The solution is:

$$A_k(x,z) = a\cos(kx - \lambda)\, e^{|k|z} \tag{3.3}$$

As defined above, k is the wavenumber and the wavelength is shown by λ. There is a constant defined by a.

In the equations above, the anomaly is represented by a single cosine function. More complex anomaly shapes may be represented by the sum of a series of cosine/sine functions with different wavelengths and amplitudes. So natural anomalies can be represented by the following series:

$$A(x,z) = \sum_{n=0}^{\infty} a_n \cos(k_n x - \lambda_n)\, e^{|k_n| z} \qquad (3.4)$$

When the anomaly is observed on the ground level (z = 0), this equation becomes:

$$A(x,0) = \sum_{n=0}^{\infty} a_n \cos(k_n x - \lambda_n) \qquad (3.5)$$

The component cosine/sine waves may be found by using Fourier analysis to assign an amplitude and phase to each wavenumber component, i.e. determine the values of a_n, and k_n for each component. The anomaly can then be transformed to that which would be observed at a different level by then changing the value of z in the exponential term for each component in the frequency domain. The inverse Fourier transform is then used to convert the upward or downward continued anomaly components back into the time domain. While working on these steps, there should be $(2N + 1)$ equally spaced field points with $2N$ intervals. The longest wavelength component that can be detected is of length L, while the shortest one has wavelength L/N. As a result of this, the wavenumber range that can be observed is between $2\pi/L$ and $2\pi N/L$ which can be shown as:

$$(2\pi/L) \le k \le (2\pi N/L) \qquad (3.6)$$

Figure 3.14 shows an example of upward continuation for grid data from the literature (Araffa et al., 2012). In this case, a total intensity magnetic data set collected at ground-level has been upward continued to an elevation of 1000 m.

Within the scope of this project, there are both profile and grid datasets to be upward continued. For profile data, this was achieved using GeoSimplex's Upward Continuation Excel sheet (GeoSimplex, 2015). This required some corrections to produce a working spreadsheet that may be used for any profile data set. Geometrics Magpick software was used for upward continuation for the grid data sets collected for the Knocklaugh Lodge and Coastal Area surveys to reduce residual anomalies. The results of upward continuation were calculated for different levels and Surfer® software was used to display them. The results of these transformations will be discussed in Chapter Four.

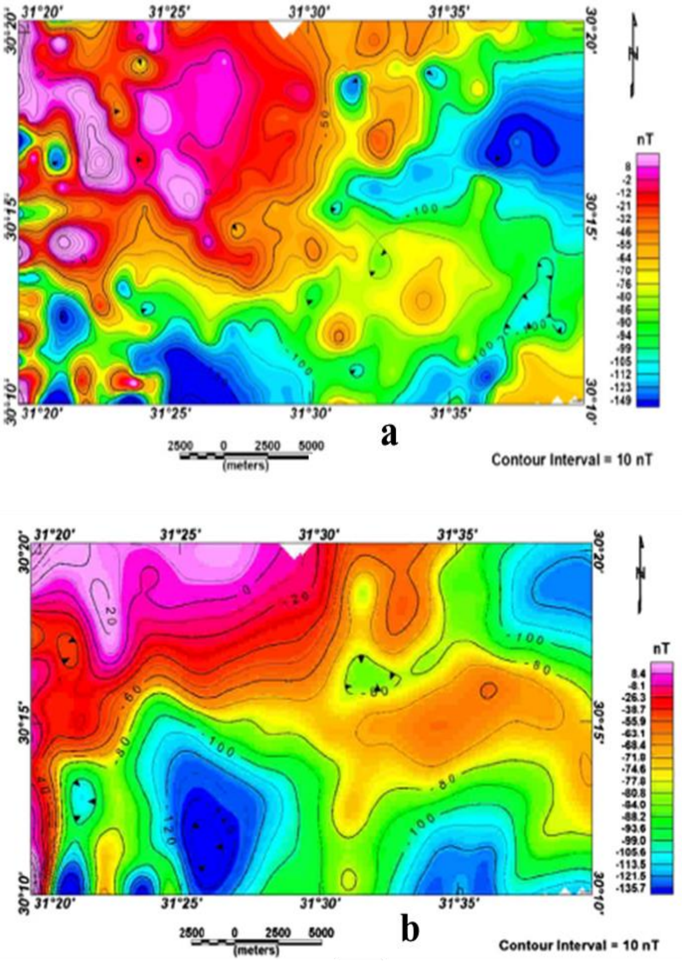

Figure 3.14. a) Total intensity magnetic map b) The result of the upward continuation for 1000 m level (from Araffa et al., 2012).

3.3 Field susceptibility results

Field susceptibility values (k) are displayed using a histogram (e.g. Figure 3.15; Gettings, 2018). Susceptibility values are transformed to $\log_{10}k$ before plotting, as low-field susceptibilities in natural materials are typically log-normally distributed (Tarling and Hrouda, 1993).

In this study, the susceptibility histograms were produced using MATLAB® for each rock type (Chapter Four). These results were used for two and three-dimensional modelling studies.

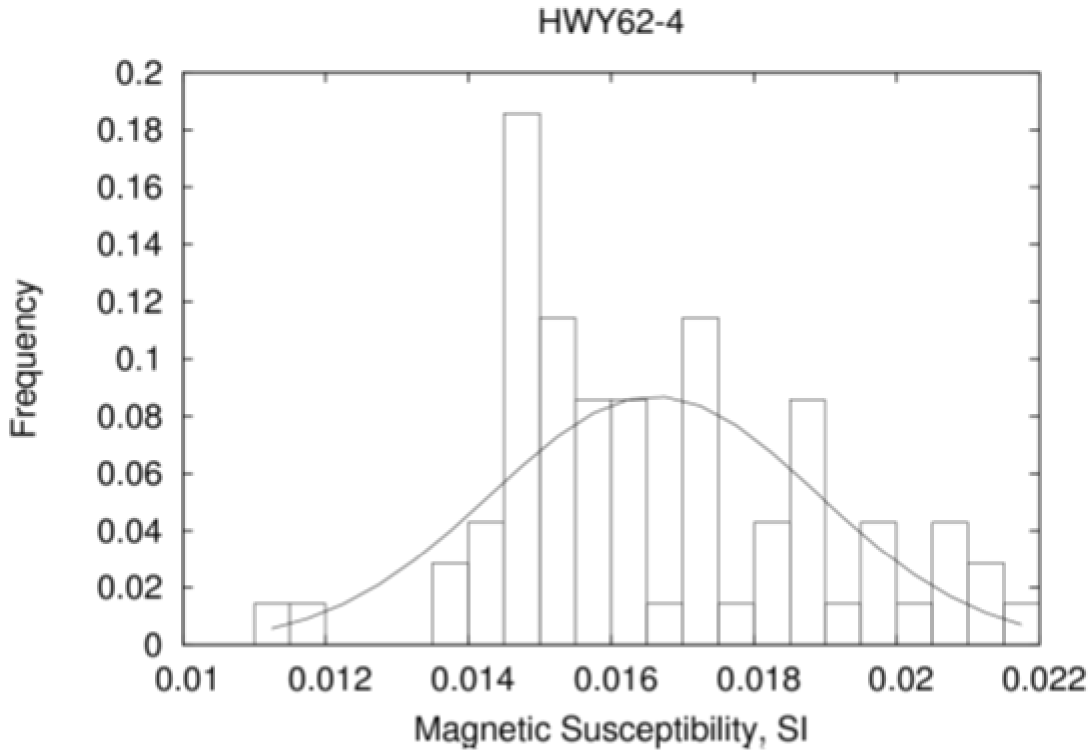

Figure 3.15. A histogram of magnetic susceptibility of an outcrop (from Gettings, 2018).

3.4 Laboratory work on oriented samples

3.4.1 Sample preparation

Hand samples were collecting in the field by recording the dip and dip direction of a suitable flat surface on each sample and marking a dip arrow and strike line directly on the oriented surface. In the laboratory lines were then drawn perpendicular to the strike line and tick marks were added to these lines in the up-dip direction. Figure 3.16 shows this marking process. These prepared hand samples were drilled perpendicular to the surface and the reference arrow was drawn along the length of the cores by extending the parallel lines for each sample. After drilling, cores were cut by using a dual-blade rock saw to produce standard specimens ~21 mm in length for AMS and NRM studies. The devices used for drilling and cutting processes are shown in Figure 3.17. Orientations of cores were specified as hade and azimuth. The hade angle is the angle between the axis of the core and the vertical and is equal to the dip of the original oriented surface of the hand sample. The core azimuth is direction relative to the north and is equal to the dip direction of the oriented surface of the hand sample ±180°. The relation between these directions is schematized in Figure 3.19.

Figure 3.16. Left: An oriented hand sample, dolerite, was collected from site four. Dip and dip direction notes were written on the left corner. Right: The same sample after preparation for drilling. Red lines were plotted perpendicular to the strike and arrows showing the up-dip direction.

Figure 3.17. Left: Drilling machine used to obtain cores from hand samples. Right: Palaomagnetic saw for cutting cores to get the specimens. The distance between the blades was selected as 21 mm to obtain a suitable specimen for measurements. These specimens were used in the AGICO KLY-5 Kappabridge for anisotropy of magnetic susceptibility (AMS) measurements and the Molspin fluxgate spinner magnetometer for Natural remanent magnetization (NRM) measurement.

Figure 3.18. An image of the specimens were used for this study. They are basalt, dolerite, gabbro, lavas, serpentinite, and siltstones. They are numbered.

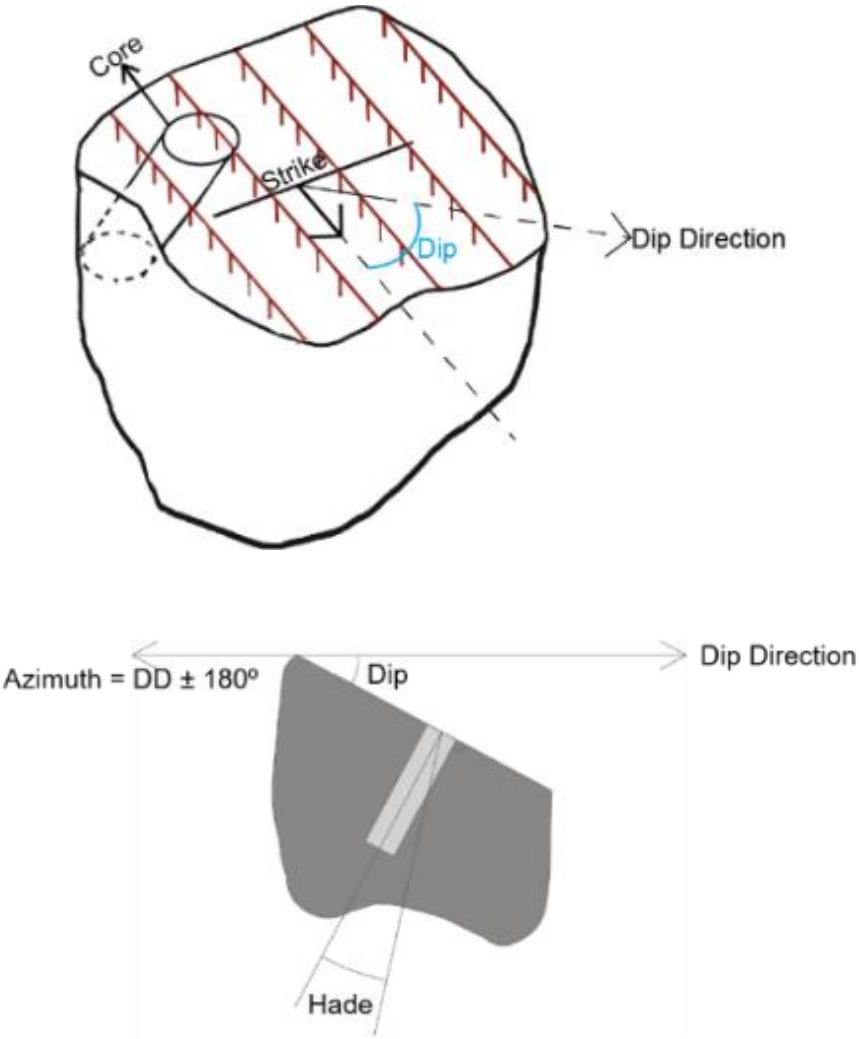

Figure 3.19. Left: Left: Illustration showing hand sample preparation for drilling. The red lines are drawn parallel to the dip direction with arrows pointing upward. Right: The relationship between core azimuth and hade angles is demonstrated in the illustration.

3.4.2 Anisotropy of magnetic susceptibility (AMS) measurements

The AMS measurements were conducted at Plymouth University using an AGICO KLY-5 Kappabridge with the Safyr 7 program being used to process the data. Each specimen was measured in three different positions to create the complete anisotropy ellipsoid and an additional measurement was used to determine the bulk susceptibility (Figure 3.20). For this study, firstly the calibration is done. Then, measurements are taken in all three positions and this provides the determination of each anisotropic component of the susceptibility tensor. With this process, the Safyr 7 software automatically combined these measurements and calculated a best-fit anisotropy ellipsoid for each specimen represented by the maximum (K_{max}), intermediate (K_{int}), and minimum (K_{min}) principal axes of the susceptibility ellipsoid (see Chapter Two). In addition to the mean susceptibility (K_{mean}), the corrected anisotropy degree (Pj) and shape parameter (T) were calculated and displayed via the Anisoft program. The result of these measurements were separated by rock types and displayed on stereonets in the geographical coordinate system and on two graphs of Pj-Kmean and T-P using the Anisoft-5 program (Figure 3.21).

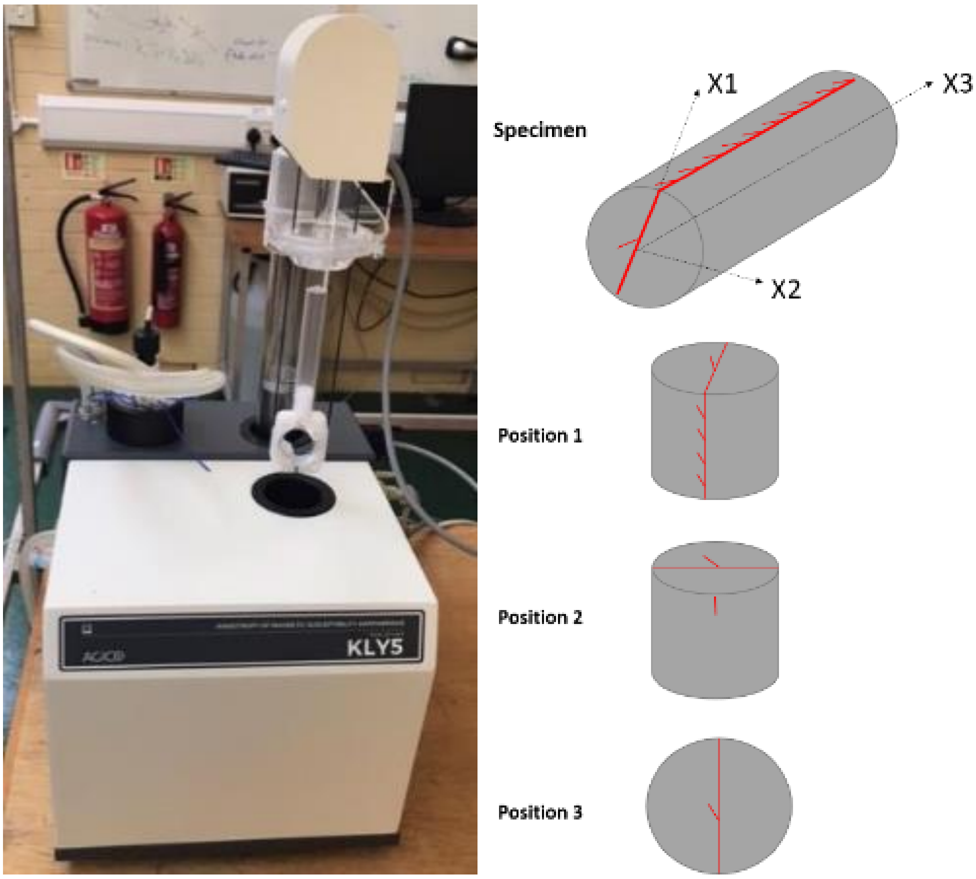

Figure 3.20. Left: AGICO KLY-5 Kappabridge. Right: Each specimen was put into the machine in these three positions for AMS measurement.

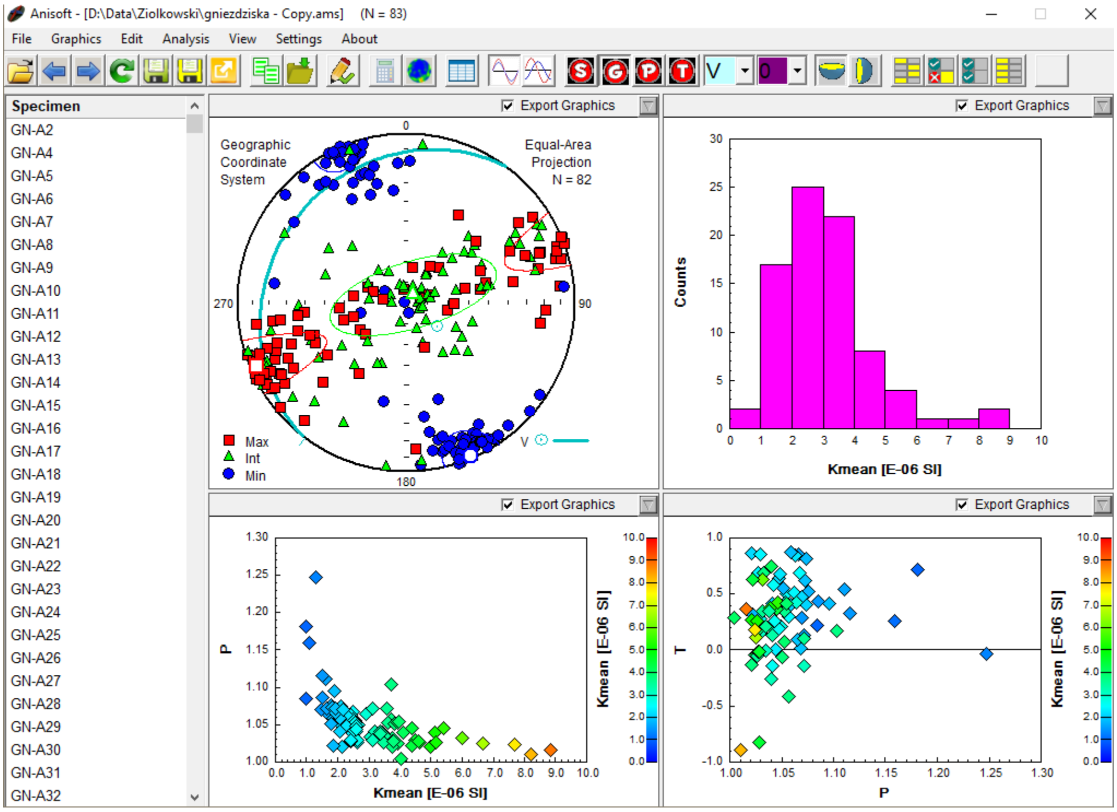

Figure 3.21. An example of AMS result displayed with the Anisoft5 program (from AGICO, 2022). The stereonet shows the principal axis for K$_{max}$, K$_{int}$, and K$_{min}$. Two graphs at the bottom represent the relation between anisotropy degree (Pj), shape parameter (T) and mean susceptibility (Kmean).

3.4.3 Natural remanent magnetization (NRM) measurements

Natural remanent magnetization is the vector sum of magnetization components obtained by a rock at different times due to various geological processes (see Chapter Two).

NRM measurements were performed at Plymouth University using a Molspin fluxgate spinner magnetometer (Figure 3.22) and its control program was used to process the data. For the measurements, the calibration is firstly done and measurements are taken in four positions for each sample. The calibration was done every 30 minutes. Intensity (mA/m) and specimen coordinates' directions (declination and inclination) were calculated by the software and then corrected to geographic coordinates.

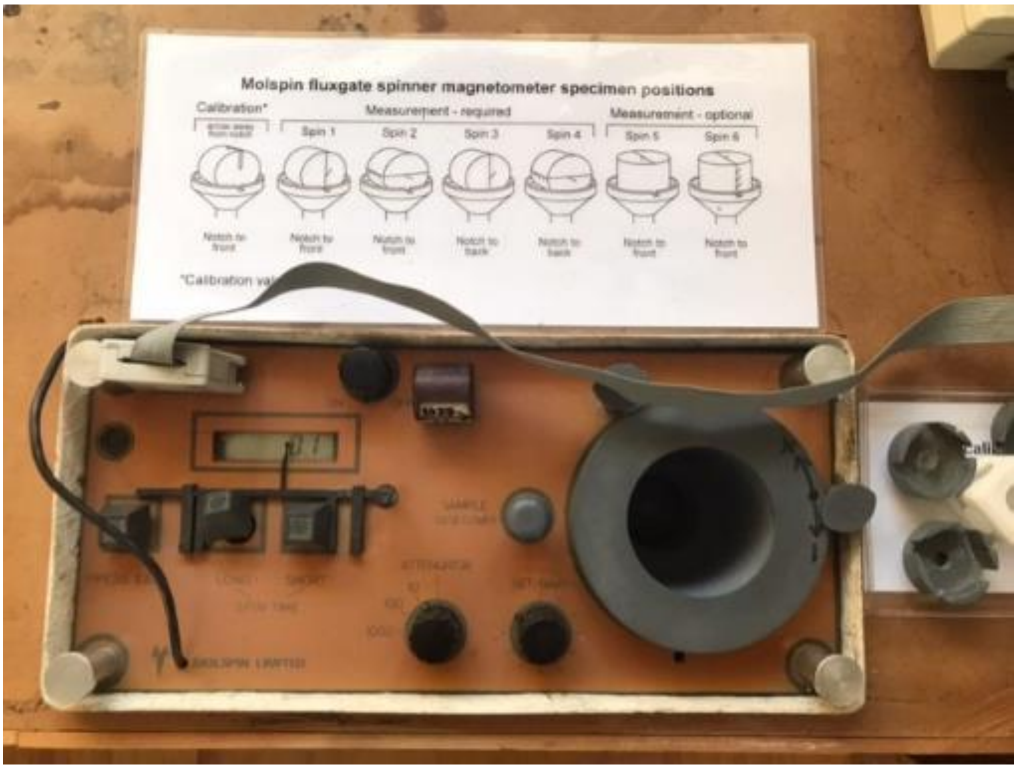

Figure 3.22. Molspin fluxgate spinner magnetometer. The positions for calibration and measurements can be seen on the picture. The calibration and the first four spin positions were used for this study. For each specimen, the intensity, declination, and inclination values were calculated by the program.

3.5 Koenigsberger ratio graphs

The Koenigsberger ratio, a dimensionless parameter, describes the magnetic characteristics of a body and shows the ratio of remanent magnetization and induced magnetization in the body (Figure 3.22).

$$Q = \frac{M_R}{M_I} \tag{3.7}$$

For plotting the Koenigsberger ratio graphs, the intensity and the mean susceptibility values were selected from the hand samples' NRM results. Intensity values had measured in milliampere per meter. They were converted into Ampere per meter for the graph. These Koenigsberger Ratio graphs were plotted using MATLAB® for each type of rock unit (see Chapter Four).

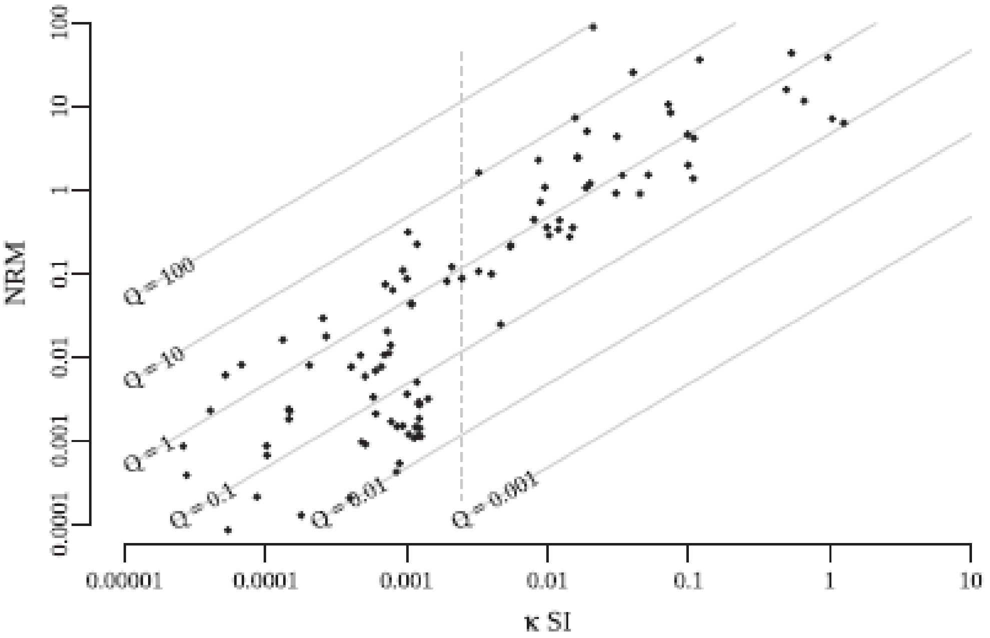

Figure 3.23. An example of Koenigsberger ratio graph (from Webber et al., 2019).

3.6 Modelling studies

Modelling studies are carried out to determine the shape and magnetisation of the subsurface bodies causing a magnetic anomaly. Although some simple anomalies may be interpreted by comparison with those calculated theoretically over simple sources such as buried spheres, this approach can only rarely be applied in practice in geologically complex situations. Since the subsurface sources in the majority of magnetic surveys have irregular structures, a forward modelling process is adopted instead, with the subsurface shape and magnetic properties of anomalous bodies being iteratively adjusted until a good fit is found between observed and calculated anomalies. The most common modelling studies are two and three-dimensional modelling.

3.6.1 Two-dimensional modelling

Information in this section is based on lecture notes regarding two-dimensional modelling as taught at the University of Plymouth (Morris, 2020), which describe the method developed by Talwani (1965).

Two-dimensional modelling assumes that the body in the subsurface has a finite cross-sectional size but extends to infinity in the third dimension perpendicular to the cross-section. To understand 2D modelling, some basic elements of the model geometry should be explained (Figure 3.24). A profile plane is a vertical plane that lies below the magnetic survey profile. It has two coordinate axes, x and z, where x is distance along the profile and z is depth. The angle α is the angle between the profile plane direction and true north. In Figure 3.24, J represents the intensity of the body's magnetisation, while J_{DEC} shows its declination, J_{INC} is its inclination. The points where the amplitude of the magnetic anomaly is measured during the magnetic survey are called field points. Each of them has its own x coordinate. For ground-level studies, their z coordinates are equal to zero. Body points represent the corners of a prism which represents the body's cross-section in the profile plane. Each body point has its own x and z coordinates. In Figure 3.24, this body

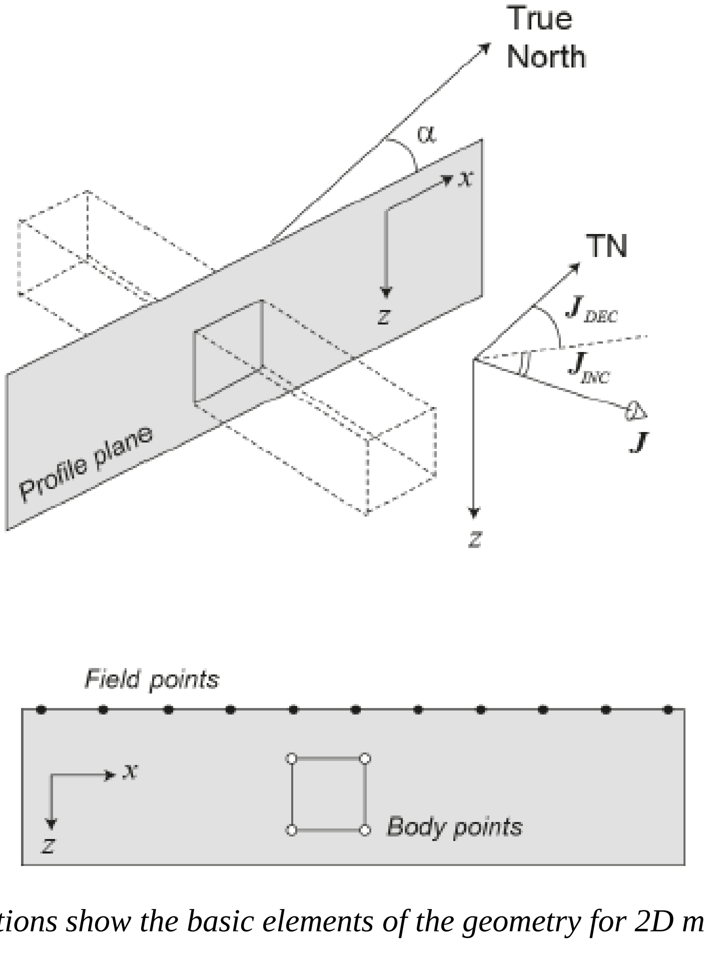

Figure 3.24. Illustrations show the basic elements of the geometry for 2D modelling (from Morris, 2020).

was described as upright rectangular. However, in the general case, the model may consist of one or multiple irregular prisms.

Only the components of the magnetization that lie within the profile plane generate an anomaly in this modelling approach (Figure 3.25). These components can be separated with trigonometry.

$$J_z = \mathrm{J}\sin(J_{INC}) \tag{3.8}$$

$$J_x = \mathrm{J}\cos(J_{INC})\cos(\alpha - J_{DEC}) \tag{3.9}$$

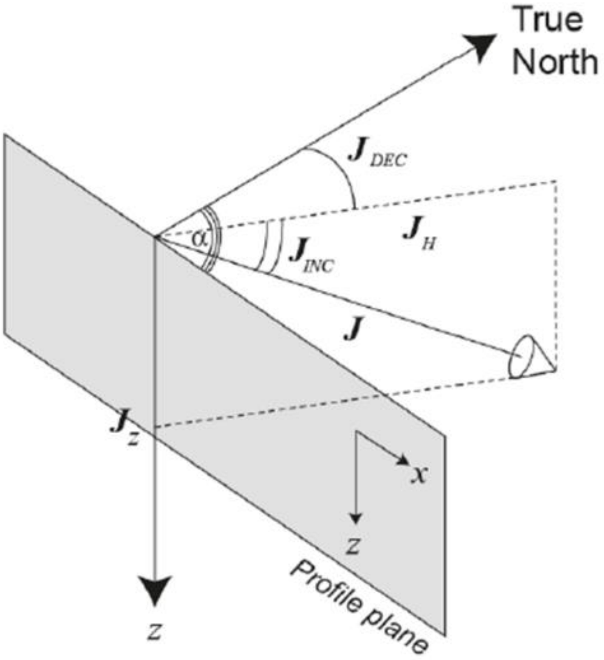

Figure 3.25. An illustration describes magnetization components on the profile plane (from Morris, 2020).

The Talwani (1965) method employs formulae for the magnetic anomaly over a two-dimensional slab with a sloping end (Figure 3.26). In this modelling framework, P defines a field point, the slope of the end of this slab is defined by an angle β (specified in radians), r_1 and r_2, represented by dash lines, are the distances between the field point P and the top and bottom body points of the sloping end of the body, and the angles between these lines and the horizontal axes are represented by Φ_1 and Φ_2 (specified in radians).

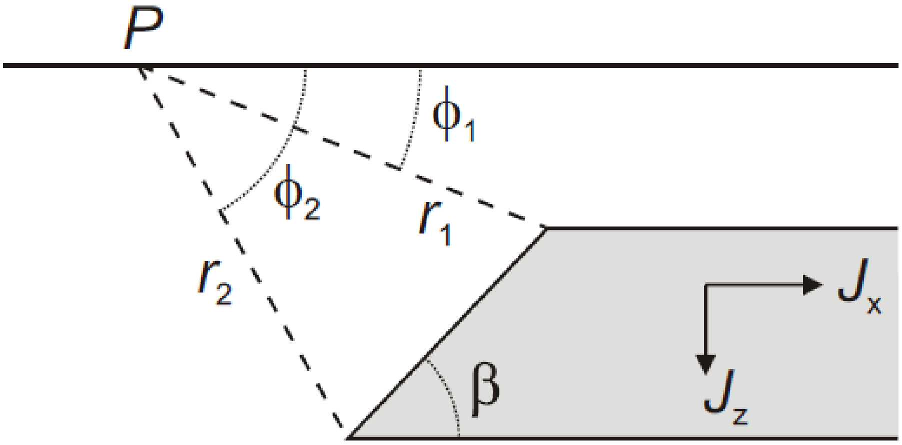

Figure 3.26. An illustration shows a 2D slab with a sloping end with parameters for 2D modelling (from Morris, 2020).

At point P, the vertical (ΔZ) and horizontal (ΔH) components of the anomaly can be calculated using the following formulae:

$$\Delta Z = \frac{\mu 0}{2\pi} sin\beta[-Jz\left\{sin\beta(\Phi 2 - \Phi 1) - cos\beta \ln\left(\frac{r2}{r1}\right)\right\}$$

$$+Jx\left\{cos\beta(\Phi 2 - \Phi 1) + sin\beta \ln\left(\frac{r2}{r1}\right)\right\}] \tag{3.10}$$

$$\Delta H' = \frac{\mu 0}{2\pi} sin\beta[Jz\left\{cos\beta(\Phi 2 - \Phi 1) + sin\beta \ln\left(\frac{r2}{r1}\right)\right\}$$

$$+Jx\left\{sin\beta(\Phi 2 - \Phi 1) - cos\beta \ln\left(\frac{r2}{r1}\right)\right\}] \tag{3.11}$$

where the magnetization components, J_x and J_z, are in Am^{-1}, and μ_0 is the magnetic permeability of free space (= $4\pi \times 10^{-7}$ N/A^2), yielding ΔZ and ΔH values in Tesla. These anomaly components are added to the local magnetic field at the survey site for modelling. Earth's magnetic field components, declination (EMF_{DEC}) and inclination (EMF_{INC}), are used for this process (3.12).

$$\Delta F = \Delta Z \sin(EMF_{INC}) + \Delta H \cos(EMF_{INC}) \cos(\alpha - EMF_{DEC}) \tag{3.12}$$

As seen above, these calculations are for a slab with a sloping end. For the modelling of any two-dimensional body shape, a polygonal prism with straight sides can be used to approximate the actual shape. This means that the irregular shape is designed as a polygonal prism with straight sides. This situation is explained in Figure 3.27.

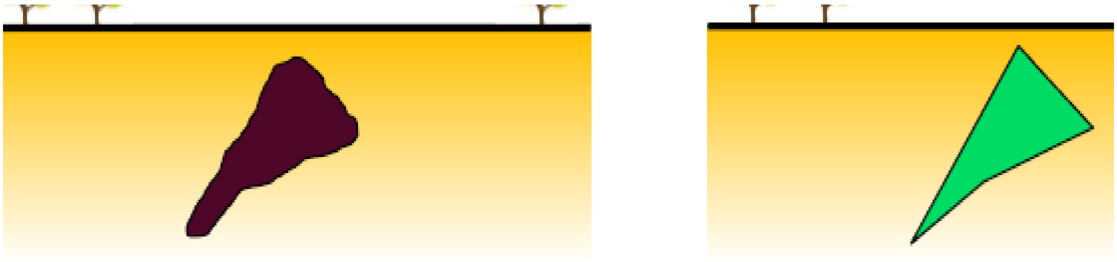

Figure 3.27. An irregular-shaped body in the subsurface is shown on the left side. The approach, using a multi-sided polygonal prism with straight sides, is shown on the right (from Morris, 2020).

With the help of this approach, the equations for the anomaly over a slab with a sloping end can be applied to calculate the anomaly due to an irregularly-shaped body (Figure 3.28).

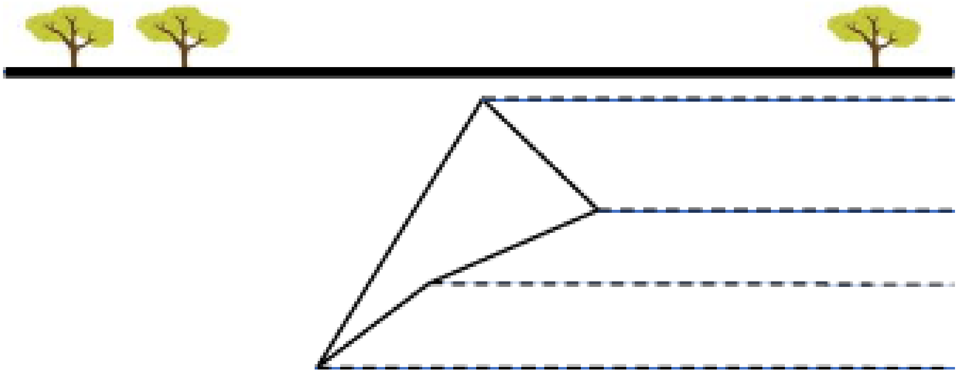

Figure 3.28. An illustration shows the sloping ends of the body using the polygonal prism approach (from Morris, 2020).

The anomaly of this prism body can be calculated by subtracting the anomalies arising from slabs connected to the sloping sides on the right of the prism from the anomalies arising from slabs connecting to those on its left side. This calculation is visualized in Figure 3.29.

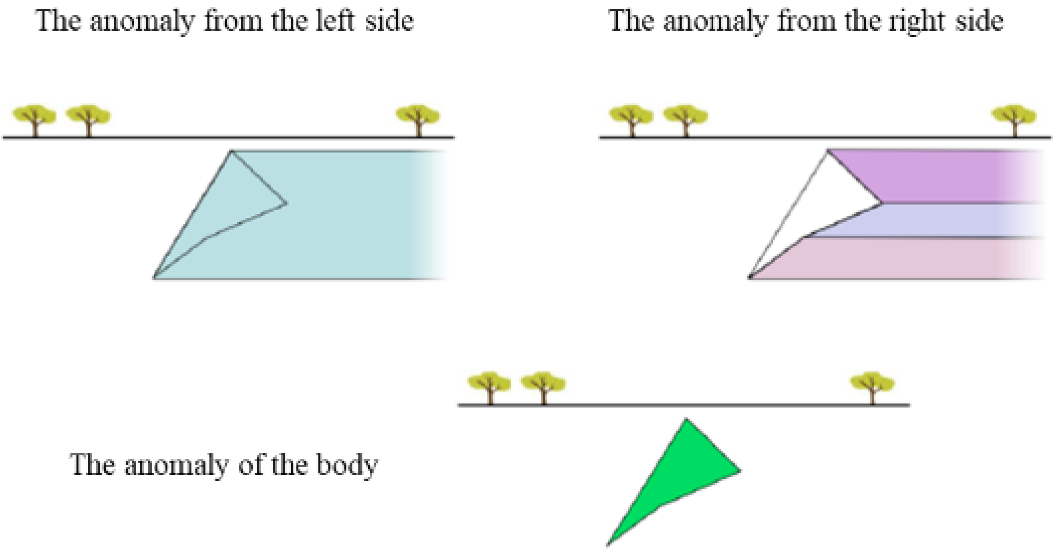

Figure 3.29. The anomaly due to the subsurface body (green) can be calculated by subtracting the anomalies from the left (blue) plate and the right (purple) plates (Modified from Morris, 2020).

Cooper (1997) created the program “Mag2dc” for implementing two-dimensional forward modelling based on this Talwani (1965) method. The program aims to compare the anomaly associated with an initial model with the observed data. The model

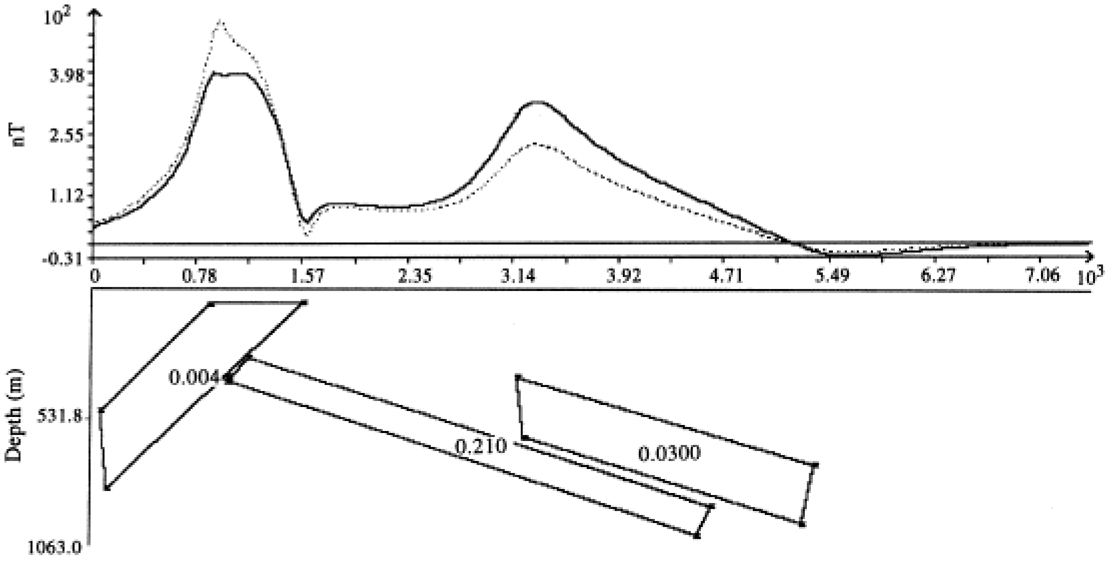

Figure 3.30. A result of two-dimensional modelling shows observed and calculated anomalies. The bold line represents the calculated anomaly while the observed one is shown by the dotted line. Each body's susceptibility value has written on it (from Cooper, 1997).

parameters are changed until the calculated and observed anomalies have a good match. A result of two-dimensional modelling can be seen in Figure 3.30.

A magnetic data file containing the dataset collected from the field should be read into this program. Then, the parameters of the study area should be introduced to the program, like the intensity, declination and inclination of remanence, and the geomagnetic field direction and initial body susceptibility. After these processes are completed, the estimated shape of the first body is introduced to the program. By changing the parameters of this body, the best match between the observed and the calculated anomaly is aimed to find. These processes are also applied to other bodies in the model as required.

In this study, the Knocklaugh Lodge profile data set was modelled using the Mag2dc program. Distances in metres and anomaly values in nanotesla were used for the input data set. For modelling, profile bearing, reference height, geomagnetic field parameters, and initial body susceptibility values were defined in the program. The results of the two-dimensional modelling will be discussed in Chapter Four.

4.6.2 Three-dimensional modelling

The theoretical background of three-dimensional modelling is more complicated than two-dimensional and is beyond the scope of this thesis. The UBC-Geophysical Inversion Facility developed algorithms for magnetic responses across a three-dimensional susceptibility distribution (UBC - Geophysical Inversion Facility, 2013) and incorporated these into a program called “Mag3d”, which is used here.

The information about this program and the three-dimensional modelling are summarized in the Mag3d program manual written by UBC-GIF. In this program, the study area is divided into three-dimensional prismatic cells and it is assumed that each cell has a constant sensitivity value. The program's algorithm works for each cell and creates a three-dimensional susceptibility model with anomaly maps. As an input document, the information about the study area (intensity, declination and inclination), easting and northing (in UTM), elevation values, and anomaly data set (nT) should be defined in the program. An example of the three-dimensional modelling can be seen in Figure 3.31.

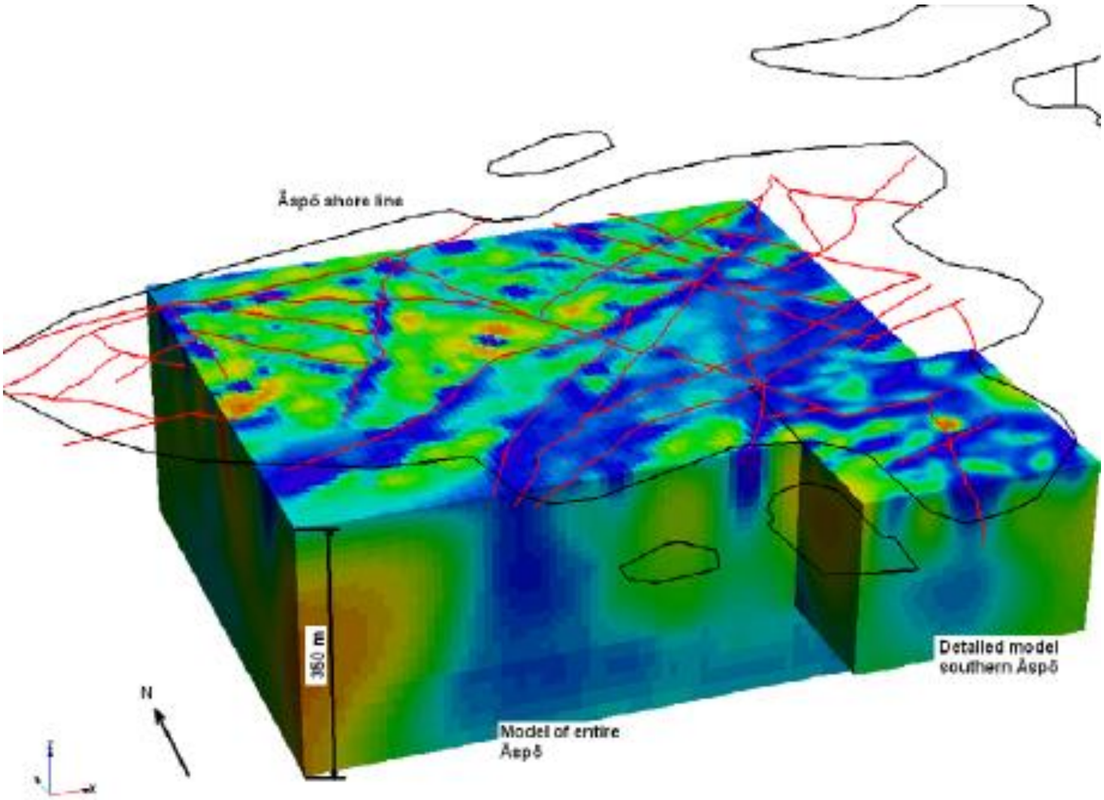

Figure 3.31. An example of three-dimensional modelling using Mag3d (from Mattsson, 2011).

In this study, the data sets from the Knocklaugh Lodge area, Coastal area and National Aeromagnetic Survey were modelled using the Mag3d program. For three-dimensional modelling, anomaly data sets were arranged to run in this program, and mesh grid documents were generated using the utility MeshTools3d. Mag3d program uses these two documents, the data set and mesh grid, to create dimensional modelling. The susceptibility range was defined in the program. The results of this modelling study will be discussed in Chapter Four.

Chapter 4 – Results

4.1 Contour maps of total magnetic field intensity data

The contour maps below were plotted using Surfer® software. The x-axis shows easting while the y-axis represents northing (UTM). The units of magnetic anomalies are nanoTesla (nT).

4.1.1. Knocklaugh Lodge survey area

Figure 4.1 shows the ground-level total magnetic field anomaly map derived from the Knocklaugh Lodge survey. This is the anomaly previously investigated by Stone et al. (1984) that is associated with a concealed serpentinite body confirmed by borehole drilling, but is defined here in much more detail than seen in the original aeromagnetic dataset used by Stone et al. (1984). The anomaly has a maximum peak-to-trough

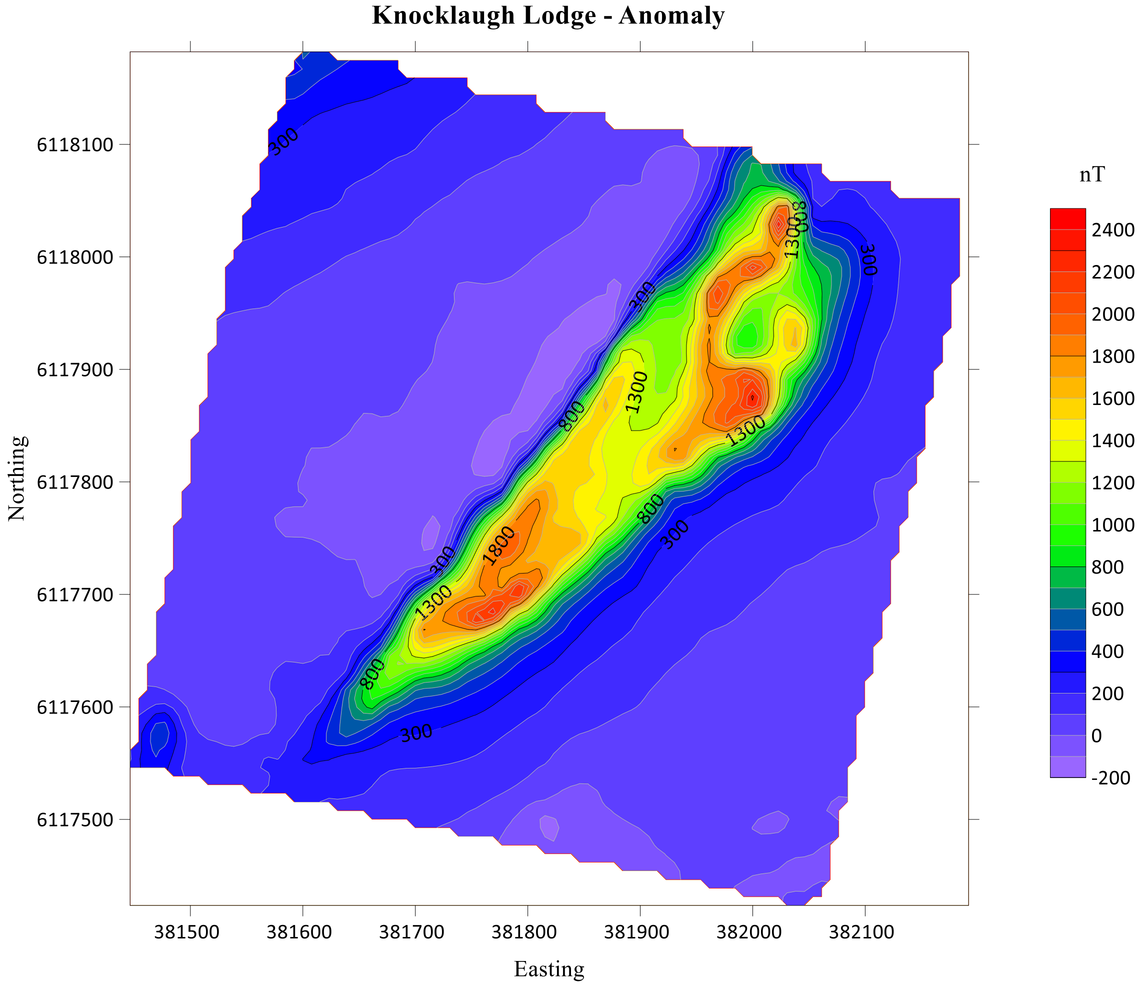

Figure 4.1. Total field magnetic anomaly map of the Knocklaugh Lodge survey area.

amplitude of ~ 2400 nT and is wedge-shaped in plan view, extending for ~610 m across the survey area from NE to SW, pinching out towards the SW. The anomaly has high magnetic gradients at its margins, which likely mark the edges of the causative serpentinite body beneath the surficial cover of boulder clay. The density of field points across the survey area (see Figure 3.6) allows details of the nature of the anomaly to be seen with confidence for the first time. Variations in peak amplitude of the anomaly within the region defined by the high field gradients at its margins are likely to originate from shallow sources (see Section 4.2 below), and probably reflect variations in the depth of superficial sediments over the proven serpentinite body that underlies the main anomaly.

4.1.2. Coastal Area survey

The ground-level total magnetic field anomaly map of the Coastal Area survey is shown in Figure 4.2, along with an inset map of the field point locations that highlights an area in the middle of the survey area where data could not be collected due to metal fences. No single anomaly can be identified in this survey area, but the anomalous field varies from -400 nT to +1400 nT. The data display a strong magnetic field gradient across the surveyed area with lowest values to the N and highest values to the S, and a more complex pattern of more local variations is superimposed on this trend. These higher spatial frequency variations are again likely to result from shallow subsurface sources, with the underlying gradient due to deeper regional sources (see Section 4.2 below).

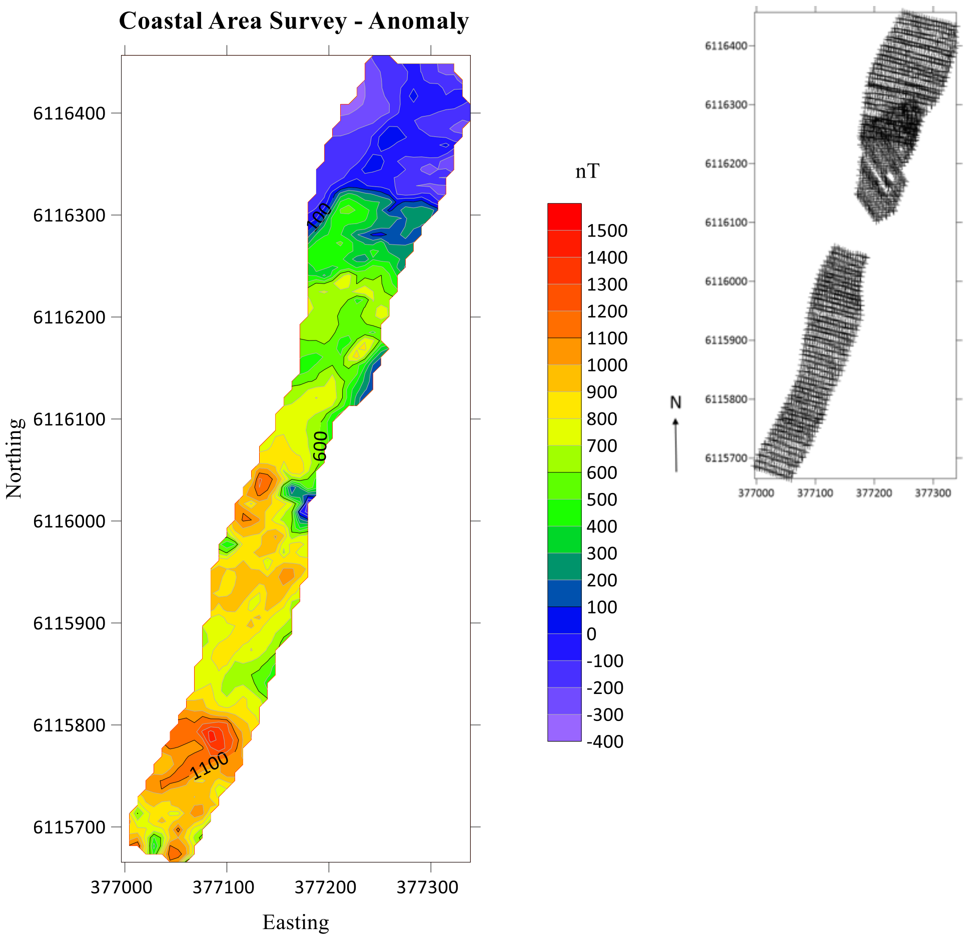

Figure 4.2. Total field magnetic anomaly map of the Coastal Area (with an inset map of field points to show the location of a small area with no data coverage).

4.1.3. Data from the UK National Aeromagnetic Survey

Figure 4.3 presents an aeromagnetic anomaly map produced using data extracted from the UK National Aeromagnetic Survey (Institute of Geological Sciences, 1972, 1980) to show the area of the current study. These data were acquired at a mean elevation of 305 m, and therefore are likely to emphasis only deep magnetic sources. This map shows two main areas of high positive magnetic anomalies. The anomaly extending to the NE away from the SW corner of the map is associated with the outcrop of the Northern and Southern Serpentinite Belts of the Ballantrae Complex. This can be divided into two parts: a large anomaly with a maximum peak of +600 nT that overlies the outcrop of the Northern Serpentinite Belt (note that the ground-level magnetic anomaly described above at Knocklaugh Lodge is indistinguishable from this anomaly due to the attenuating effect of observing at elevation during the aeromagnetic survey); and a lower amplitude anomaly with a peak intensity of +450nT over the Southern Serpentinite Belt. The second main anomaly extends northeastwards from the centre of the map and overlies the outcrop of the Tappins Group, which contains the highly magnetic Traboyack Formation (see Section 1.3.2). This has a maximum peak of +500 nT towards its SW end and subsidiary peaks of +250 nT and +150 nT at its centre and NE end respectively.

All three anomaly maps are discussed again in Chapter 5.

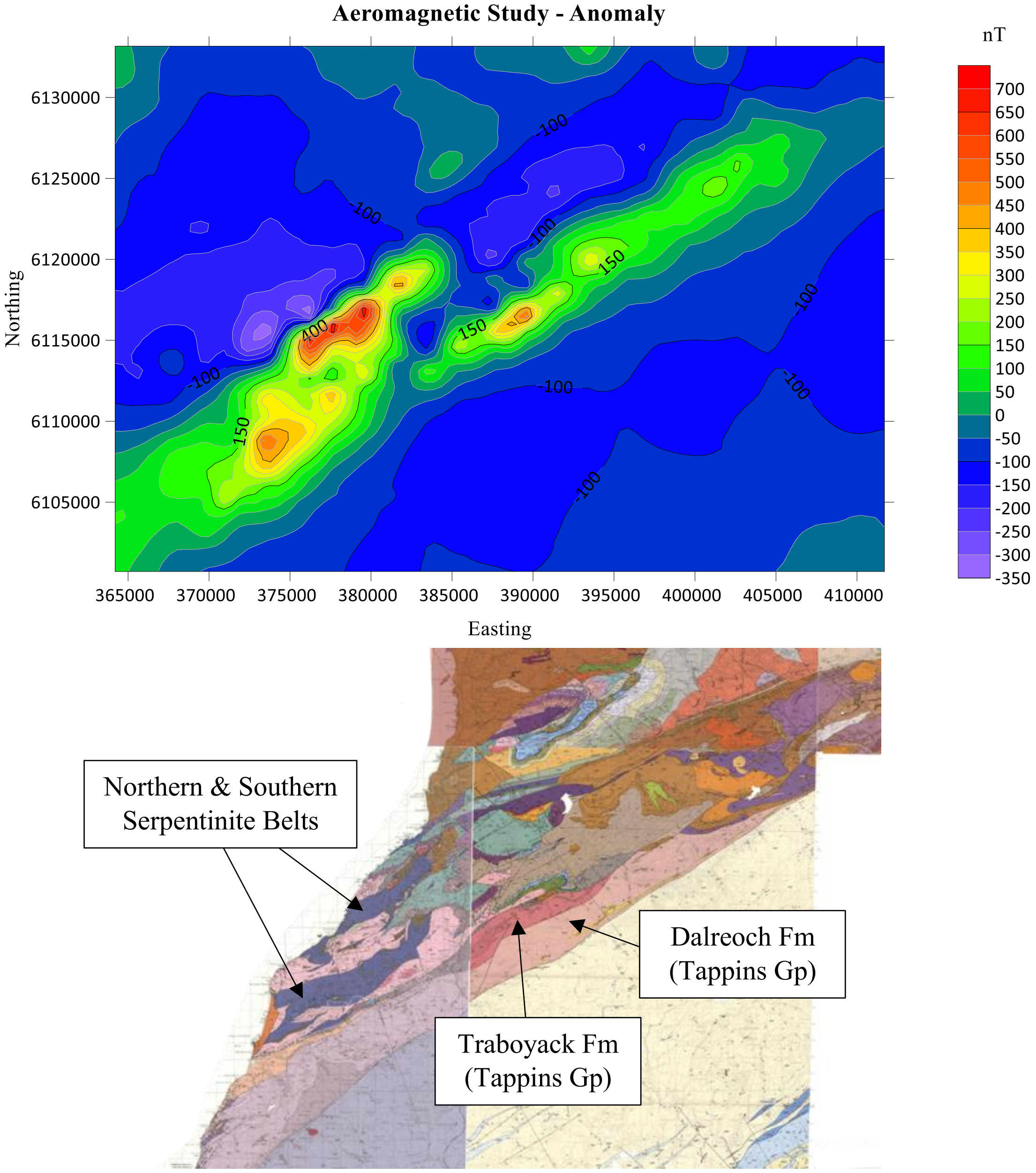

Figure 4.3. Top: Total field magnetic anomaly map using a subset of data drawn from the UK National Aeromagnetic Survey (Institute of Geological Sciences, 1972, 1980); Bottom: compilation of BGS geological maps covering the same area.

4.2 Contour maps of magnetic gradiometer data

Contour maps of the magnetic gradiometer data were plotted to infer the possible boundaries of the subsurface serpentinite body for the two-dimensional modelling of the Knocklaugh Lodge ground-level magnetic profile and to give insights into the pattern of near-surface sources for the grid surveys of Knocklaugh Lodge and the Coastal Area.

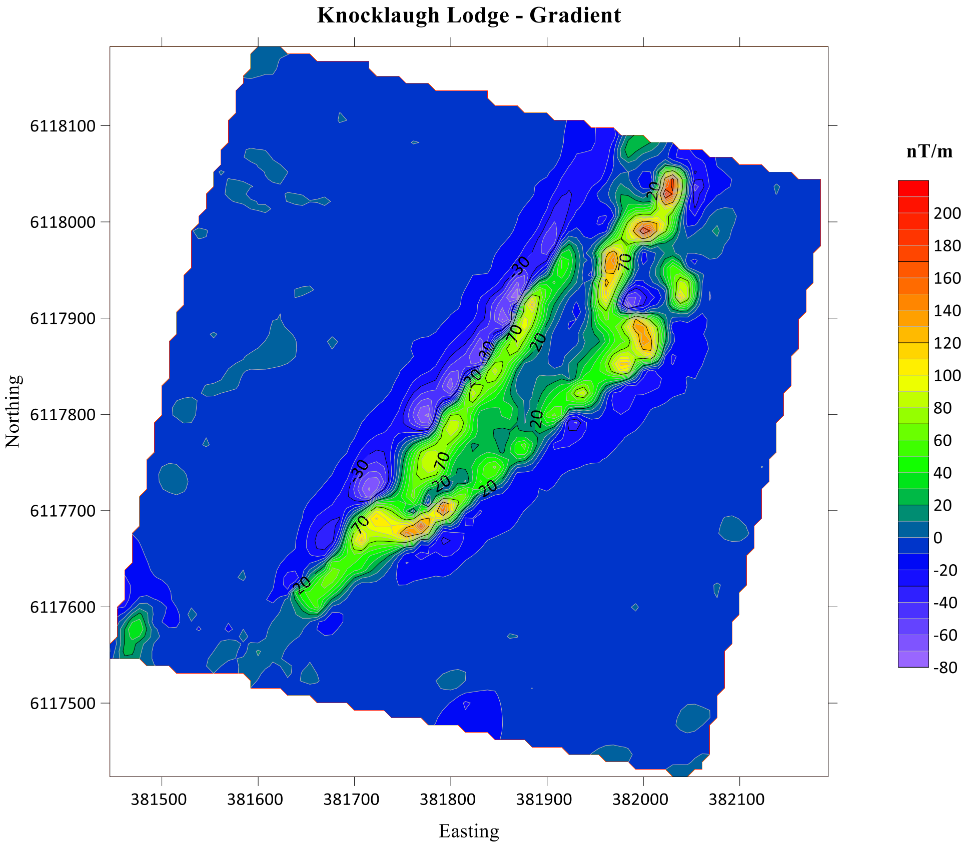

Figure 4.4. Magnetic gradient map for the Knocklaugh Lodge area.

4.2.1. Knocklaugh Lodge survey area

Figure 4.4 shows the gradiometer contour map for the Knocklaugh Lodge area. This shows high gradients along the margins of the main anomaly described above which are likely to directly overlie the edges of the buried serpentinite body in the subsurface. This information was used to delineate the location of the margins of the body used to explain this anomaly in the 2D modelling of the profile extending from Knocklaugh Lodge to the coast (over the Northern Serpentinite Belt). Peaks in magnetic gradient along the SE margin of the anomaly and its NE termination are likely to reflect variations in the depth of glacial overburden and may represent areas where the highly magnetic serpentinite comes closer to the surface, noting that small changes in the depth of such sources when close to the surface can produce significant changes in anomaly amplitude and gradients.

4.2.2. Coastal Area survey

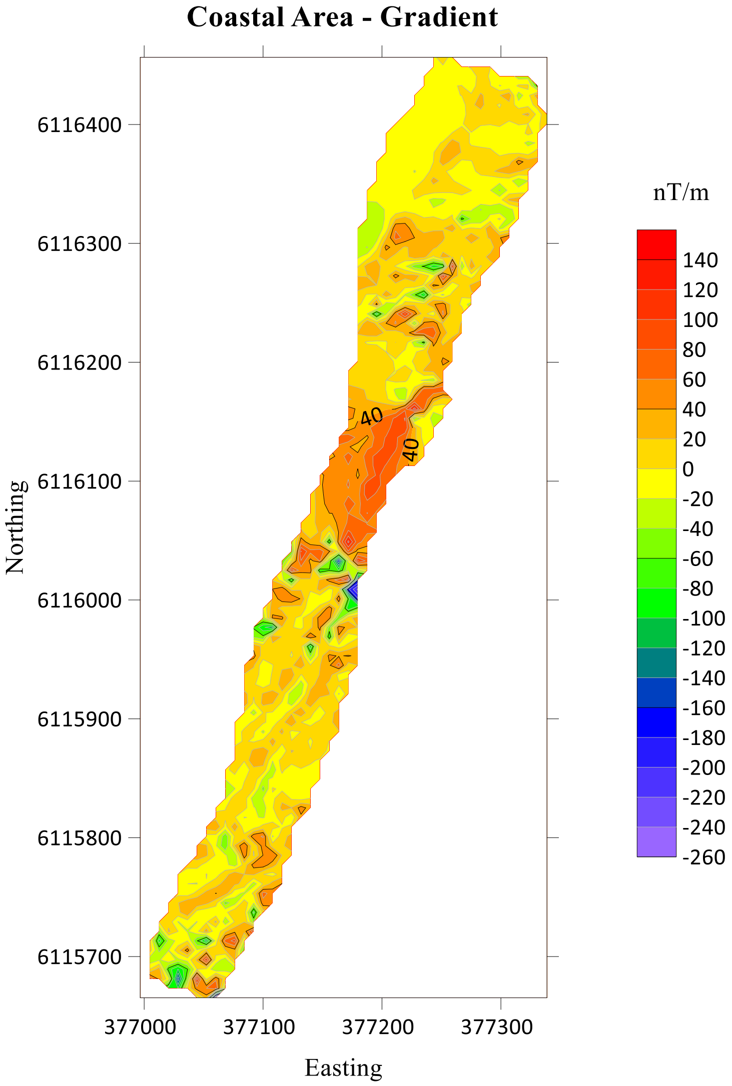

Figure 4.5. Magnetic gradient map of the Coastal Area.

Figure 4.5 shows the gradiometer contour map for the Coastal Area. The high magnetic gradients in the central area of this map correspond to the area where no data was collected (compare with the inset map of Figure 4.2) and are purely artefacts of the contouring process. Elsewhere, the gradiometer data appear to delineate a series of NE-SW-trending features that are likely to be of near-surface origin. The trend of these features is similar to that of the exposures of dolerite sheets intruded into the Northern Serpentinite Belt that are seen on the BGS geological map of the area. The subsurface form of these bodies is impossible to model using the total field data as individual anomalies cannot be isolated, but they probably reflect the paleotopography of the contact between the bedrock and raised marine terrace deposits (plus surficial sediments/soils) (see Chapter 5 for more discussion of this hypothesis).

4.3 Ground-level total magnetic field anomaly profile across the Knocklaugh Lodge and Northern Serpentinite Belt anomalies

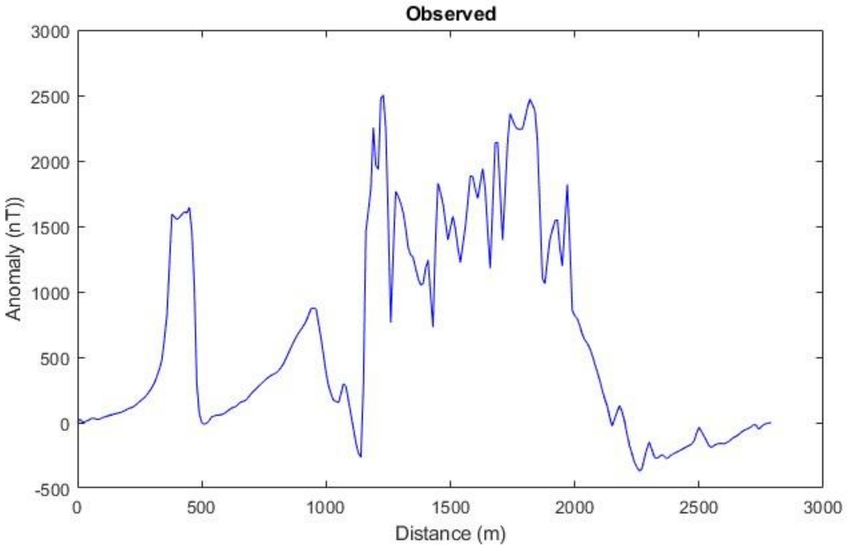

Figure 4.6. The ground-level total field magnetic anomaly profile between Knocklaugh Lodge and NW side of the Northern Serpentinite Belt.

The location of this profile and its relation to the grid survey at Knocklaugh Lodge is shown in Figure 3.5. It extends SE-NW for approximately 2.8 km from UTM grid reference 30U 382043E, 6117416N to 30U 380593E, 6119795N. The anomaly profile (Figure 4.6) can be divided into four main parts: (i) a discrete anomaly of 1600 nT amplitude centred at ~400 m along the profile which is the anomaly associated with the buried serpentinite body at Knocklaugh Lodge; (ii) a lower amplitude (~800 nT) anomaly with its peak at ~950 m along the profile which occurs over ground with no exposed rocks that is mapped as sedimentary bedrock by the BGS; (iii) a complex zone of high amplitude anomalies from ~1100 – 2000 m along the profile that corresponds to the mapped extent of the Northern Serpentinite Belt. This zone is marked by high spatial frequency variations in field intensity with peak-to-trough amplitudes of ~100 nT. These suggest the presence of zones within the Northern Serpentinite Belt with variable susceptibilities and/or remanence intensities, or spatial variations in the proximity of the highly magnetic serpentinites to the surface; and (iv) a zone at the NW end of the profile of very low (essentially zero) magnetic anomalies associated with mapped outrcops of sedimentary rocks.

4.4 The results of upward continuation

The background of upward continuation was explained in Chapter Three. The data sets were divided into two main parts, a profile data set and grid data sets.

4.4.1. Upward continuation of the profile across the Knocklaugh Lodge and Northern Serpentinite Belt anomalies

GeoSimplex's Upward Continuation Excel sheet (GeoSimplex, 2015) was used to upward continue this profile data set in 50 m steps from 50 m to 300 m and results were displayed using MATLAB® software. Figure 4.7 show the results this process, where blue lines represent the observed ground-level profile and red lines shows the upward continued profile.

As seen in these graphs, as the upward continuation level increases, the profile becomes smoother. This is because the short wavelength components originating from shallow sources are supressed by the upward continuation, enhancing the anomalies due to deeper geological sources. The profile resulting from upward continuation to 100 m elevation was selected for 2D modelling. In this result, the deep source anomalies can be observed clearly while the effect of the short wavelength, residual anomalies is suppressed. It gives information from deep sources without the shallow bodies' effect, and represents the best compromise in terms of retaining the trough in anomaly amplitudes seen in the anomaly over the Northern Serpentinite Belt that likely reflects a significant variation in subsurface bulk magnetic properties.

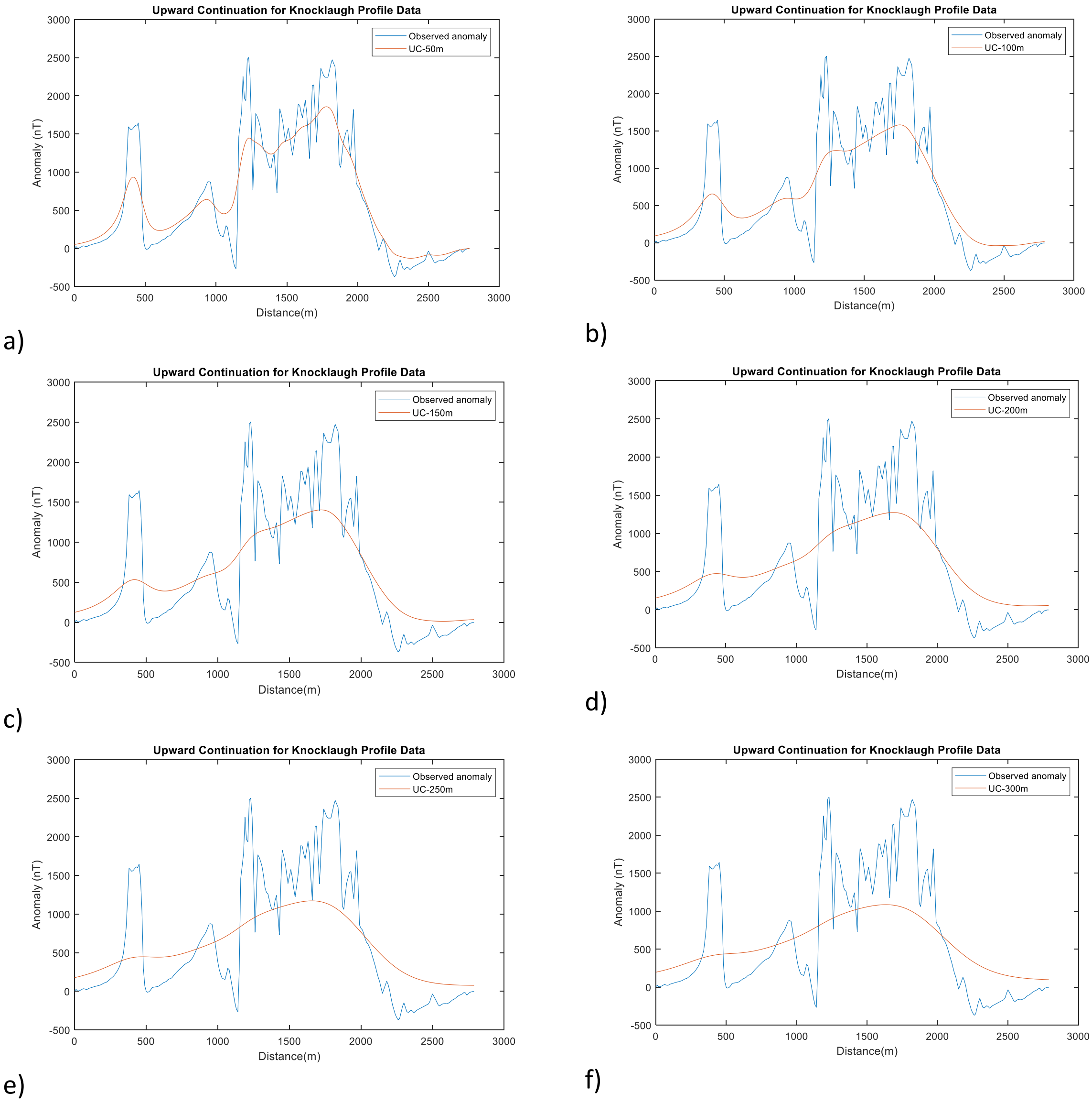

Figure 4.7. Upward continuation of the ground-level magnetic anomaly profile to an elevations of (a)50 m, (b)100 m, (c)150 m, (d) 200 m, (e) 250 m and (f) 300 m. SE is to the left, NW to the right.

4.4.2. Upward continuation of the Knocklaugh Lodge survey dataset

Magpick software was used for upward continuation of the grid data sets from the Knocklaugh Lodge and the Coastal Area surveys to emphasise the deeper sources of the anomalies. This software allows calculation of upward continued data but also calculates the residual anomalies resulting from subtracting the upward continued data from the ground-level data, hence allowing assessment of both deep and shallow anomaly sources. Upward continuation was again applied to different elevations and Surfer® software was used to demonstrate the results.

The original anomaly for the Knocklaugh Lodge survey can be seen in Figure 4.8, while. Figures 4.9 – 4.12 shows the anomaly after upward continuation to various elevations from 5 to 250 m. The maps at the left side show the results while the maps at the right side represent the residual values removed from the original anomaly. Eastings and northings are on the x- and y-axes, respectively (UTM), with anomalies shown in nT.

The dataset upward continued to 100 metres was again selected for modelling (Figure 4.11), for consistency with the associated profile data.

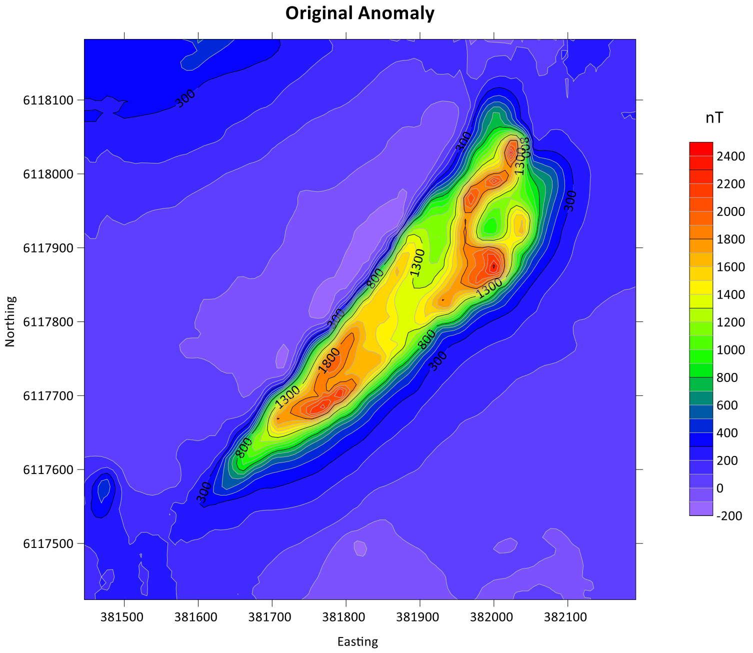

Figure 4.8. The ground-level total field magnetic anomaly map for Knocklaugh Lodge.

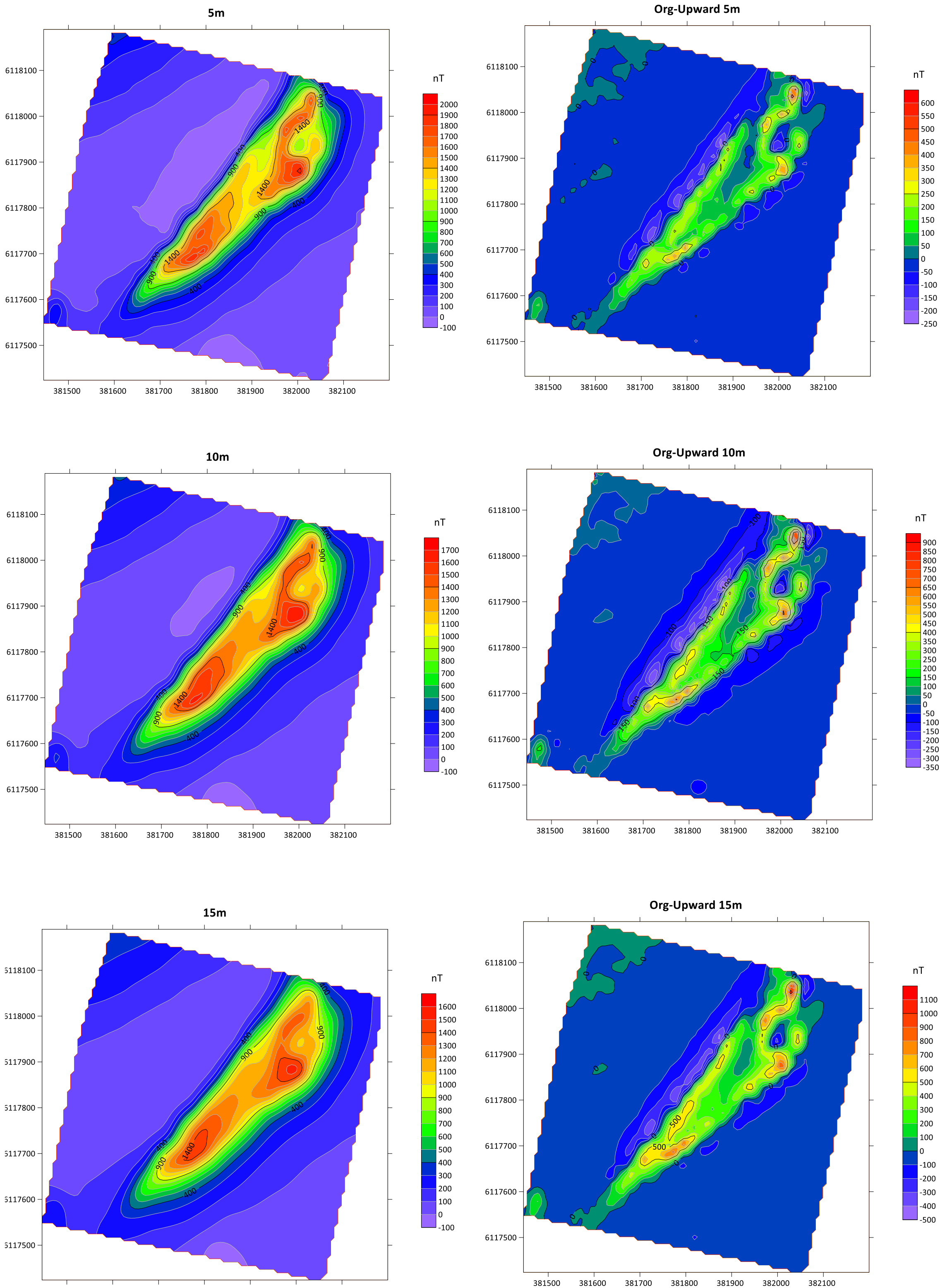

Figure 4.9. Upward continuation for the Knocklaugh Lodge survey data. Maps on the left show upward continuation to 5, 10 and 15 metres. The maps at the right represent the residual anomaly values after removal of the upward continued data from the original ground-level data.

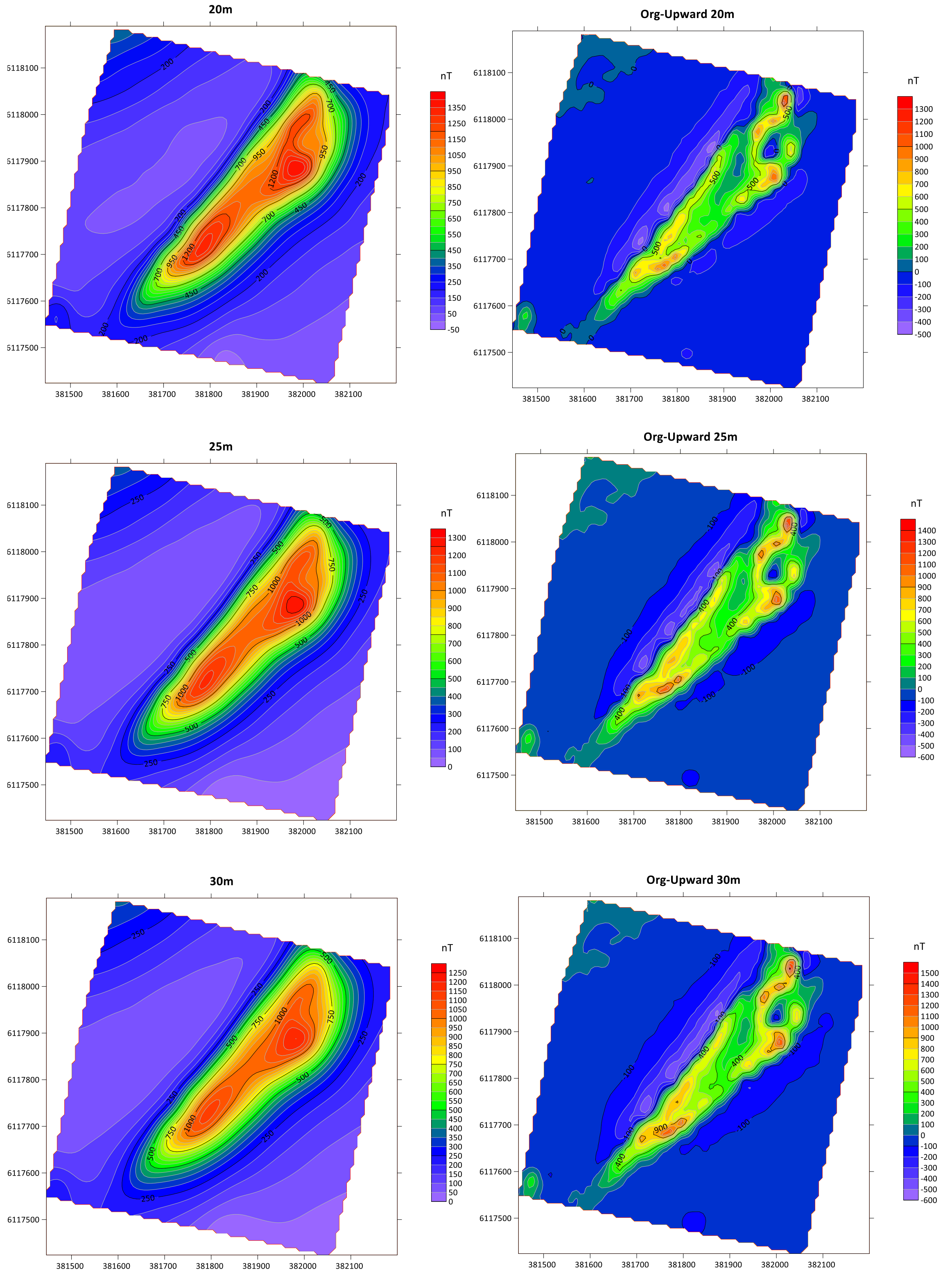

Figure 4.10. Upward continuation for the Knocklaugh Lodge survey data. Maps on the left show upward continuation to 20, 25 and 30 metres. The maps at the right represent the residual anomaly values after removal of the upward continued data from the original ground-level data.

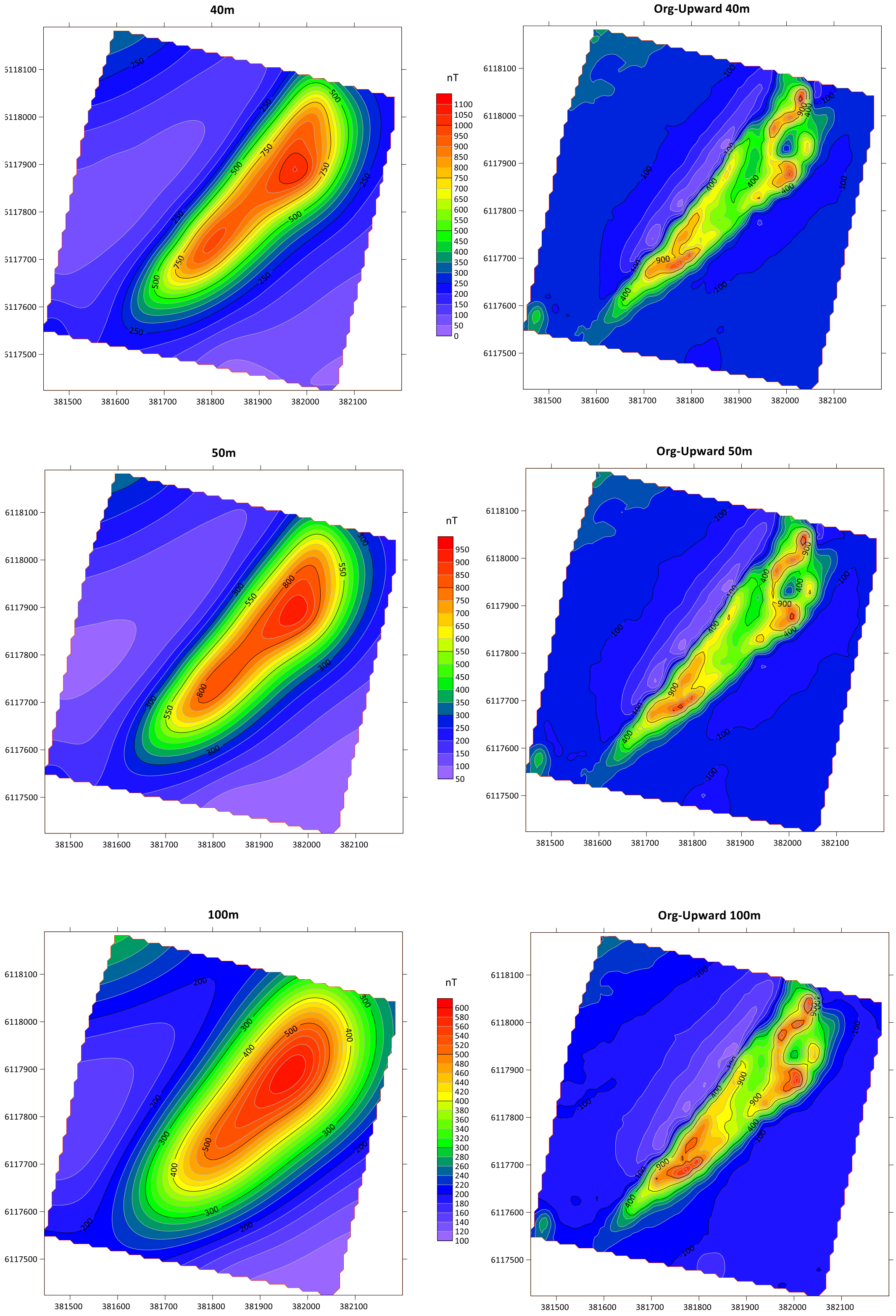

Figure 4.11. Upward continuation for the Knocklaugh Lodge survey data. Maps on the left show upward continuation to 40, 50 and 100 metres. The maps at the right represent the residual anomaly values after removal of the upward continued data from the original ground-level data.

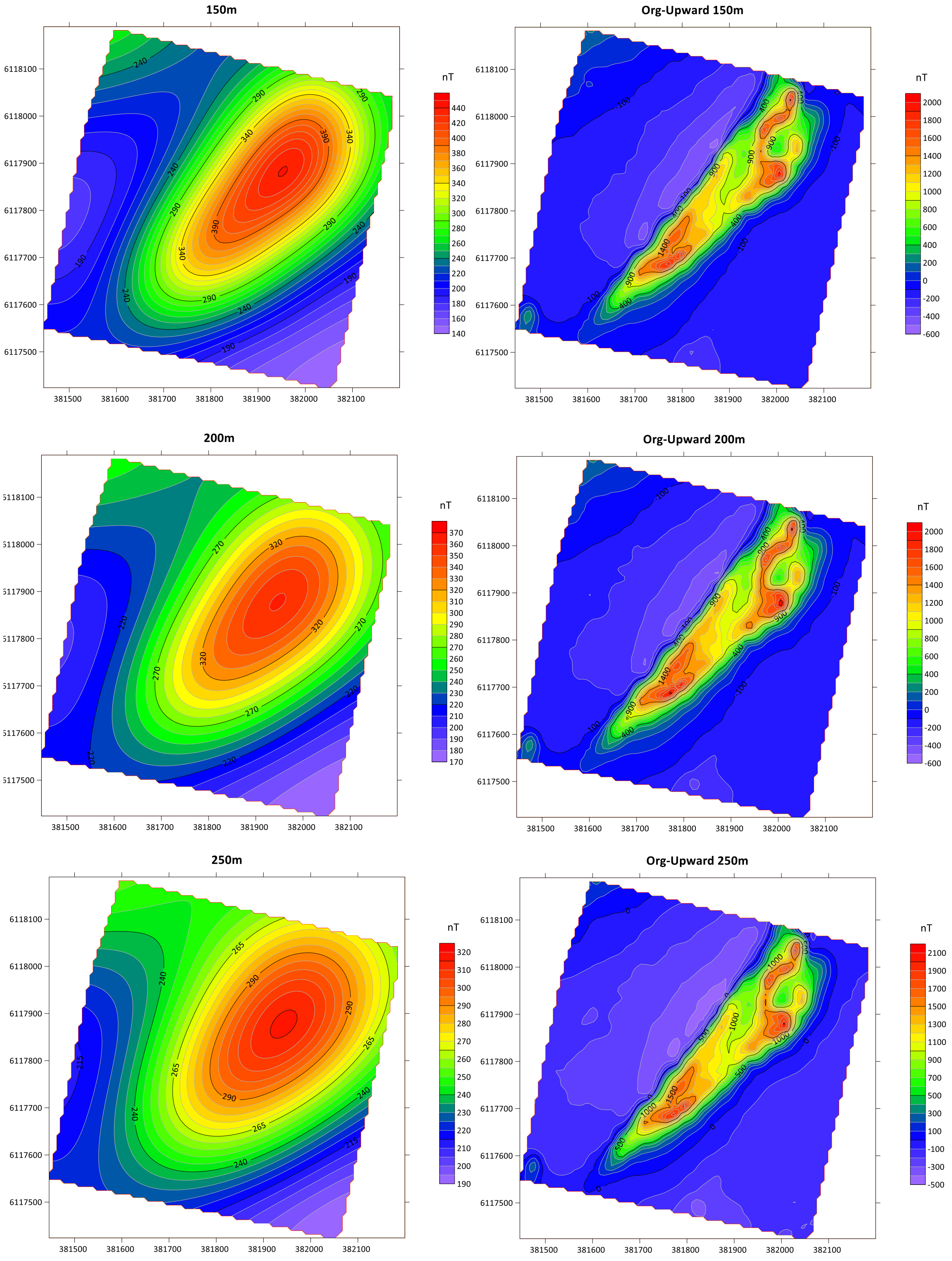

150m

Org-Upward 150m

200m

Org-Upward 200m

250m

Org-Upward 250m

Figure 4.12. Upward continuation for the Knocklaugh Lodge survey data. Maps on the left show upward continuation to 150, 200 and 250 metres. The maps at the right represent the residual anomaly values after removal of the upward continued data from the original ground-level data.

4.4.3. Upward continuation of the Coastal Area survey dataset

The original anomaly for the Coastal Area can be seen in Figure 4.13 along with the results of upward continuation to 5 m. The results for other elevations are shown in Figures 4.14 – 4.19. The results obtained by upward continuation to elevations of 100 m and above reveal that the deep source anomaly is a regional gradient increasing to the south. Such regional gradients cannot be modelled magnetically and are usually removed from datasets prior to any attempt at interpretation. In this case, the de-trended data are provided by the residual anomaly maps for elevations above 100 m, but these are dominated by near-surface sources with no clear isolated anomalies that can be modelled quantitatively. However, qualitative interpretation of these residual anomalies is attempted in Chapter 5 in terms of the geological and geomorphological setting of the Coastal Area as a raised marine terrace.

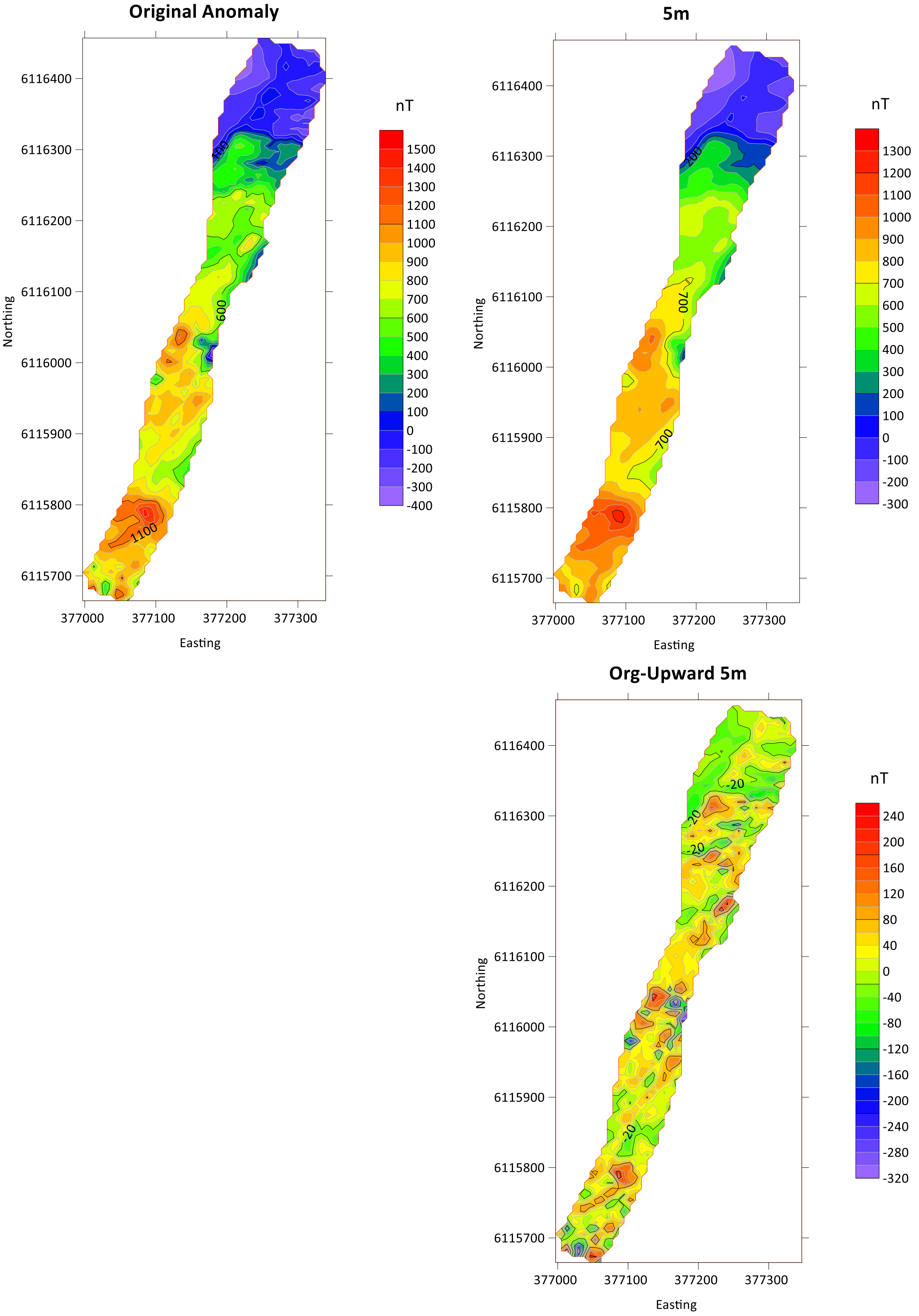

Figure 4.13. Top left: Original ground-level anomaly map for the Coastal Area. Top right: The result of upward continuation to 5 metres. Bottom right: residual anomaly values after removal of the upward continued data from the original ground-level data.

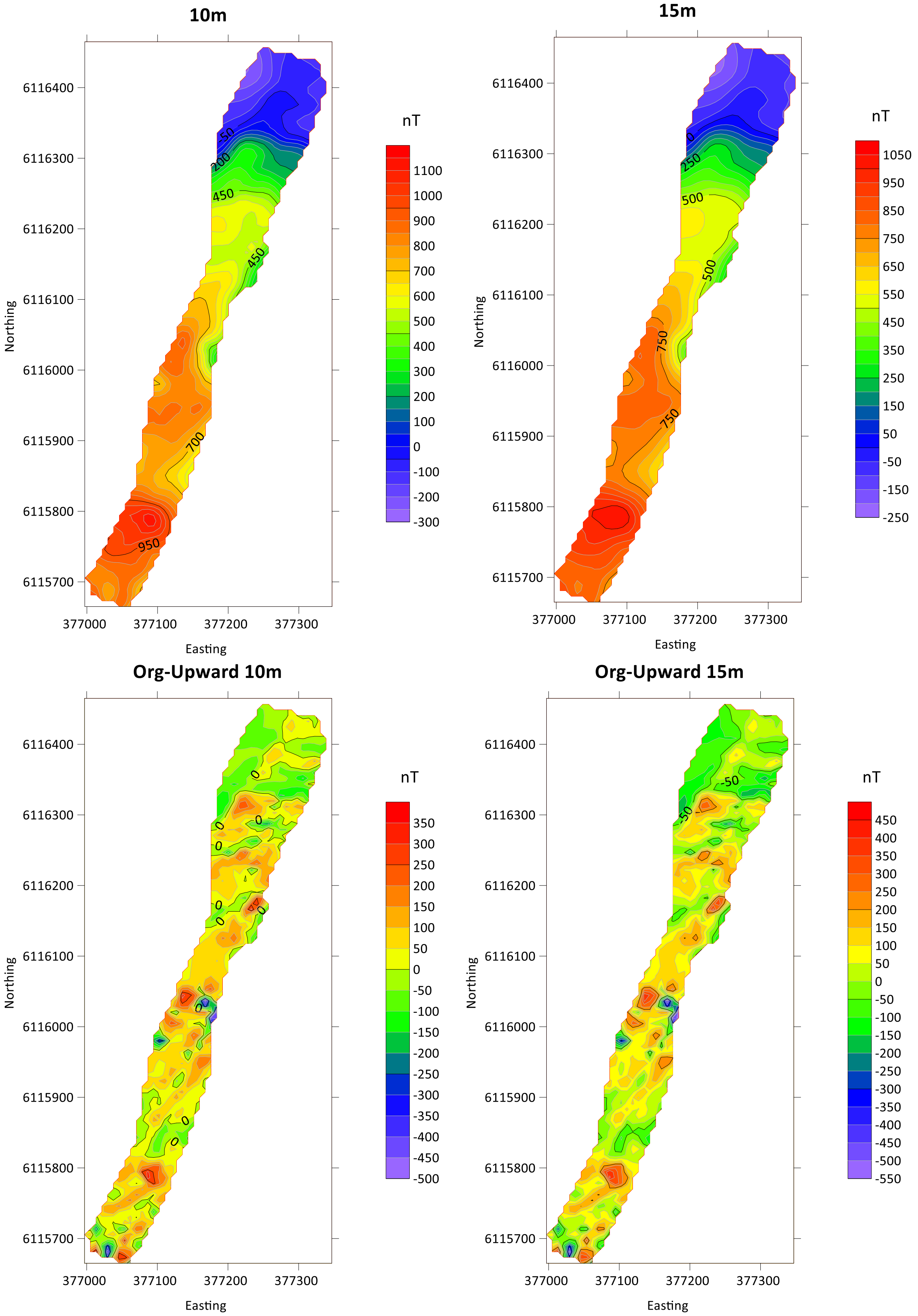

Figure 4.14. Upward continuation of the Coastal Area data to elevations of 10 m and 15 m. Left: upward continued data; Right: residual anomaly values after removal of the upward continued data from the original ground-level data.

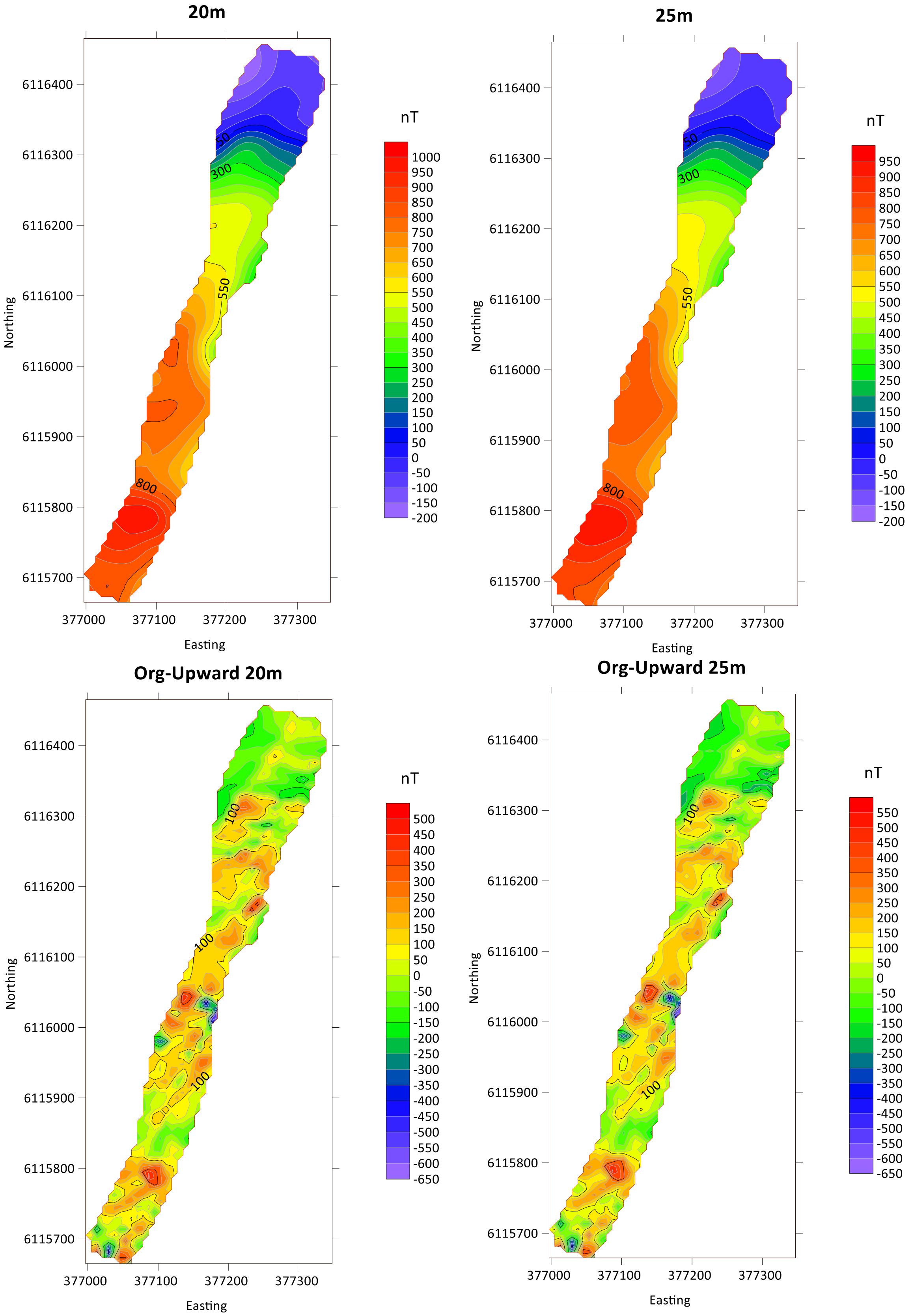

Figure 4.15. Upward continuation of the Coastal Area data to elevations of 20 m and 25 m. Left: upward continued data; Right: residual anomaly values after removal of the upward continued data from the original ground-level data.

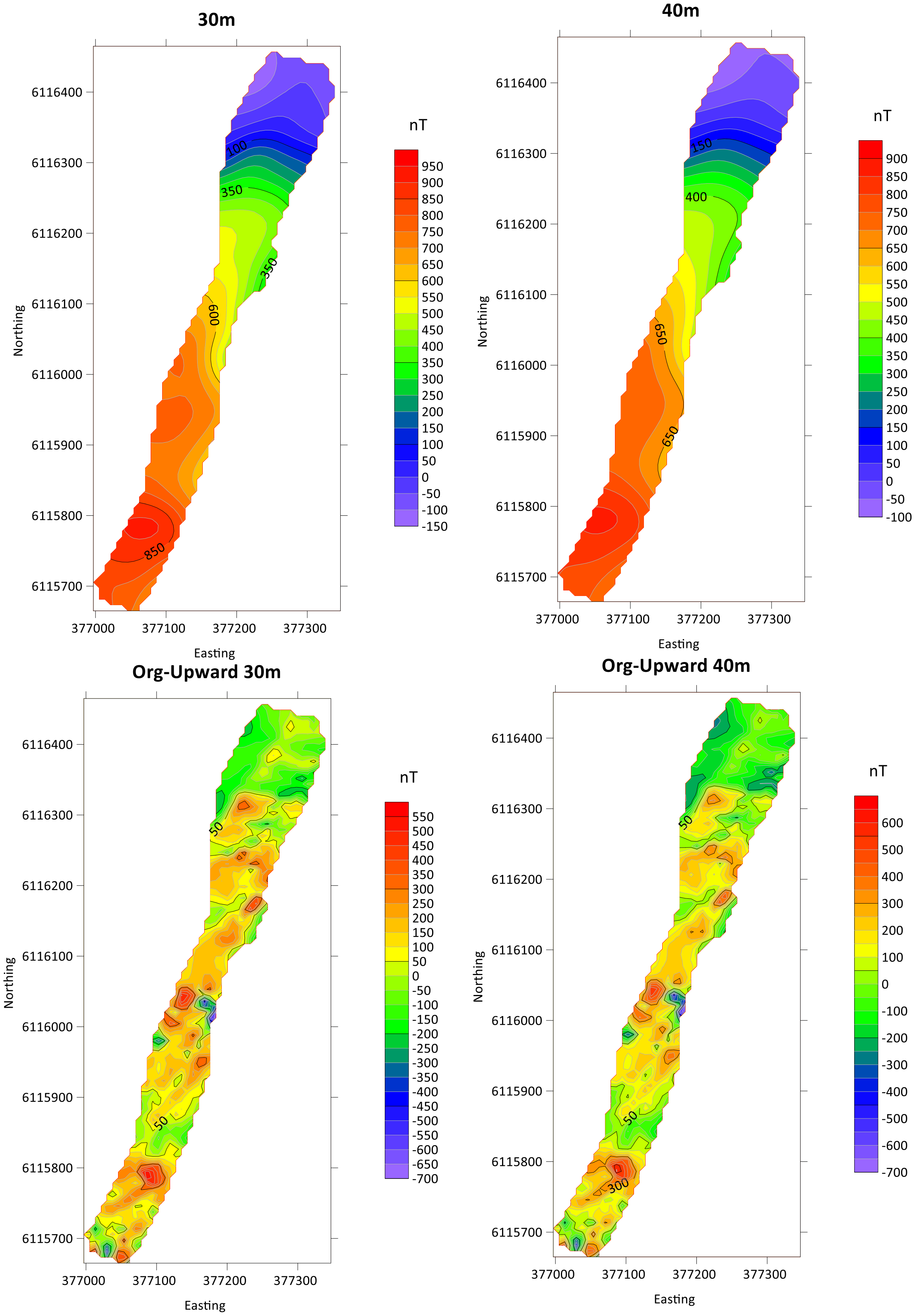

Figure 4.16. Upward continuation of the Coastal Area data to elevations of 30 m and 40 m. Left: upward continued data; Right: residual anomaly values after removal of the upward continued data from the original ground-level data.

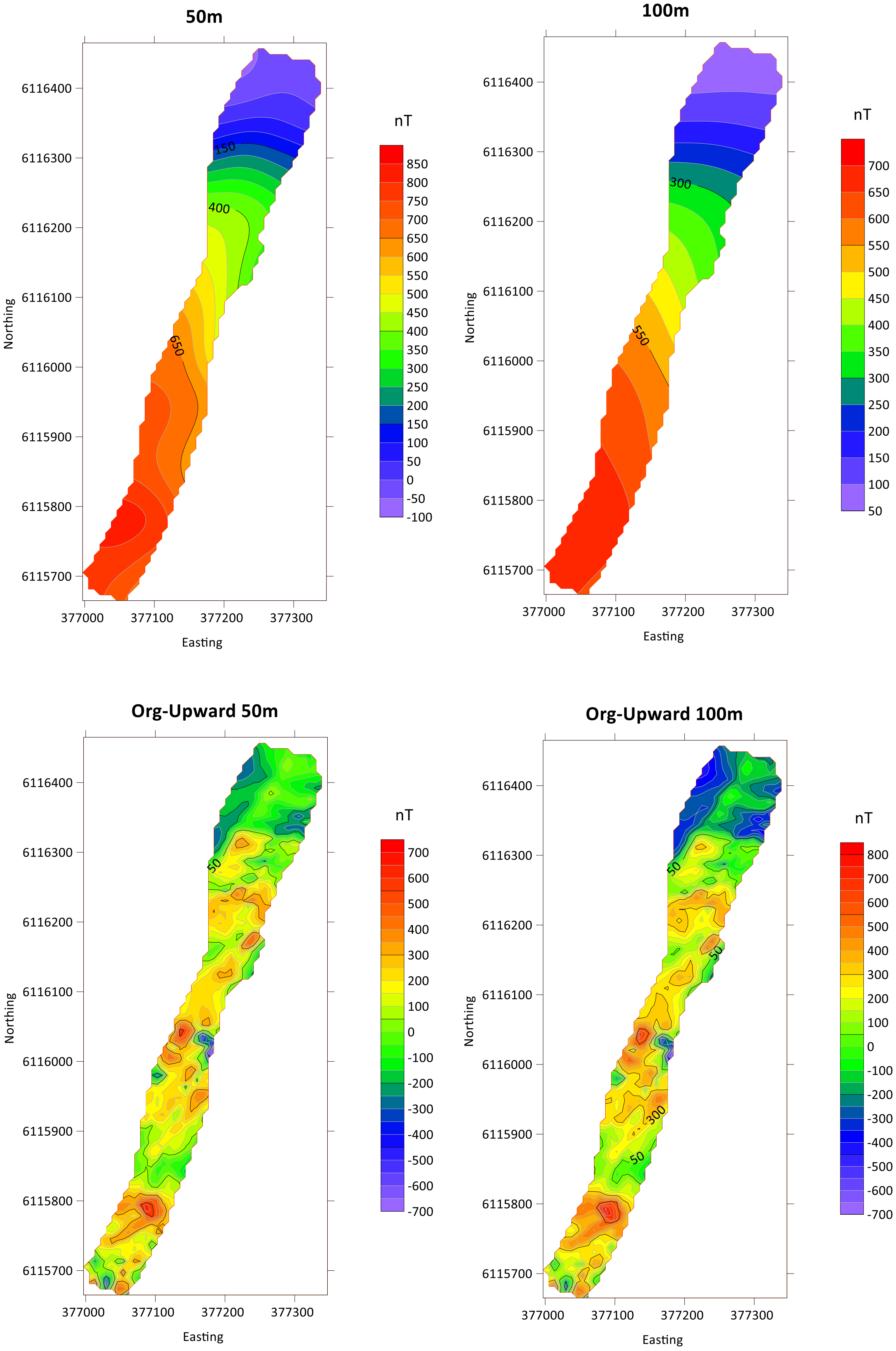

Figure 4.17. Upward continuation of the Coastal Area data to elevations of 50 m and 100 m. Left: upward continued data; Right: residual anomaly values after removal of the upward continued data from the original ground-level data.

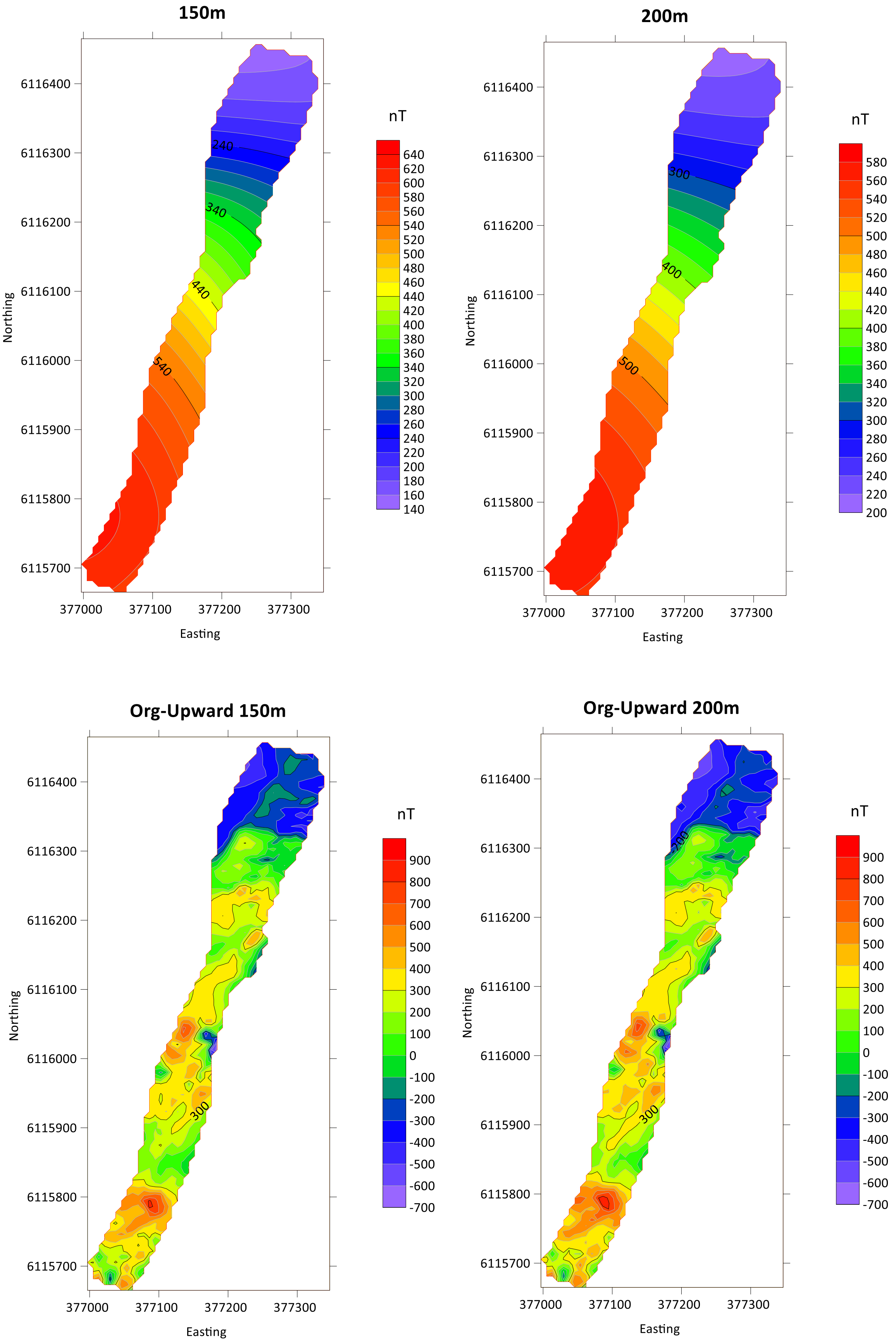

Figure 4.18.Upward continuation of the Coastal Area data to elevations of 150 m and 200 m. Left: upward continued data; Right: residual anomaly values after removal of the upward continued data from the original ground-level data.

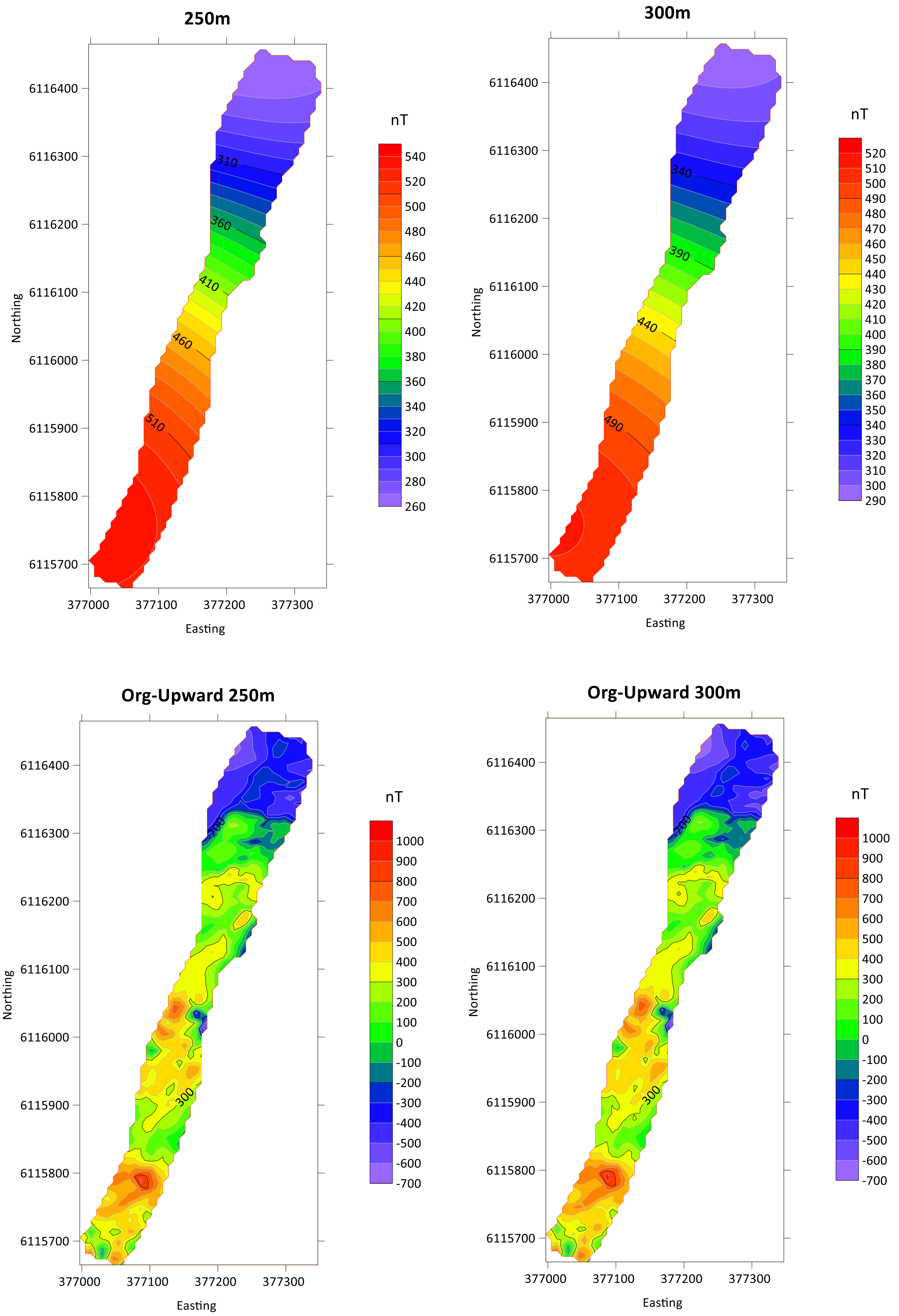

Figure 4.19. Upward continuation of the Coastal Area data to elevations of 250 m and 300 m. Left: upward continued data; Right: residual anomaly values after removal of the upward continued data from the original ground-level data.

4.5 Bulk magnetic properties of rocks in the study area

4.5.1 Low field magnetic susceptibilities

The histograms of Figures 4.20 and 4.21 show the variation of susceptibility (k, in SI units) according to rock type. The locations where the susceptibility values were collected can be seen in Figure 3.2. X-axes show $\log_{10}$ values of susceptibility, y-axes represent the frequency.

It can be seen that the serpentinites have the highest susceptibilities of any of the rocks analysed within the Ballantrae Complex, with a mean susceptibility of 4 x 10^{-2} SI (and a range of 2 x 10^{-2} to 6 x 10^{-2} SI. These values are slightly lower than the mean susceptibility

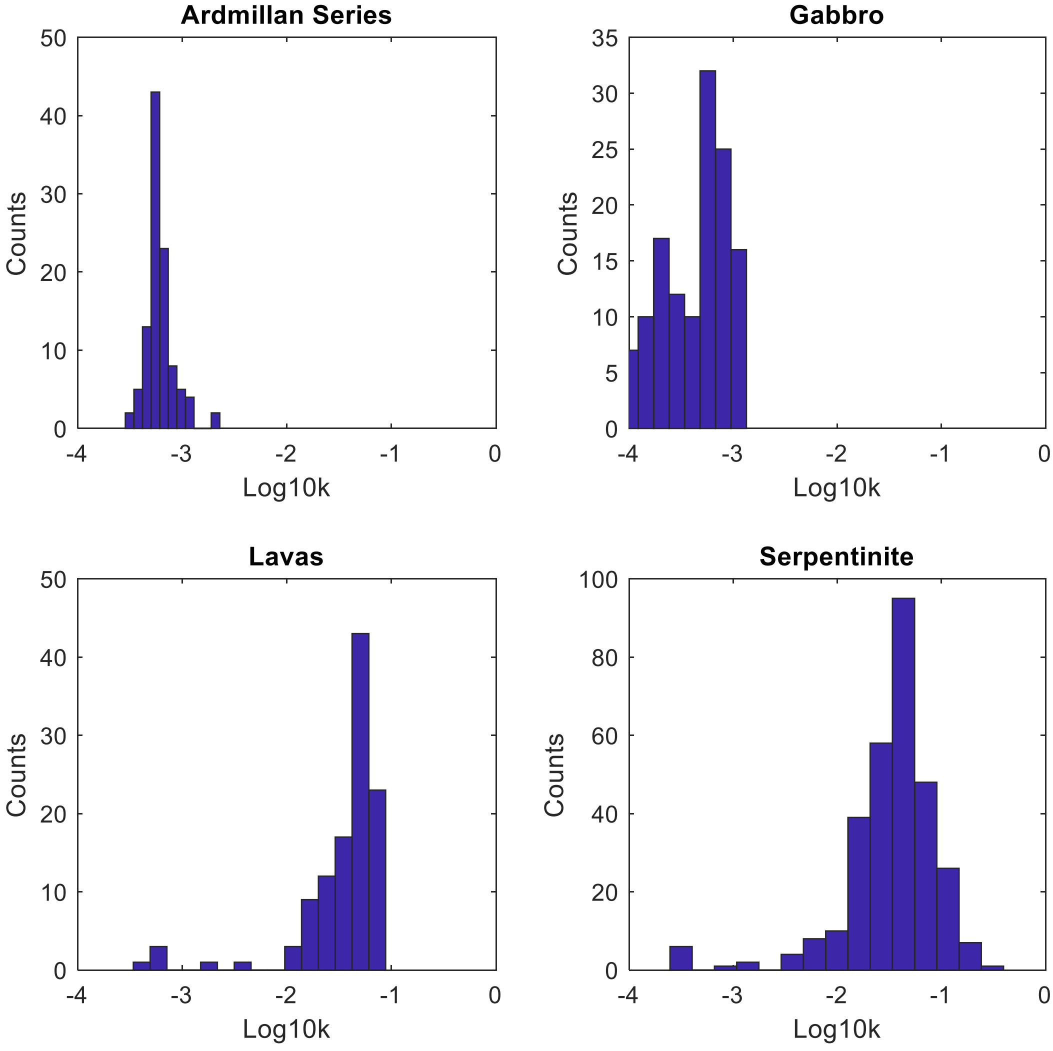

Figure 4.20. Histograms showing the susceptibilities of each of the main rock types within the Ballantrae Complex in the study area.

reported by Powell (1978) of 7 x 10^{-2} (SI) (see Chapter One). Lavas of the Ballantrae Complex have lower susceptibilities than the serpentinites but are exposed outside the area studied here and are not considered further. The Ardmillan Series is typical of the sedimentary rocks found in the study area and have similar susceptibilities as the gabbros, of around 6 x 10^{-4} SI. This is two orders of magnitude lower than the mean susceptibility of the serpentinites, and so both the sediments and gabbros do not contribute significantly to the observed magnetic anomalies. However, the presence of significant volumes of gabbro intruded into the Northern Serpentinite Belt along the line of the magnetic profile survey conducted here may result in a reduction of their bulk susceptibility, and this effect is included in the 2D forward modelling of these data.

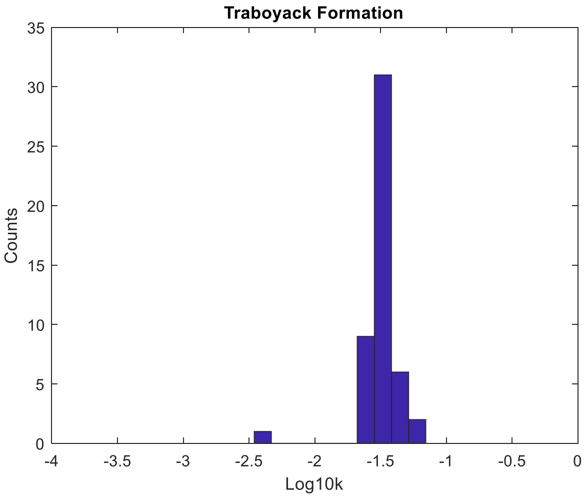

Figure 4.21. A histogram of susceptibilities of sedimentary rocks of the Traboyack Formation.

Susceptibilities of sedimentary rocks of the Traboyack Formation can be seen in Figure 4.21. As mentioned in Chapter One, the Traboyack Formation belongs to the Tappin Group. Floyd and Kimbell (1995) a mean susceptibility for these rocks of around 4 x 10^{-2} SI, which falls in the range of values found here (between 2 x 10^{-2} and 6 x 10^{-2} SI). As discussed in Chapter One, the serpentinite and the Traboyack Formation have the highest susceptibility values in the region.

Note that the anisotropy of magnetic susceptibility (AMS) results from the samples collected for this project are not relevant to the interpretation of the observed magnetic anomalies are presented separately in the Appendix to this thesis.

4.5.2. Natural Remanent Magnetization (NRM) results

NRM measurements were performed on all samples collected for this study, but only data from the serpentinites and Traboyack Formation sediments gave consistent results. Since these are the only rocks with high enough susceptibilities to contribute to the magnetic anomalies in the region, only the results from these two units are presented here.

The equal area stereographic projections of Figure 4.22 show the NRM directions from the Traboyack Formation and serpentinite samples, respectively, and their mean directions, mean NRM intensities and range of NRM intensities are listed in Table 4.1.

Table 4.1. Summary of NRM data for the Traboyack Formation and serpentinite samples.

	Mean NRM direction (dec/inc)	α_{95}	Mean NRM intensity (mA/m)	NRM intensity range (mA/m)	n
Traboyack Formation	317/76	2.4	770	569 – 1173	40
Serpentinites	175/74	8.5	821	88 – 14360	58

Both units have well-defined, near-vertical NRM mean directions, although the serpentinites have a greater dispersion than the sediments. In a full paleomagnetic study, these samples would have been subject to stepwise demagnetization experiments in the laboratory to establish their characteristic remanence directions. However, for the purposes of modelling of magnetic anomalies, only the NRM directions and intensities are relevant, and the values listed in Table 4.1 have been used to constrain the magnetization of modelled bodies in the 2D analysis of the profile data.

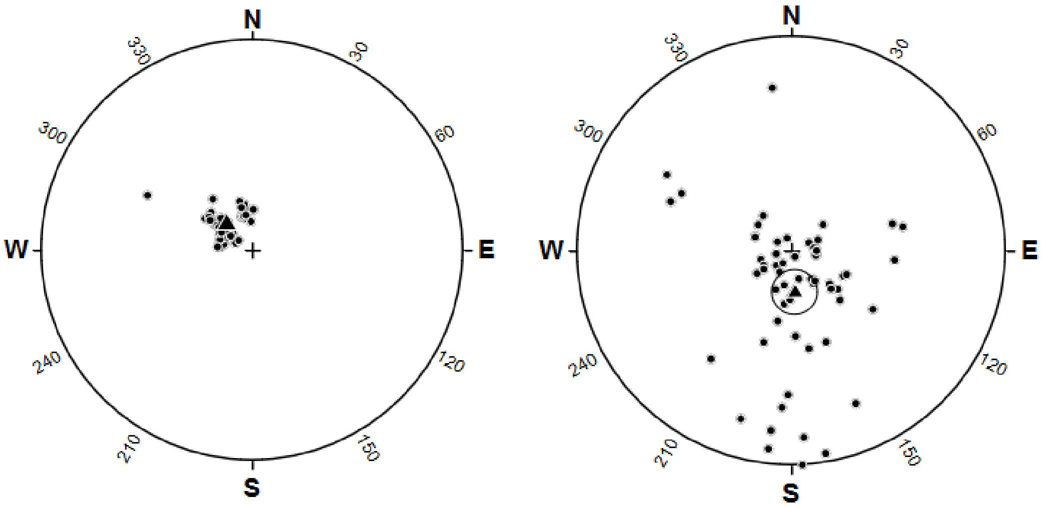

Figure 4.22. Equal area stereographic projections showing NRM directions of the sedimentary rocks of the Traboyack Formation (left) and serpentinites of the Ballantrae Complex (right)

4.5.3. Koenigsberger ratios

The Koenigsberger ratio (Q) allows a comparison of the relative contributions of induced and remanent magnetizations in analysed rocks to observed magnetic anomalies. They are commonly plotted on graphs of NRM intensity against low field magnetic susceptibility that include lines connecting points of equal Q. If Q is higher than 1, remanent magnetization is more dominant. Figures 4.23 and 4.24 show Q values for the serpentinites of the Ballantrae Complex and sedimentary rocks of the Traboyack Formation, respectively. In both cases, the majority of samples have Q values > 10, indicating that the dominant magnetisations contributing to the observed magnetic anomalies are the sub-vertical remanent magnetizations of each rock unit.

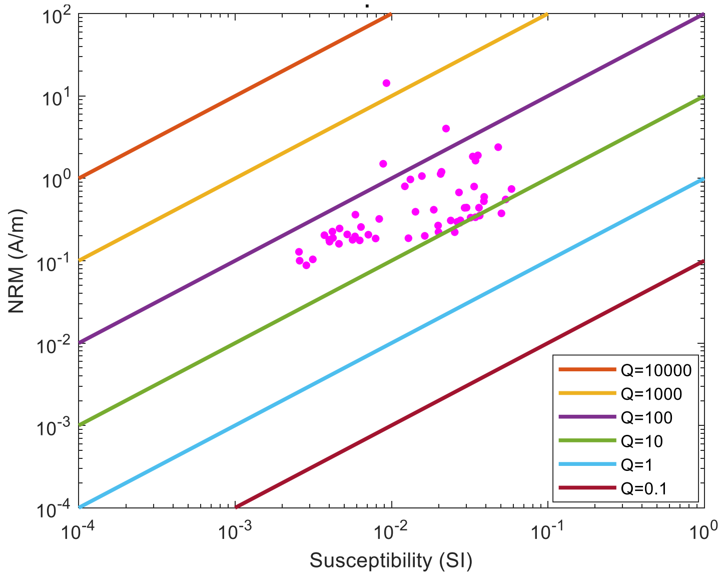

Figure 4.23. Koenigsberger ratios of serpentinite samples.

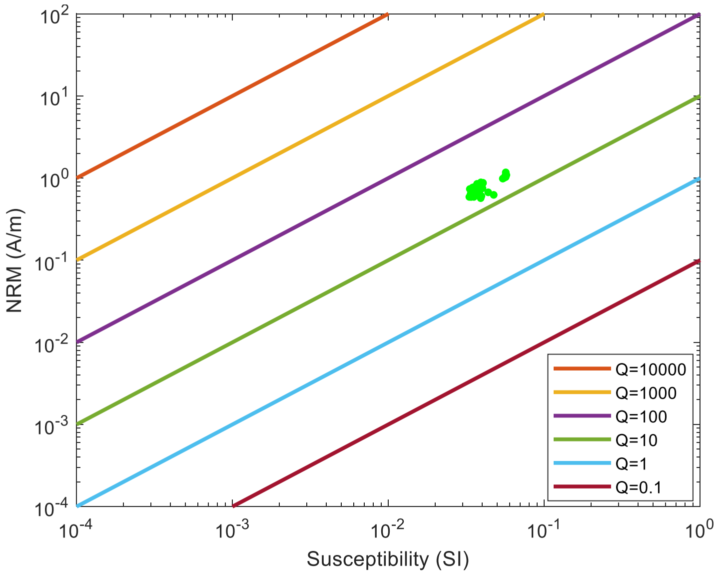

Figure 4.24. Koenigsberger ratios of samples from the Traboyack Formation.

4.6 The modelling results

4.6.1 Mag3D modelling of the Knocklaugh Lodge grid survey data

As discussed in Chapter Three, the Mag3D program developed by the UBC-Geophysical Inversion Facility was used for the three-dimensional modelling. The Knocklaugh Lodge survey data set upward continued to 100 m elevation was used for this modelling study.

The result of this modelling can be seen in Figure 4.39. The initial model susceptibility is defined in the modelling program as 4 x 10^{-2} SI and the lower and upper limits as 8 x 10^{-3} and 6 x 10^{-2} SI. These values were selected using the susceptibility histograms above (see Section 4.5.1). The colour bar shows these susceptibility values in SI units.

The susceptibility range was cut to display the body without the low susceptibility surroundings in order to emphasise the shape and size of high susceptibility rocks in the subsurface. This range is between 2 x 10^{-2} and 6 x 10^{-2} SI units. The anomaly map was added to the model view to see the correlation between anomalies and modelled bodies. The results are shown from different viewpoints and positions to show the details.

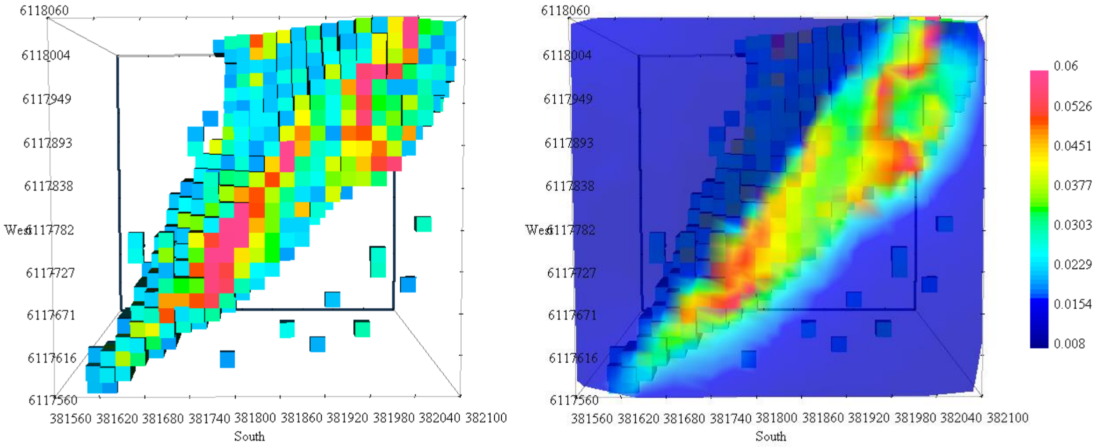

Figure 4.25. A bird's eye view of the Knocklaugh Lodge Mag3D model (left), overlain by the observed contour map (right).

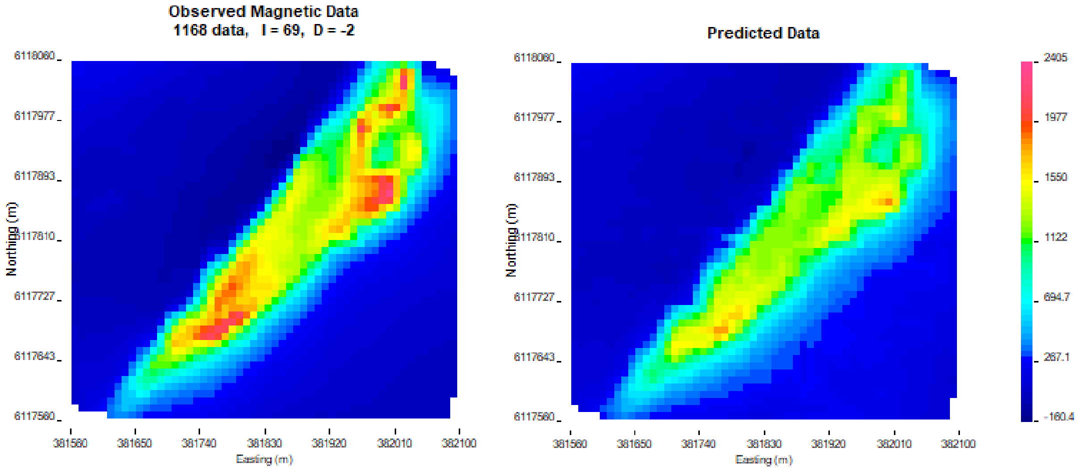

Figure 4.26. The observed and the predicted anomaly maps.

As can be seen in Figures 4.25 and 4.26, the 3D model is compatible with the observed anomaly map. The modelled high susceptibility body has an orientation which extends from southwest to northeast like the anomaly. Figure 4.26 shows the predicted anomaly map generated with from the model alongside the observed anomaly map. The colour bar represents the magnetic field values in nT. The model also does a good job of accounting for the details of magnetic variations within the wedge-shape anomaly that remain after upward continuation.

Figure 4.27 shows the model from two different viewpoints to demonstrate the shape of the body. It can be seen that the body is expanding in width and becoming deeper towards the northeast.

Figures 4.28a to c show the model results from a constant view point looking towards the NNE and show sequential slices through the subsurface susceptibility model as the south side of the modelled cuboid is swept through the model towards the north.

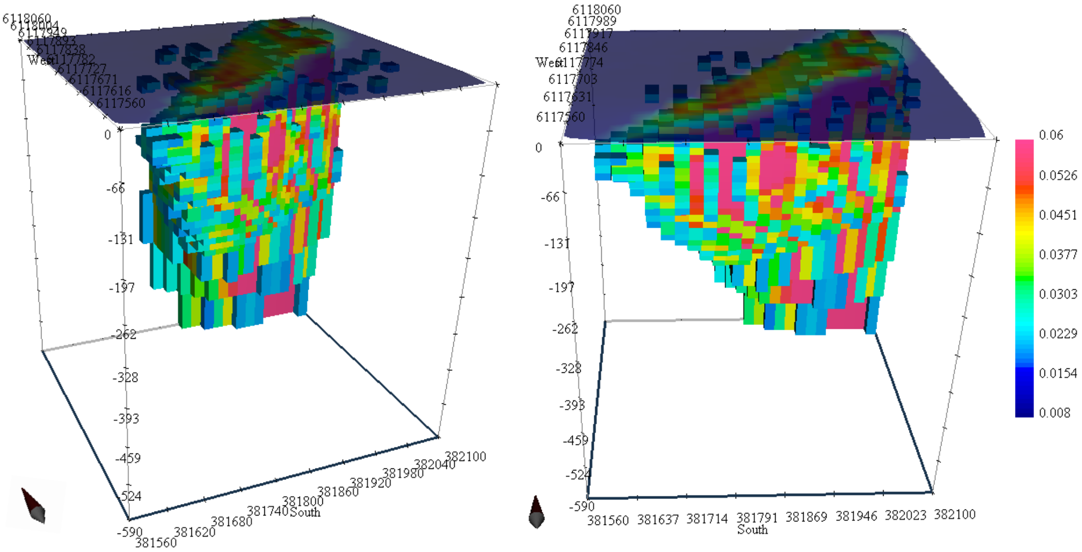

Figure 4.27. Two different model views. The north has been shown by a compass arrow to the bottom left of the model.

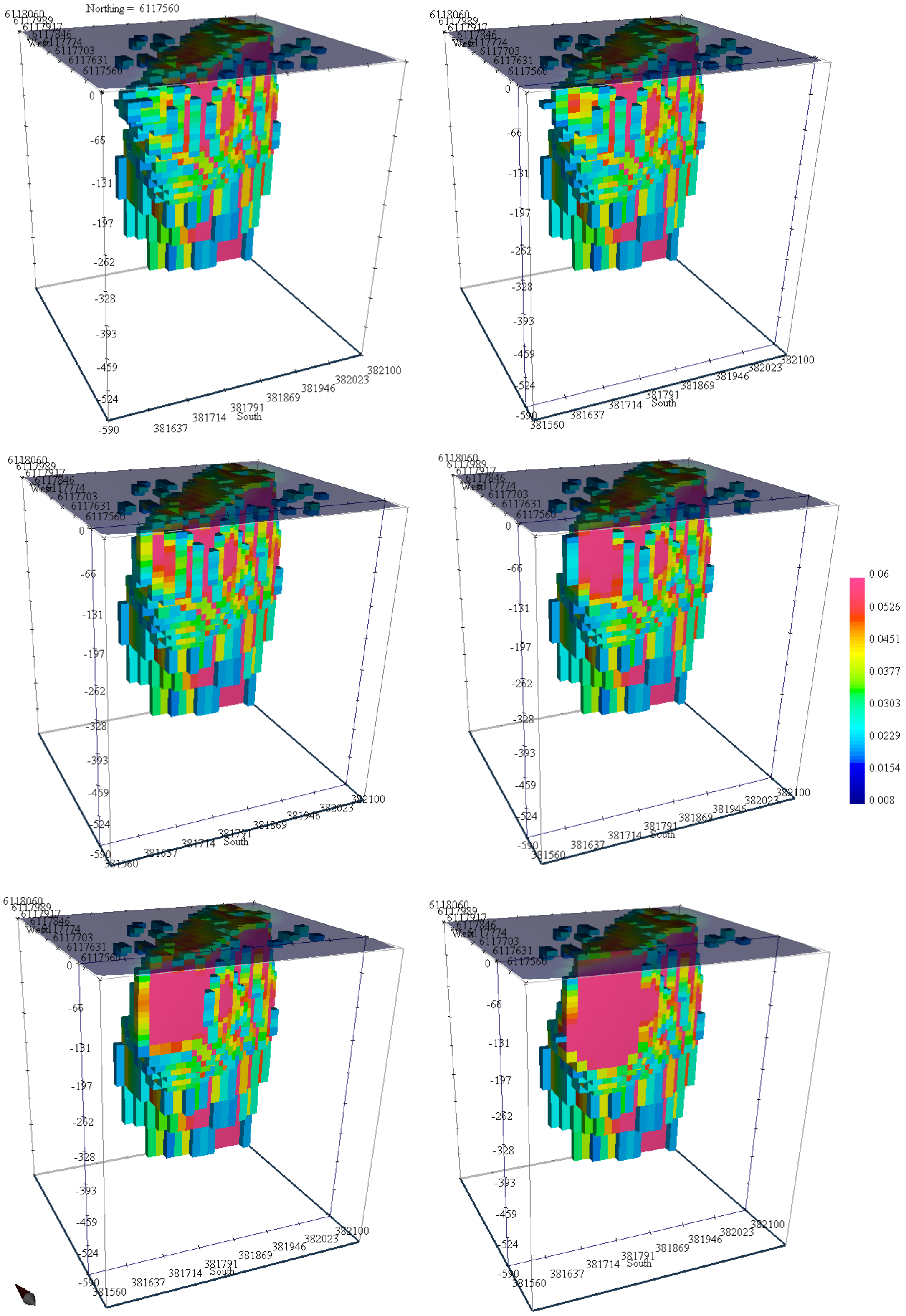

Figure 4.28a. Sequential slices through the subsurface susceptibility model of the Knocklaugh Lodge anomaly produced by scrolling the southern side of the model cuboid progressively to the north.

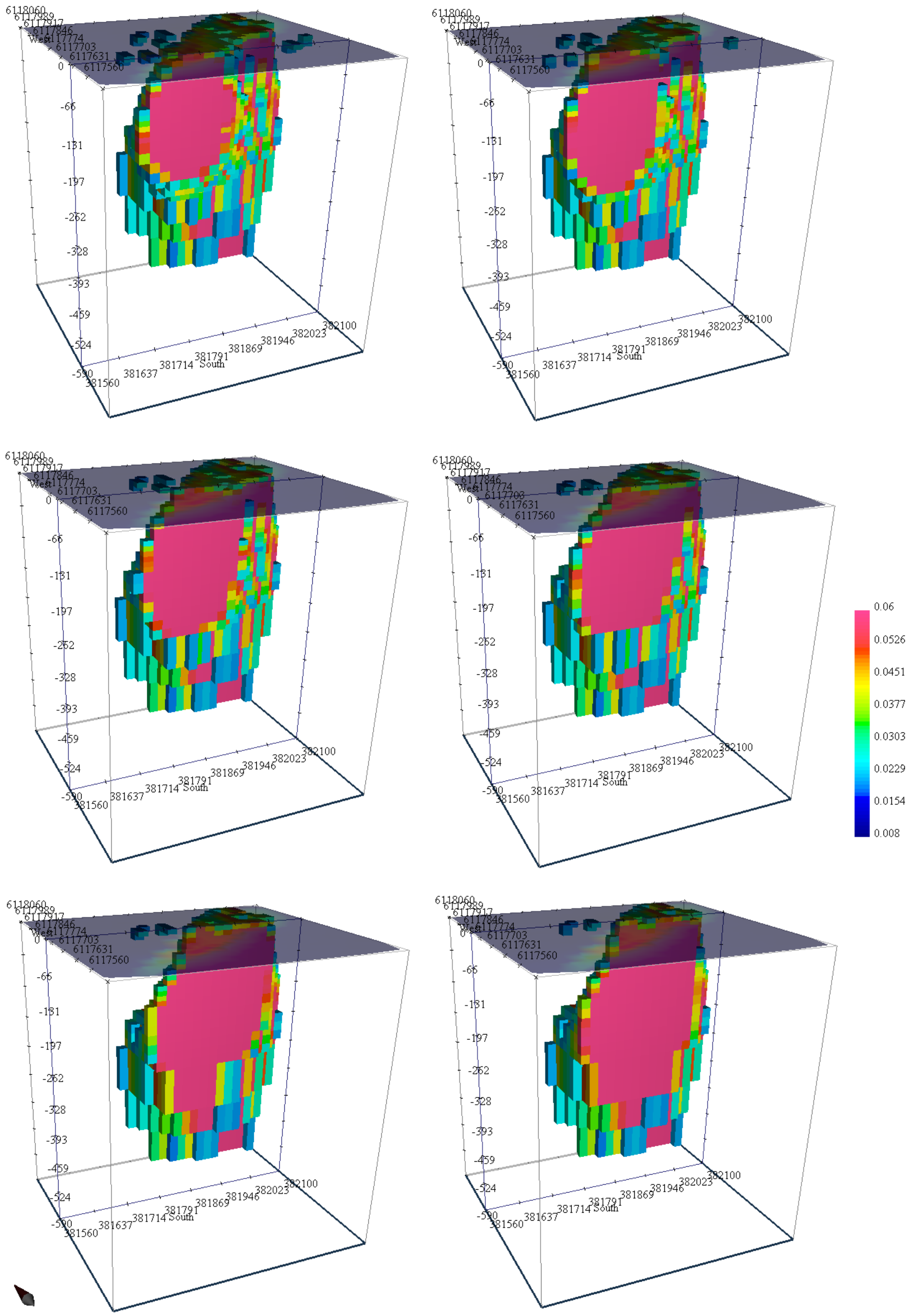
6118060
6117989
6117917
6117846
6117774
6117703
6117631
6117560
West
0
-66
-131
-197
-262
-328
-393
-459
-524
-590
381560
381637
381714
381791
381869
381946
382023
382100
South
0.06
0.0526
0.0451
0.0377
0.0303
0.0229
0.0154
0.008

Figure 4.28b.

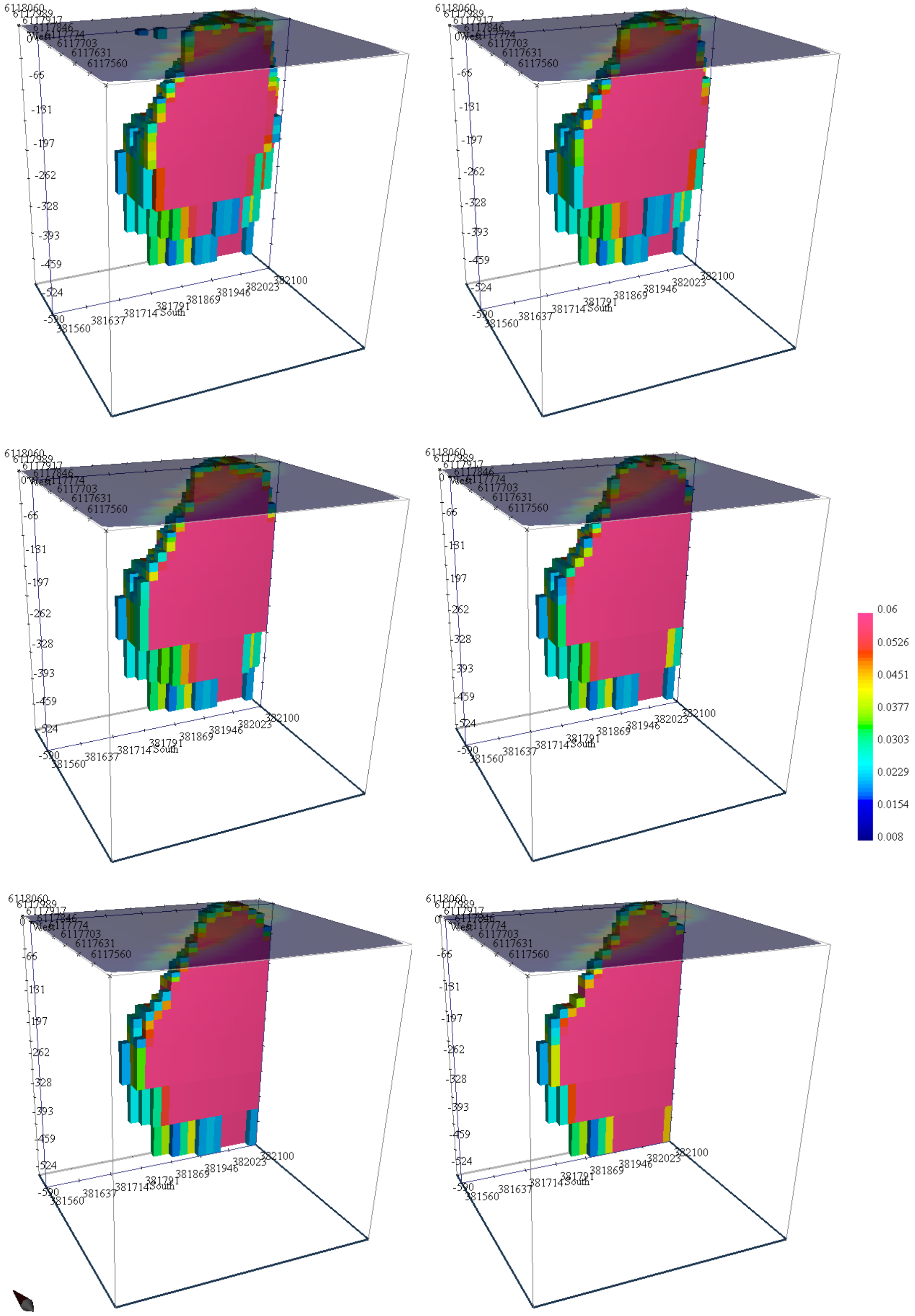
6118060
6117989
6117917
6117846
6117774
6117703
6117631
6117560
0
West
-66
-131
-197
-262
-328
-393
-459
-524
-590
381560
381637
381714
South
381791
381869
381946
382023
382100
0.06
0.0526
0.0451
0.0377
0.0303
0.0229
0.0154
0.008

Figure 4.28c.

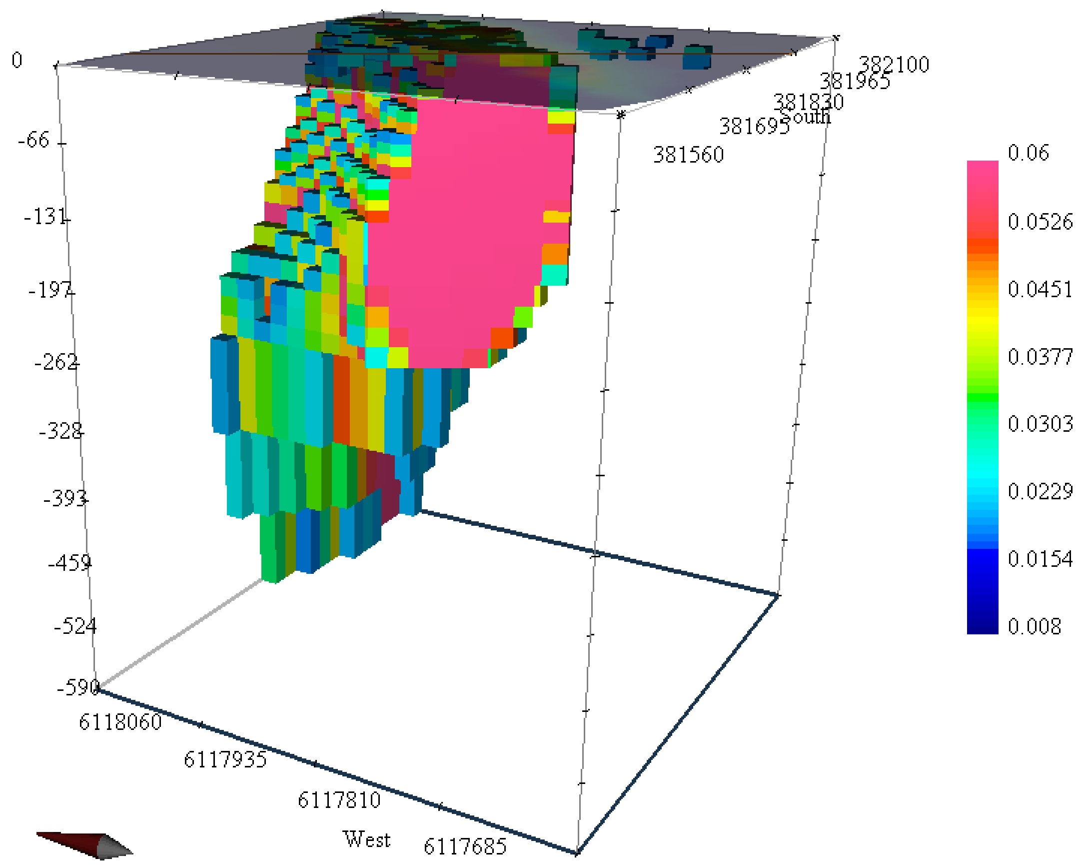

Figure 4.29. A view of the model sliced along the Knocklaugh Lodge profile line, looking perpendicular to the line.

As can be seen in Figure 4.29, the depth of the body with high susceptibilities in the region where the ground-level total field magnetic anomaly profile plane cuts the body is around 290 m, with a susceptibility of ~ 6 x 10^{-2} SI. This perspective also shows that the depth of the modelled high susceptibility region then increases to a maximum depth of 590 m further to the NE.

4.6.2. Mag2dc modelling of the profile across the Knocklaugh Lodge and Northern Serpentinite Belt anomalies

As mentioned in Chapter 3, the Mag2dc program was to interpret the profile data across the Knocklaugh Lodge and Northern Serpentinite Belt anomalies upward continued to 100 m elevation. Results are shown in Figure 4.30, where the upper graph compares the observed anomaly (dashed green line) with the calculated anomaly (solid black line). The lower part of the figure shows the best-fit 2D model, with distance in metres on the x-axis and depth in metres on the y-axis (note that the distances are represented at approximately twice the scale of the depths). Four bodies labelled B1, B2, B3 and B4 are required to achieve a close fit between calculated and observed anomalies, and their susceptibilities

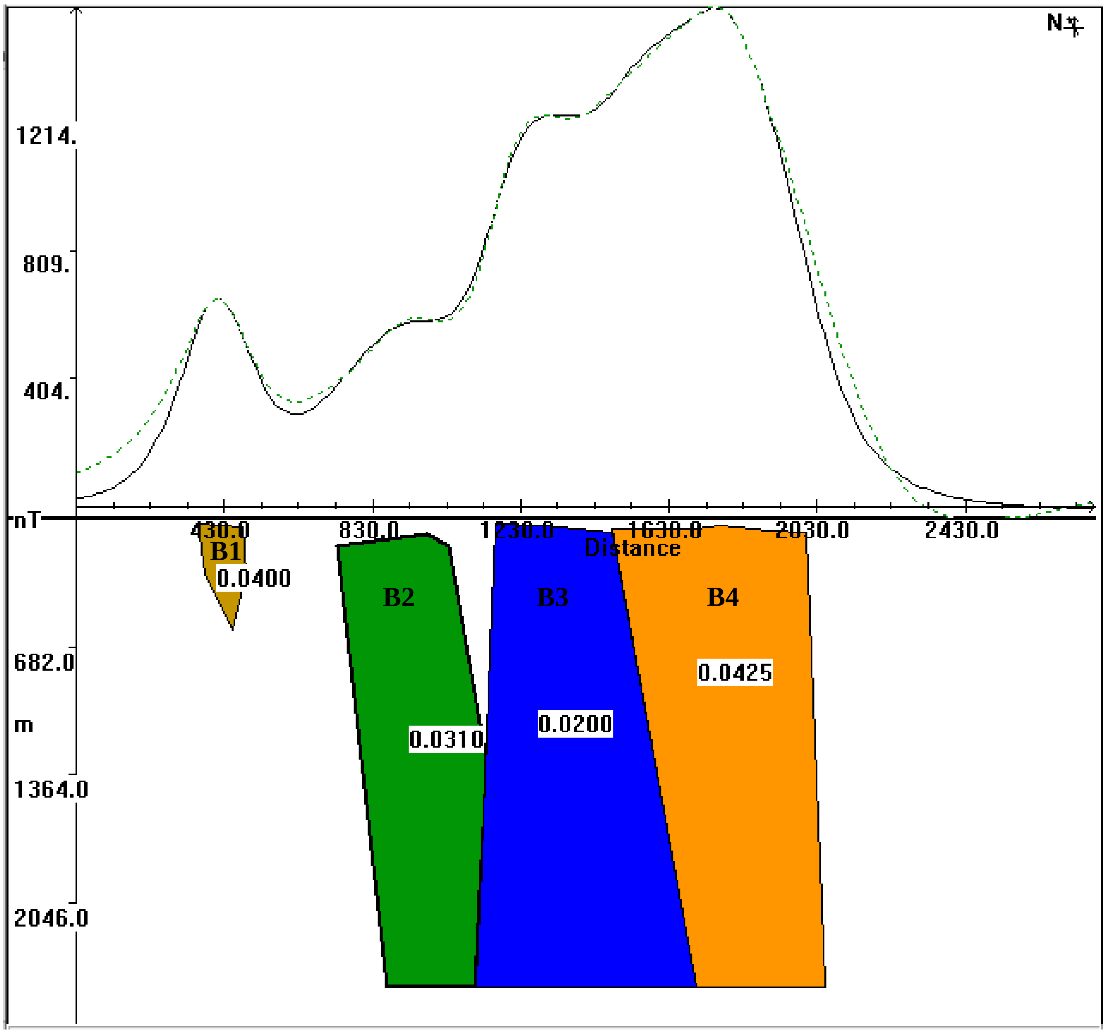

Figure 4.30. The best-fitting 2D subsurface model for the total field magnetic anomaly profile upward continued to 100 m elevation. SE to the left, NW to the right.

(shown in SI units by the numbers over each body) are within the range of observed values for the serpentinites of the Ballantrae Complex. The Mag2dc model also incorporates the magnetic remanence of the bodies, and these were all set to the intensity and direction of the mean NRM found for the serpentinites (i.e., dec = 175, inc = 74, intensity = 821 mA/m, as listed in Table 4.1 above). All other geological units traversed by this profile, as shown on the BGS geological map extract in Figure 4.31, have susceptibilities two orders of magnitude less than that of the serpentinites (and negligible NRM intensities) and so these units are considered as part of the non-magnetic background host of the model (shown in white in the model of Figure 4.30).

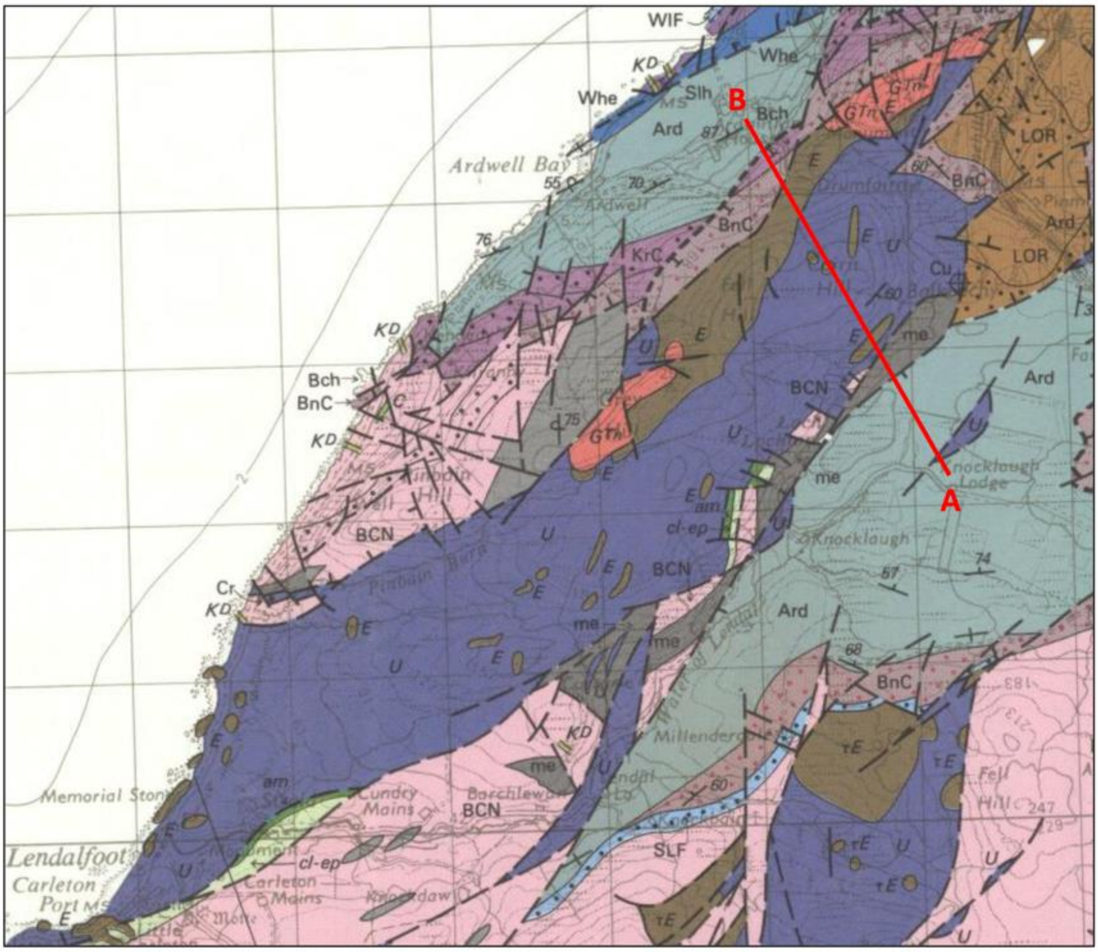

Figure 4.31. Geological map showing the Knocklaugh Lodge profile line from A to B and the geological units (modified from BGS, 1988). Ard: Ardwell Formation, me: Sedimentary mélange, E: Diorite and gabbro, U: Serpentinite.

In developing this model, the Knocklaugh Lodge gradiometer map was used to fix the locations of the boundaries of body B1. The SE side of body B3 corresponds to the faulted contact along the SE margin of the Northern Serpentinite Belt as mapped by the BGS (Figure 4.31), and the NW side of body B4 to its NW mapped contact with a gabbro body (Figure 4.31). Bodies B1 and B4 are assigned the mean susceptibility of the serpentinites determined in this study (4 x 10^{-2} SI). In order to account for the reduction in magnetic anomaly amplitude over the SE margin of the Northern Serpentinite Belt and its shape seen at approximately 1230 m along the profile (Figure 4.30), it was necessary to use a lower susceptibility value of 2 x 10^{-2} SI (at the lower end of the range of observed serpentinite susceptibilities). However, BGS mapping and field observations indicate that the Northern Serpentinite Belt along this part of the profile contains a significant volume of gabbroic intrusions that have been shown here to have susceptibilities two orders of magnitude lower than the host serpentinites. It is likely that these intrusions are responsible for lowering the overall bulk susceptibility in this part of the serpentinites therefore.

Body B2 is interpreted as a serpentinite body with a mean susceptibility of 3.1 x 10^{-2} SI that is concealed beneath essentially non-magnetic sedimentary rocks of the Ardwell Formation and is required to account for the subsidiary bump in the anomaly profile at approximately 850 m along the profile. The required shape of this body implies that the small, fault-bounded outcrop of sedimentary mélange along the SE margin of the Northern Serpentinite Belt ("me" on Figure 4.31) forms a downward narrowing wedge of essentially non-magnetic material sandwiched between fault-bounded slices of serpentinite.

Finally, it should be noted that during iterative modification of this four-body model, it was realised that changing the maximum depth of bodies 2 – 4 had very little effect on the fit between calculated and observed anomalies. A constant maximum depth of 2.5 km has been used in the final 2D model to be consistent with the results of the Mag3D modelling of the subsurface beneath the Northern Serpentinite Belt that suggests that rocks with susceptibilities of ~4 x 10^{-2} SI do not extend deeper than ~2.5 km.

4.6.3. Mag3D modelling of the UK National Aeromagnetic Survey data set

The aeromagnetic data described in Section 4.1.3 were modelled using Mag3D using a mesh of 71280 cells, each of 500 m side length. The initial model susceptibility was defined in the modelling program as 4 x 10^{-2} SI while the lower and upper limits were set as 8 x 10^{-4} and 6 x 10^{-2} SI. The anomaly map with the elevation values was plotted over the model to assess the correlation (Figure 4.32) between the model and the anomaly.

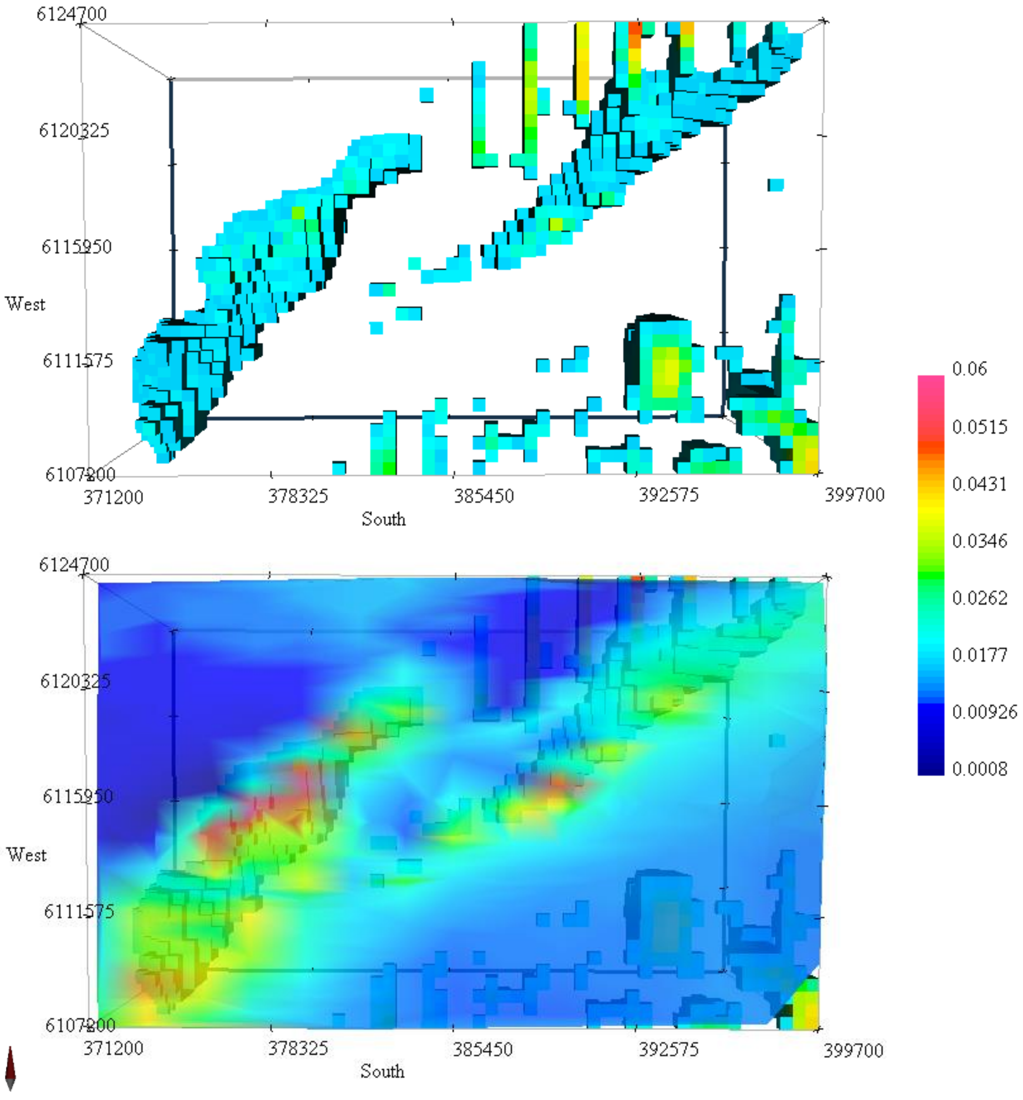

Figure 4.32. A bird's eye view of the Mag3D model of the aeromagnetic data (top), overlain by the observed contour map (bottom).

The observed magnetic data, the predicted anomaly and the elevation maps can be seen in Figure 4.33. The data collection points were added to the observed anomaly map as dots and shows that the southeast of the study area has fewer observations and will therefore be less well constrained. The program assigns some high susceptibilities to cells in this area (e.g. Figure 4.34), but these are considered to be artefacts of the modelling process.

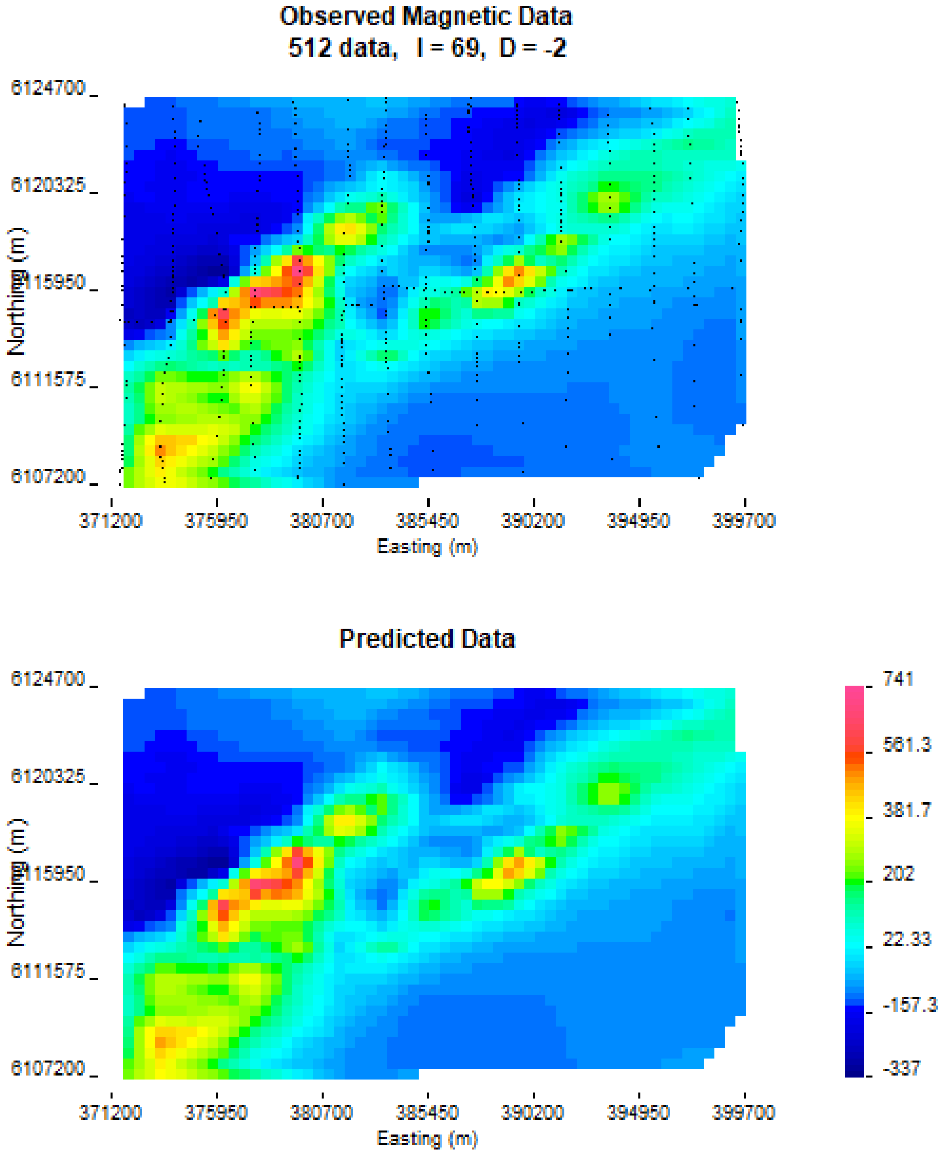

Figure 4.33. Maps showing the observed aeromagnetic data map (top) and that predicted by the Mag3D model (bottom).

A side view of the resulting Mag3D model can be seen in Figure 4.34. The depth axis (z) has been plotted at double the scale of the x and y-axes to show the bodies clearly.

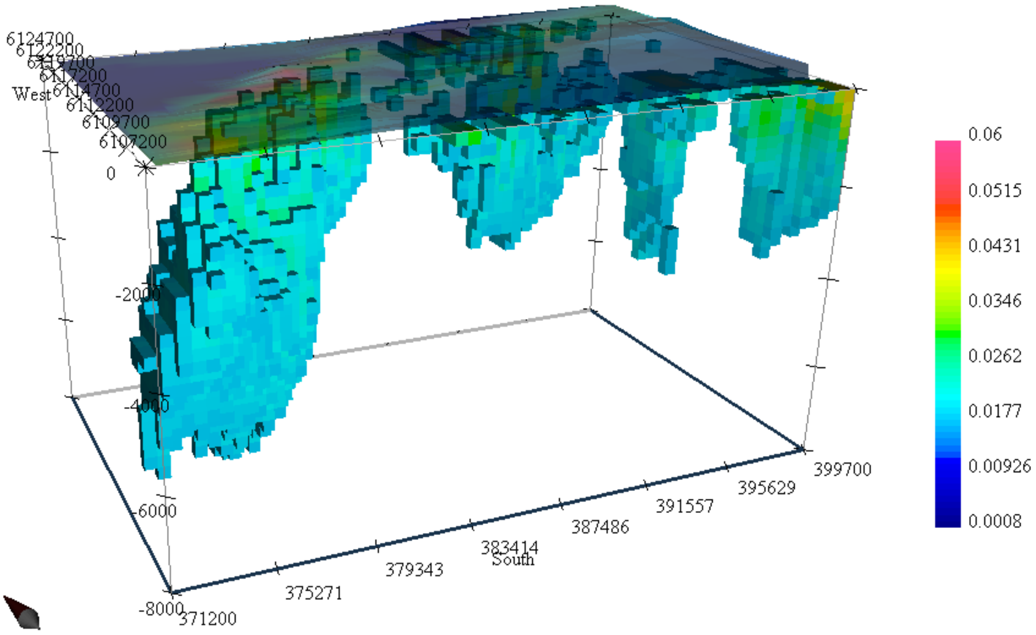

Figure 4.34. A model view showing the subsurface bodies. North is indicated by the compass (bottom left).

Sequential slices through the model are shown in Figure 4.35a-g looking to the NNE to demonstrate the changes in susceptibility and body shape as the south side of the model is swept to the north.

Excluding the modelling artefacts in the SE corner of the model (discussed above), two main high susceptibility bodies were created by the modelling program in order to fit the observed dataset: (i) a tongue-shaped body on the western half of the model volume that extends to near the base of the model mesh and that has a core of very high susceptibility cells extending to depths of approximately 2.5 km. This body underlies the mapped outcrops of the Northern and Southern Serpentinite Belts and provides information on their subsurface form that will be discussed further in Chapter 5; and (ii) a shallower elongate body in the NE quadrant of the model volume that correlates with the mapped outcrop of the Traboyack Formation of the Tappins Group, that has been shown here to have mean susceptibilities comparable to that of the serpentinites of the Ballantrae Complex. Again, this will be discussed in more detail in Chapter 5.

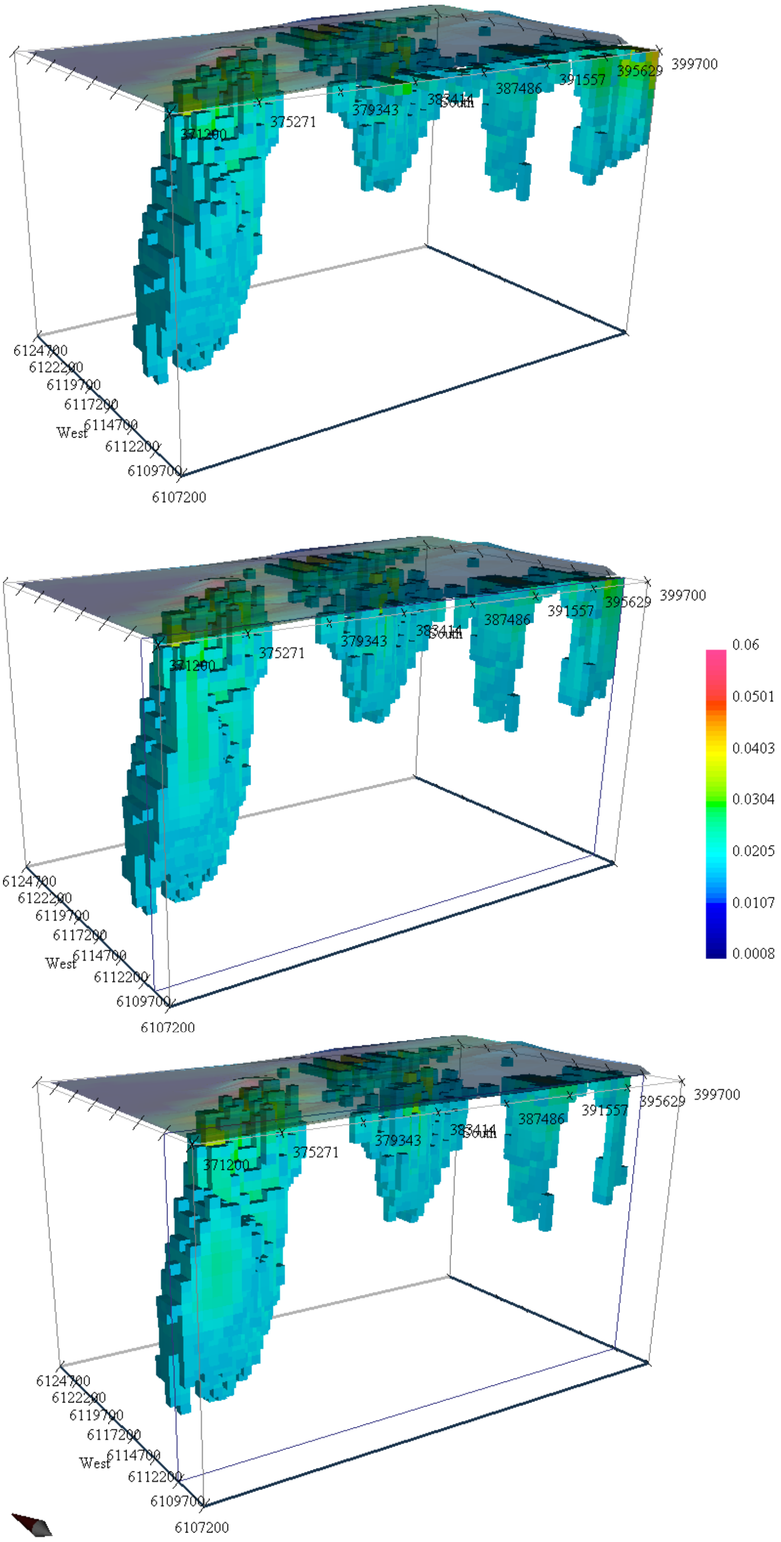

Figure 4.35a. Sequential slices through the subsurface susceptibility model of the aeromagnetic anomaly map produced by scrolling the southern side of the model cuboid progressively to the north.

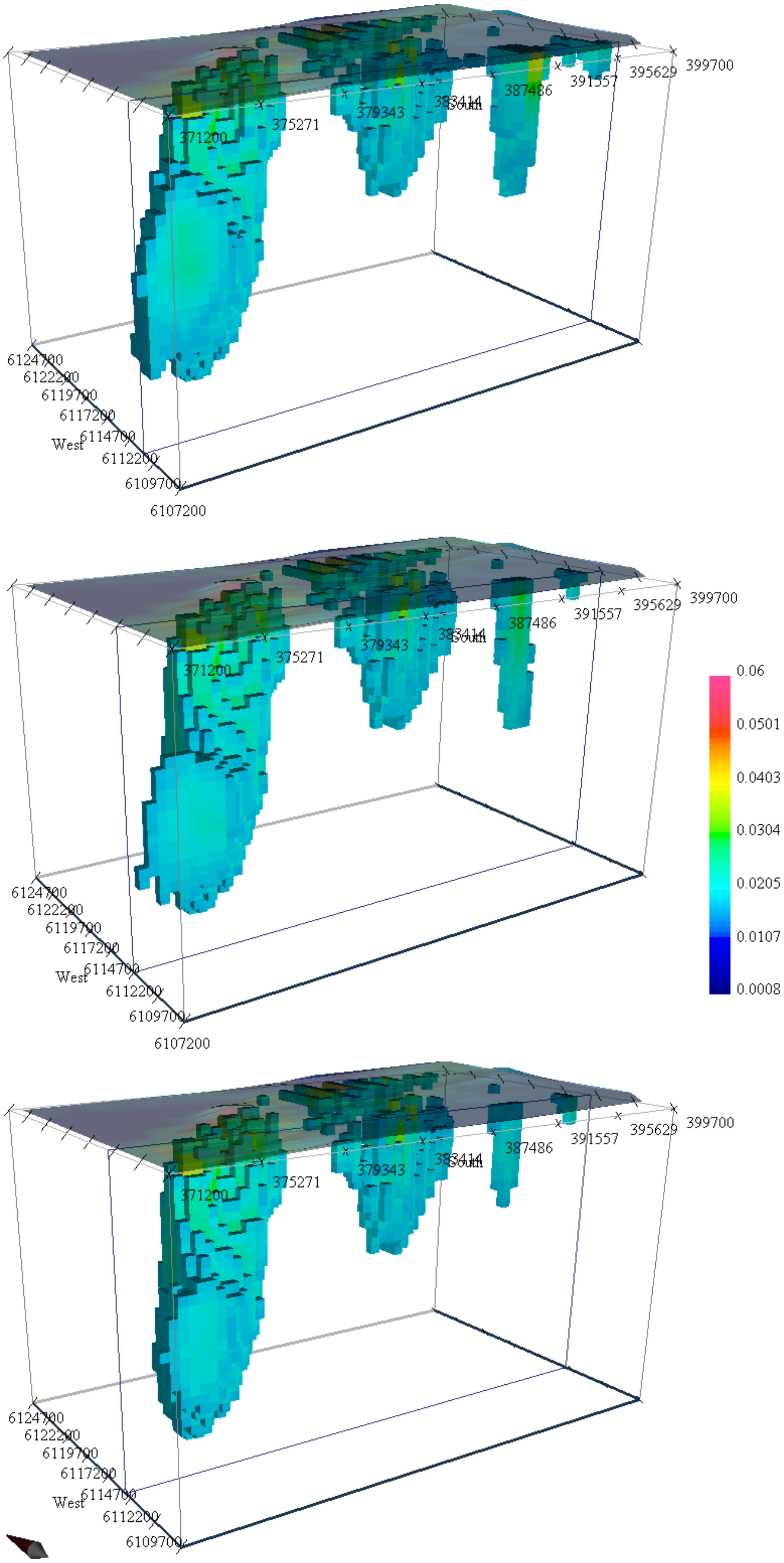
399700
395629
391557
387486
383414
South
379343
375271
371200
6124700
6122200
6119700
6117200
West
6114700
6112200
6109700
6107200
399700
395629
391557
387486
383414
South
379343
375271
371200
6124700
6122200
6119700
6117200
West
6114700
6112200
6109700
6107200
0.06
0.0501
0.0403
0.0304
0.0205
0.0107
0.0008
399700
395629
391557
387486
383414
South
379343
375271
371200
6124700
6122200
6119700
6117200
West
6114700
6112200
6109700
6107200

Figure 4.35b.

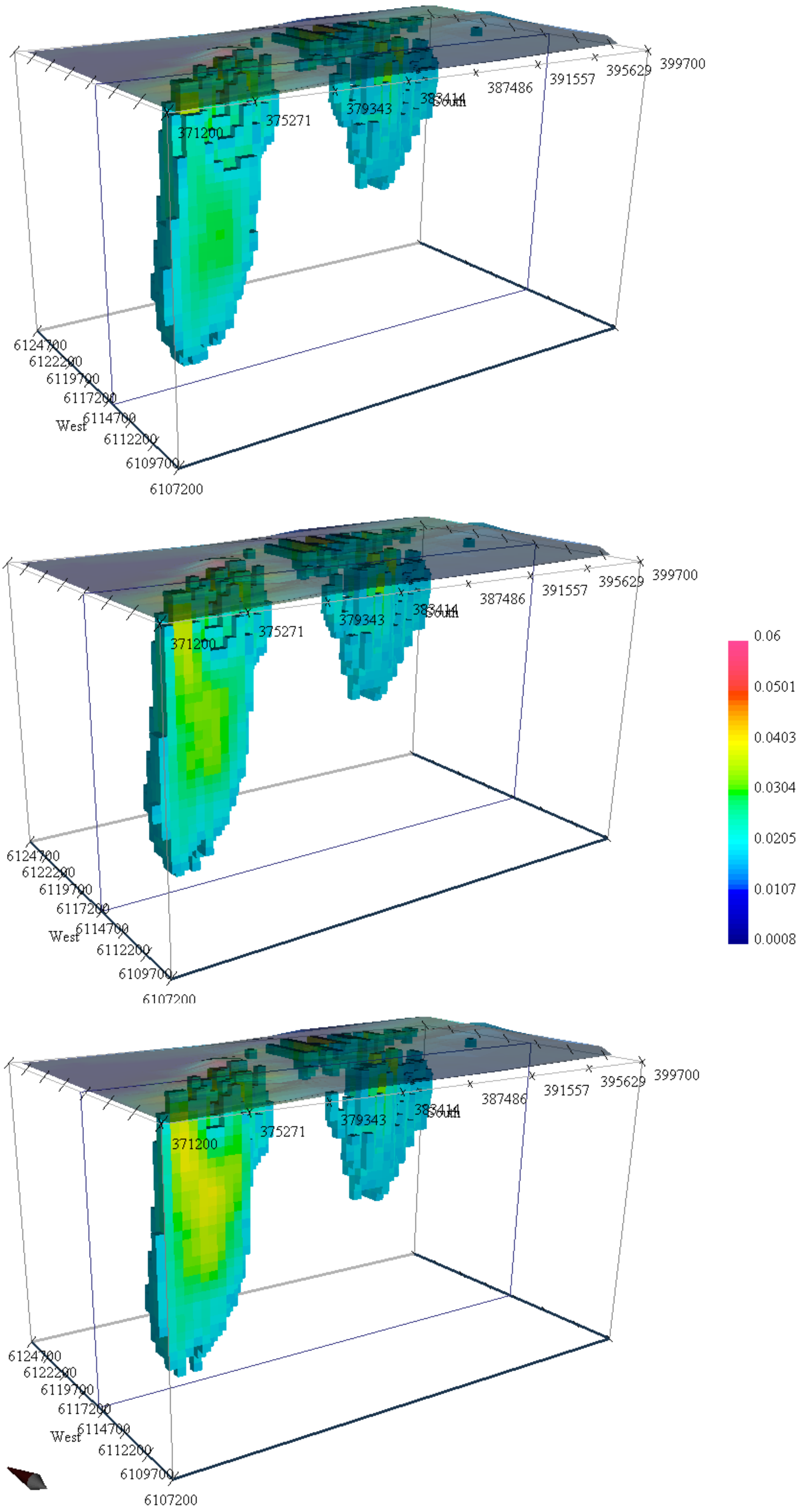
371200
375271
379343
383414
South
387486
391557
395629
399700
6124700
6122200
6119700
6117200
West
6114700
6112200
6109700
6107200
0.06
0.0501
0.0403
0.0304
0.0205
0.0107
0.0008

Figure 4.35c.

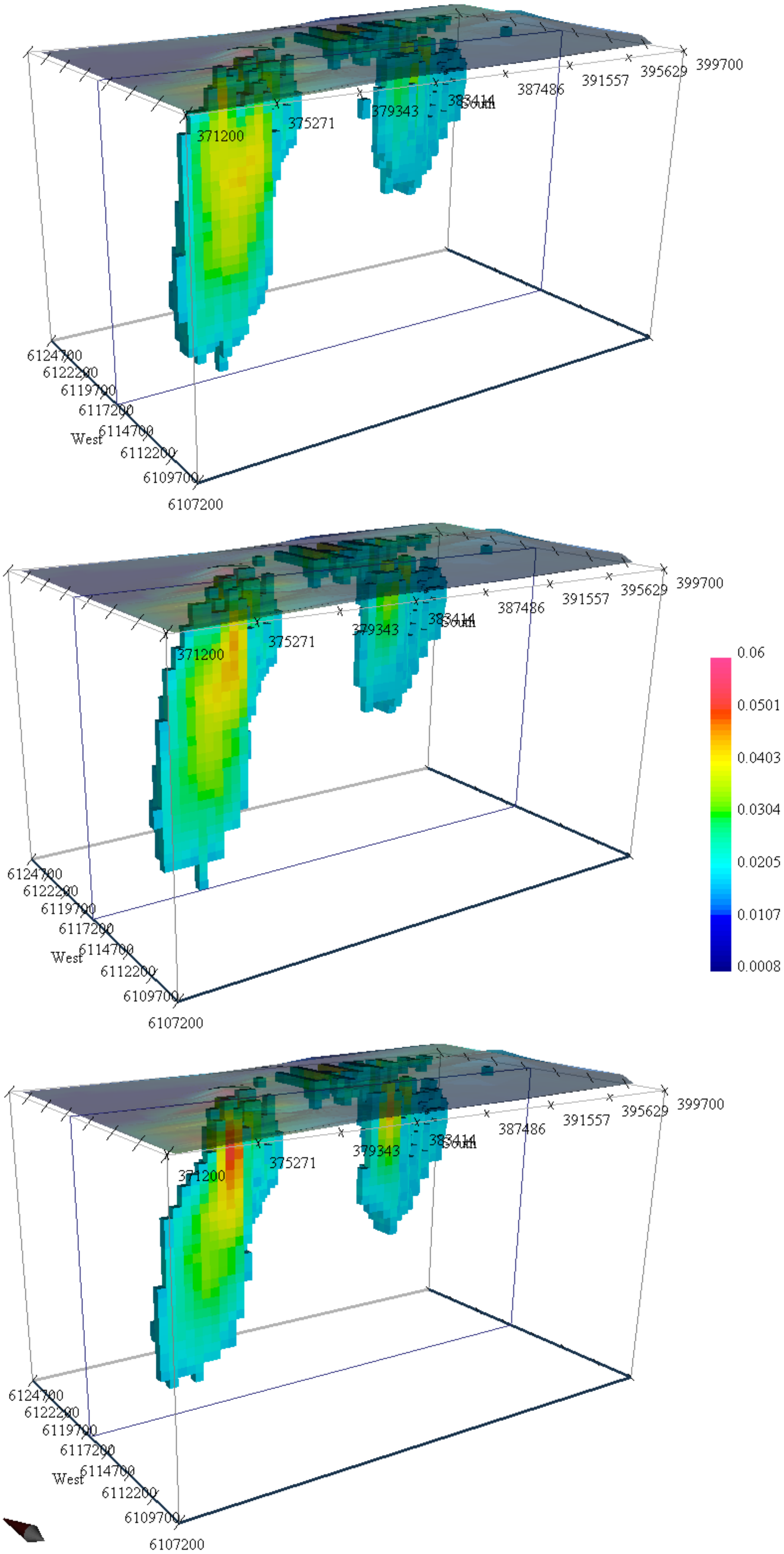
399700
395629
391557
387486
383414
South
379343
375271
371200
6124700
6122200
6119700
6117200
West
6114700
6112200
6109700
6107200
399700
395629
391557
387486
383414
South
379343
375271
371200
6124700
6122200
6119700
6117200
West
6114700
6112200
6109700
6107200
0.06
0.0501
0.0403
0.0304
0.0205
0.0107
0.0008
399700
395629
391557
387486
383414
South
379343
375271
371200
6124700
6122200
6119700
6117200
West
6114700
6112200
6109700
6107200

Figure 4.35d.

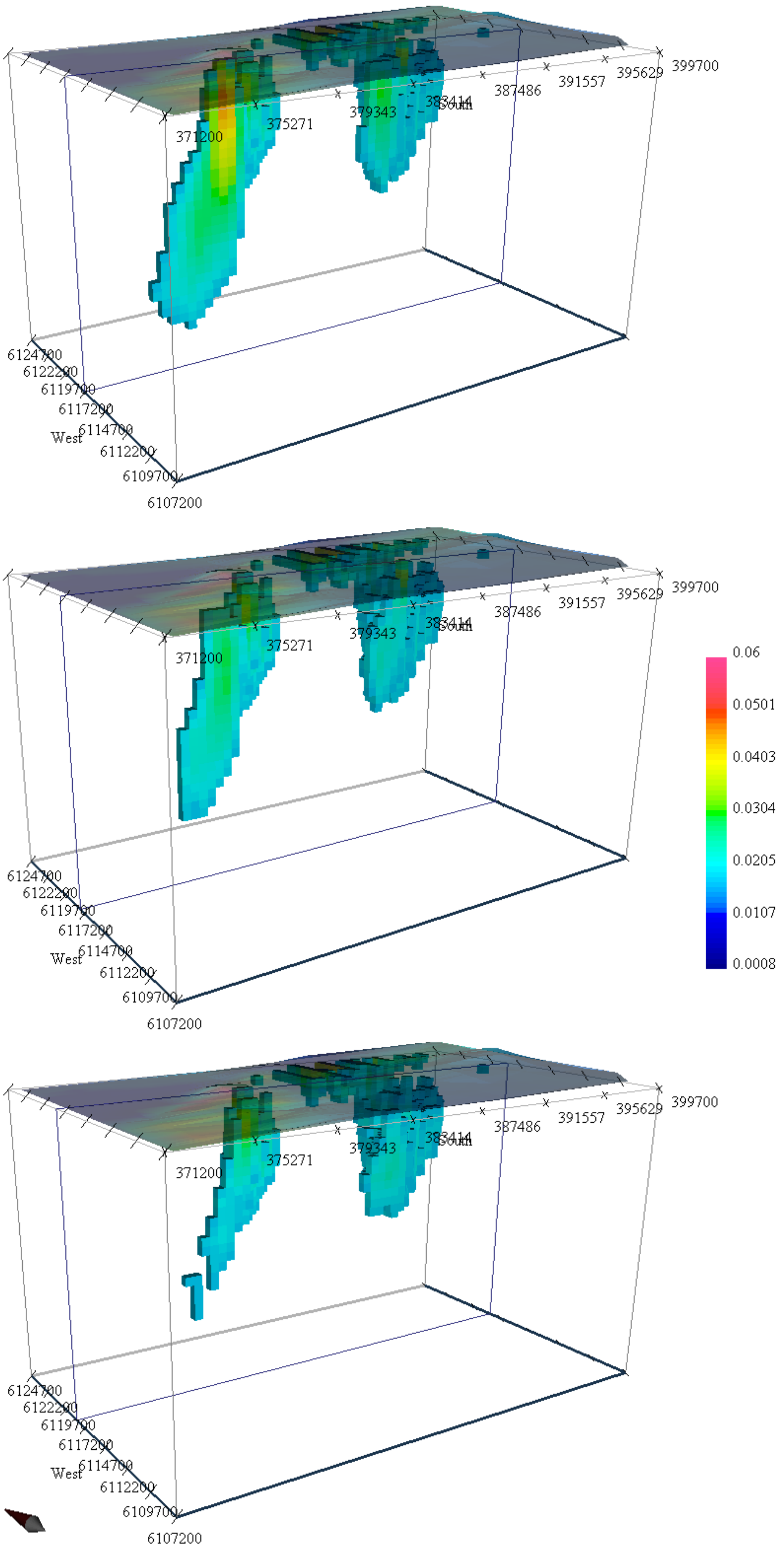
371200
375271
379343
383414
South
387486
391557
395629
399700
6124700
6122200
6119700
6117200
West
6114700
6112200
6109700
6107200
0.06
0.0501
0.0403
0.0304
0.0205
0.0107
0.0008

Figure 4.35e.

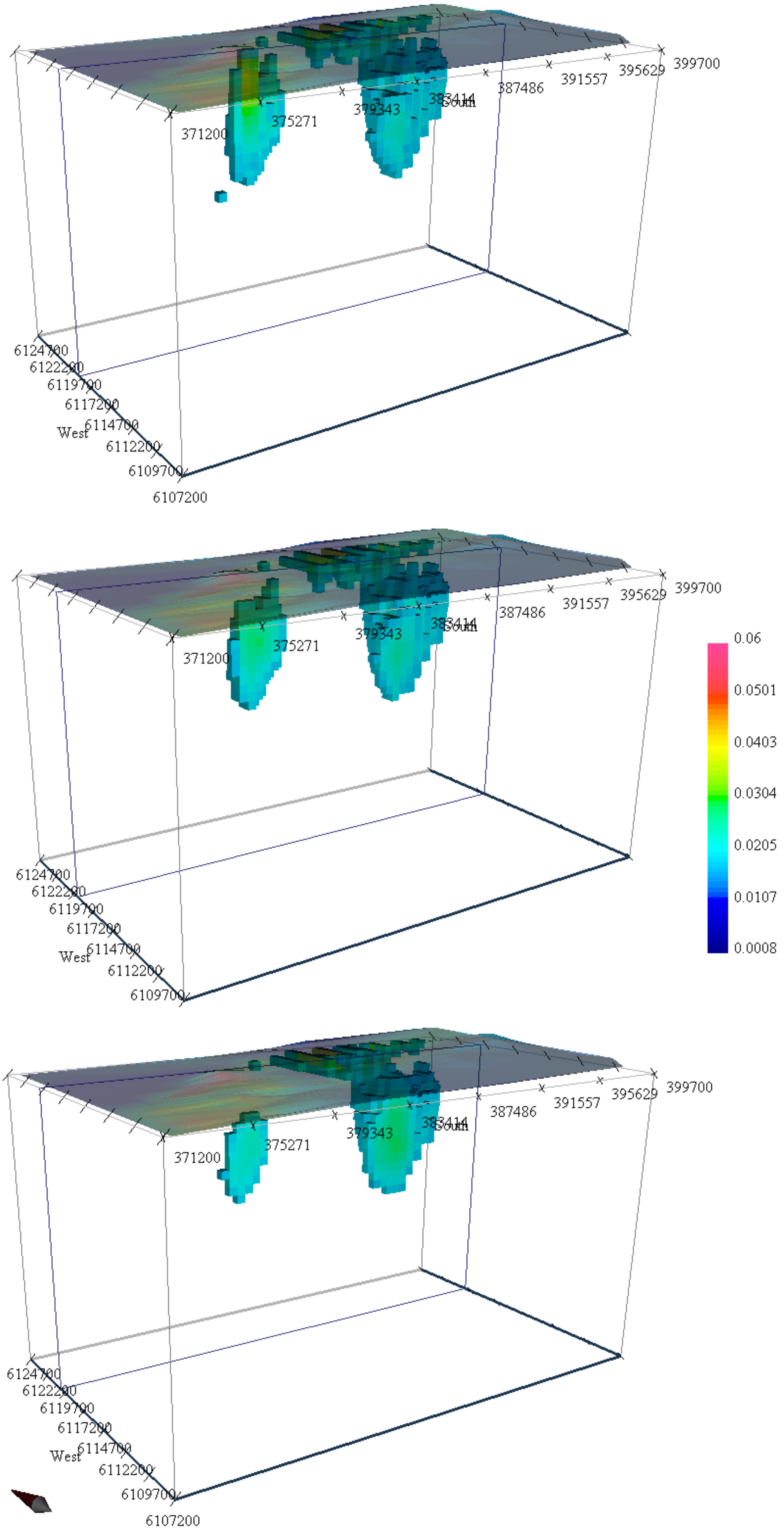
399700
395629
391557
387486
383414
South
379343
375271
371200
6124700
6122200
6119700
6117200
West
6114700
6112200
6109700
6107200
0.06
0.0501
0.0403
0.0304
0.0205
0.0107
0.0008

Figure 4.35f.

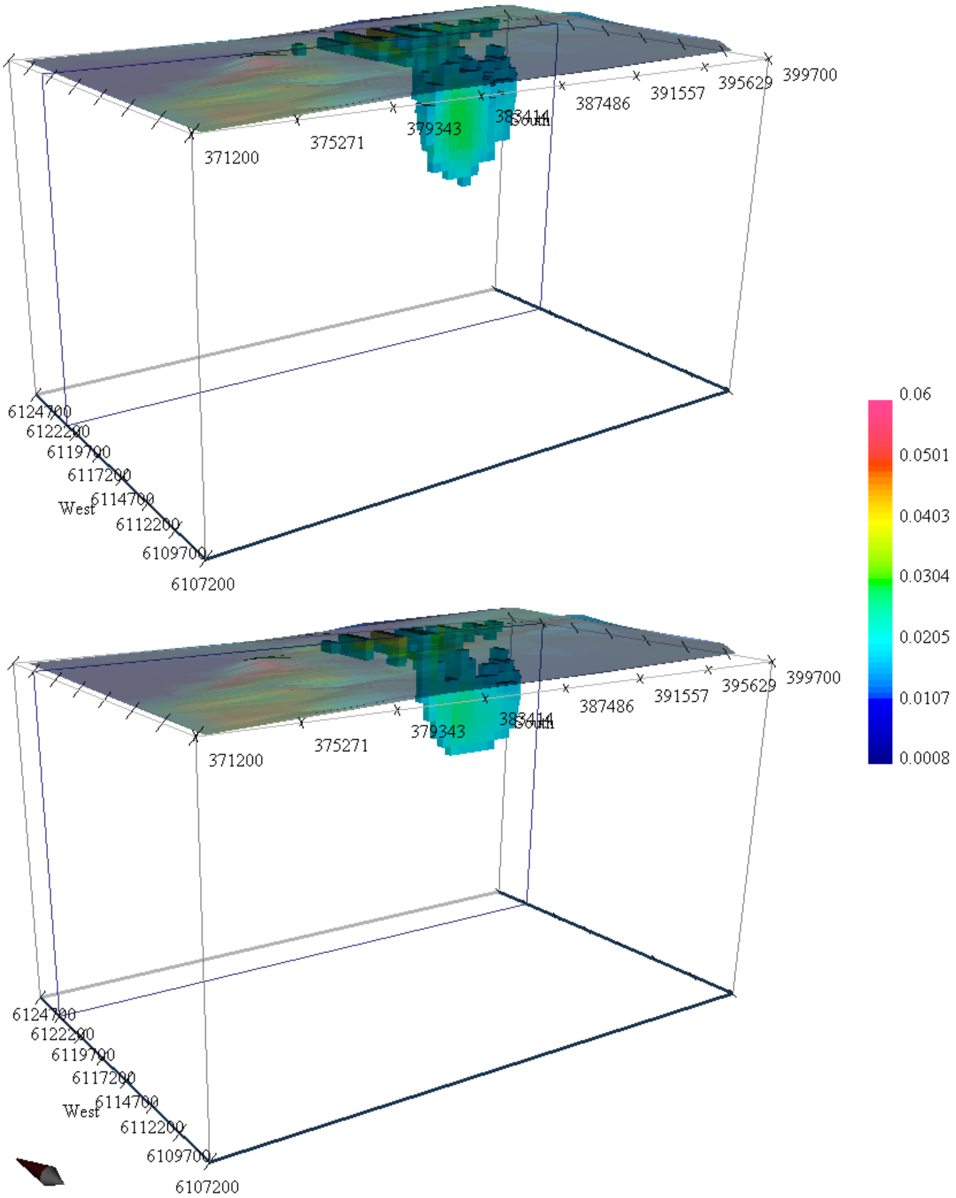
399700
395629
391557
387486
383414
South
379343
375271
371200
6124700
6122200
6119700
6117200
West
6114700
6112200
6109700
6107200
0.06
0.0501
0.0403
0.0304
0.0205
0.0107
0.0008
399700
395629
391557
387486
383414
South
379343
375271
371200
6124700
6122200
6119700
6117200
West
6114700
6112200
6109700
6107200

Figure 4.35g.

Chapter 5 - Discussion

As mentioned in Chapter One, 2D modelling of the magnetic anomalies over the Northern and Southern Serpentinite Belts was previously attempted by Powell (1978). However, the 3D magnetic modelling presented here represents the first-ever attempt to use a 3D approach to understand the source of the aeromagnetic and ground-level magnetic anomalies that characterise the Girvan-Ballantrae region.

5.1 The Knocklaugh Lodge area

The Mag3D model of the Knocklaugh Lodge magnetic anomaly is shown again in Figure 5.1 (after applying susceptibility cut-offs of 2 x 10^{-2} to 6 x 10^{-2} SI that corresponds to the range of susceptibilities observed in data collected in this study). This shows an inferred SW-NE-striking serpentinite body extending to a depth of 590 m that has high susceptibility values. It is clear that the body becomes deeper and broader towards the NE (Figure 5.1). The shape of this body suggests that it represents a small fault-bounded sliver, that could either be an isolated thrust slice or have been entrained along a strike-

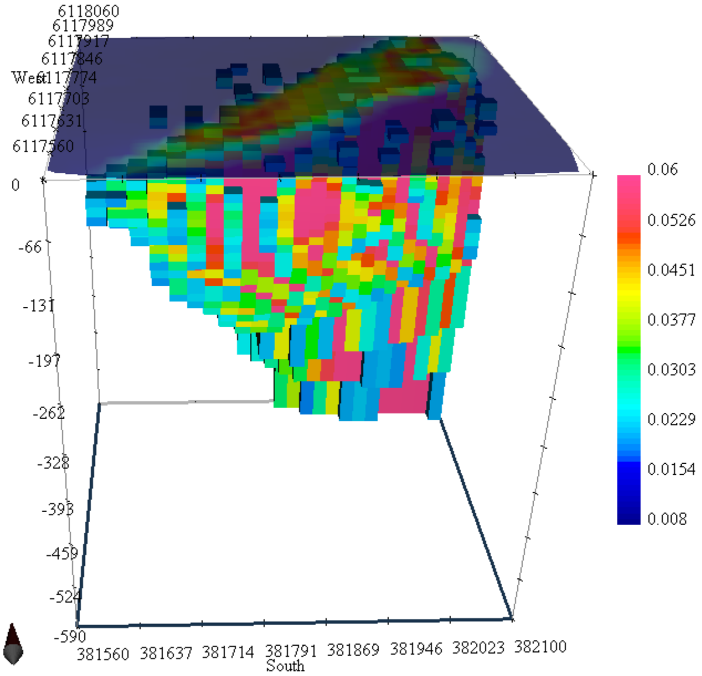

Figure 5.1. The Mag3D model of the Knocklaugh Lodge anomaly showing the orientation and depth of the subsurface serpentinite body.

slip fault system. The fault-bounded nature of this body is confirmed by borehole drilling at this location (Stone et al., 1984), which showed that its SE margin is marked by a sheared and imbricated fault zone containing pervasively silicified and carbonated serpentinite (Figures 1.8 and 1.9). Stone et al. (1984) suggest that this fault zone forms part of a more extensive NE-SW fault system cutting the upper Ordovician Ardmillan Series that merges with other major structures to the SW through a tectonic mélange zone at Knockormal (to the south of Lendalfoot) (Bloxam, 1980).

2D modelling of the upward continued profile from Knocklaugh Lodge to the coast across the Northern Serpentinite Belt (Figure 5.2) suggests the presence of four high-susceptibility bodies in the subsurface, three of which extend down to 2.5 km (although the model is not sensitive to increases in the depth of the base of these bodies to greater than 2.5 km, as noted in Chapter 4). The first of these bodies (B1 in Figure 5.2) is that modelled using the superior 3D approach above at Knocklaugh Lodge. Body B2 suggests presence of a previously unknown serpentinite body located concealed beneath a mapped unit of mélange along the SE margin of the Northern Serpentinite Belt, whereas bodies B3 and B4 model the subsurface form of the exposed belt itself. The shape of these modelled bodies again suggested that they are fault-bounded slices of serpentinite, with the SE side of body B3 corresponding to the fault mapped along the SE margin of the Northern Serpentinite Belt (BGS, 1988). Again, the faults separating the modelled blocks could be either high-angle thrust or strike-slip faults. Unfortunately, no detailed structural analysis of the faults associated with the serpentinite belts has been published, and even the BGS memoir accompanying the Girvan geological map (Cameron et al., 1986) focuses solely on petrographic and lithological descriptions. However, Fujisaki et al. (2015) provide evidence for presence of thrust duplexes in sedimentary rocks associated with the Ballantrae Complex, and so an interpretation of the modelled subsurface geometry of the serpentinite as a series of thrust slices is adopted here.

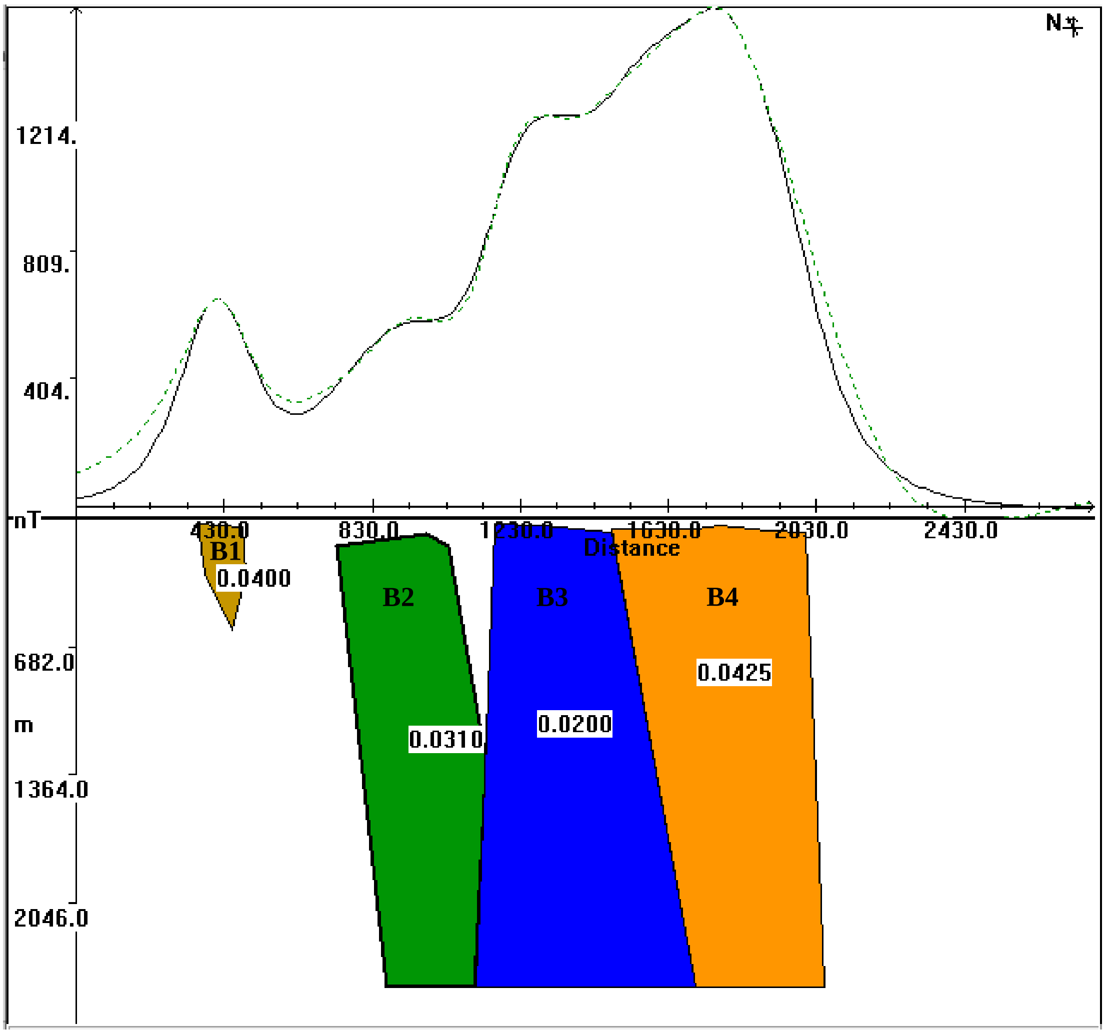

Figure 5.2. The 2D model showing the serpentinite bodies under the Knocklaugh Lodge profile.

5.2 The regional aeromagnetic study

The 3D model of the regional aeromagnetic study is created using susceptibility cut-offs of 1.8 x 10^{-2} to 6 x 10^{-2} SI which corresponds to the range of susceptibilities observed in data collected in this study. However, the model also assigns lower susceptibilities to other cells in the mesh that are not shown when the models are presented using these cut-offs.

5.2.1. Subsurface form and extent of the Northern and Southern Serpentinite Belts

The model was sliced along the line of profiles A-A and B-B of Powell (1978). These slices can be seen in Figures 5.3 and 5.4. As can be seen in Figure 1.6, the A-A profile of Powell (1978) crosses only the Northern Serpentinite Belt while the B-B profile crosses both the Northern and Southern Serpentinite Belts. When sliced along the line A-A profile line of Powell (1978), the 3D model developed here shows high susceptibility rocks of

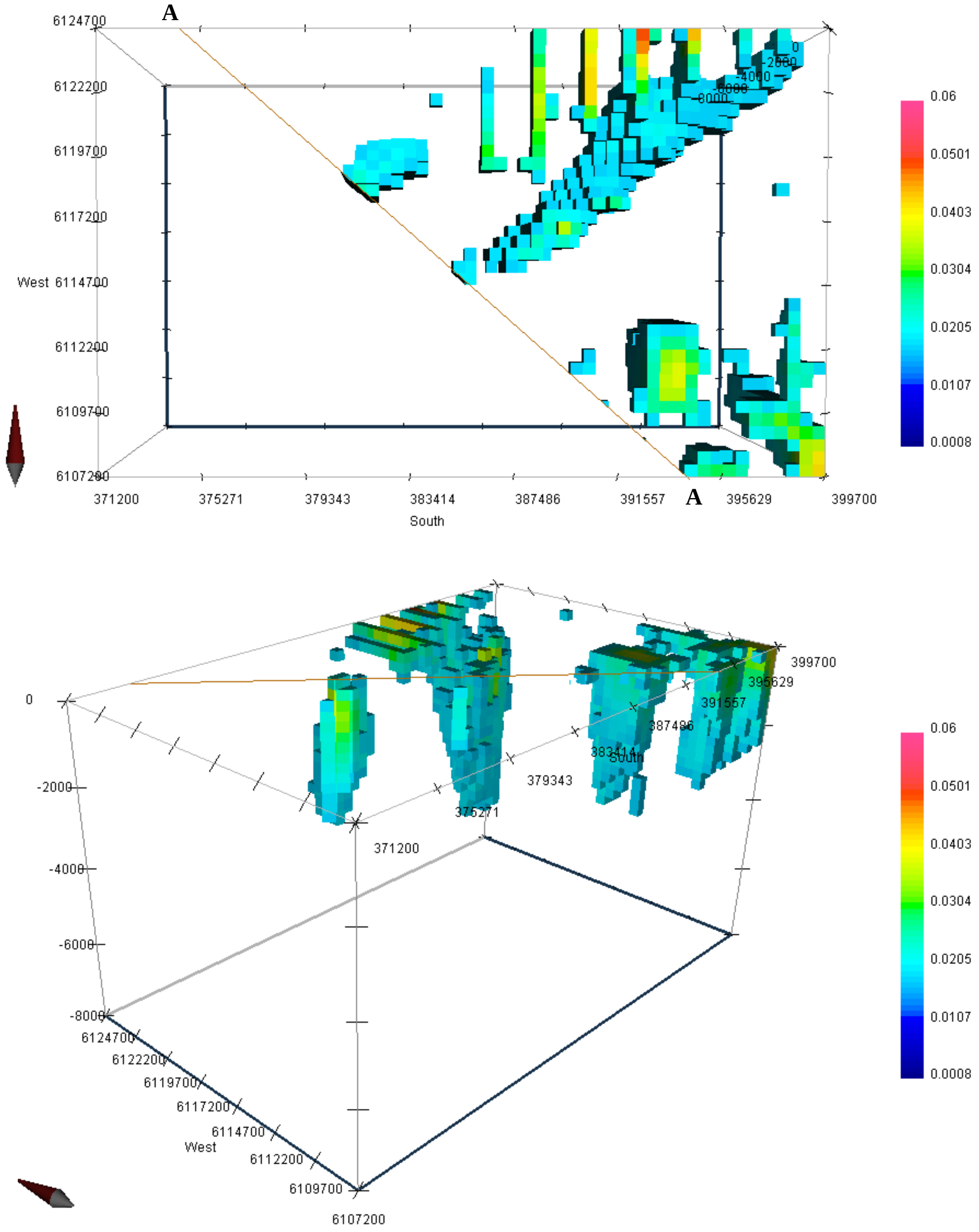

Figure 5.3. Top: A bird's eye view showing the location of the A-A profile of Powell (1978). Bottom: A view of the Mag3D model looking perpendicular to the A-A profile line.

the Northern Serpentinite Belt extending down to ~3.25 km below the surface. This depth is comparable to that determine in the 2D modelling carried out by Powell (1978), who modelled the Northern Serpentinite Belt as a sub-vertical sheet extending to 3.5 km (Figure 1.7). However, the full Mag3D model shows a connection between the Northern and Southern Serpentinite Belts in the subsurface (discussed further below), in contrast

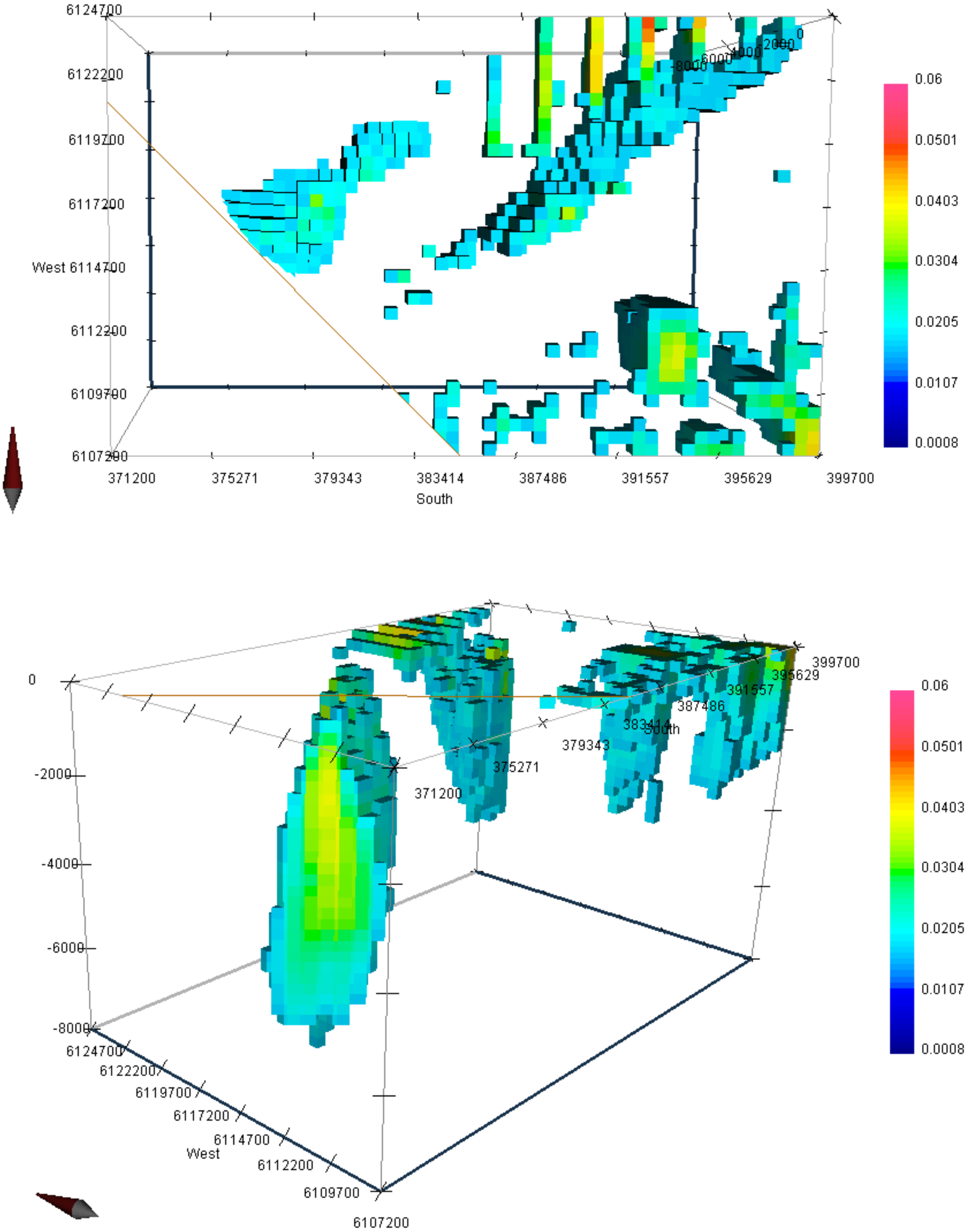

Figure 5.4. Top: A bird's eye view showing the location of the B-B profile of Powell (1978). Bottom: A view of the Mag3D model looking perpendicular to the B-B profile line.

to Powell’s (1978) 2D model. This reflects the fact that the 3D model is based on BGS aeromagnetic data surveyed at an elevation of 305 m, whereas Powell’s (1978) analysis was based on ground-level magnetic anomaly data. Therefore, at aeromagnetic altitudes, the anomalies due to the Northern and the Southern Serpentinite Belt merge into one broad anomaly (on the left side in Figure 4.32), whereas the ground-level survey reported by Powell (1978) identified two distinct anomalies over the exposed serpentinite belts.

The 3D model of the serpentinite belts shows a complex subsurface distribution of susceptibilities, extending to variable depths. Under the outcrop of the Northern Serpentinite Belt, the 3D model demonstrates high susceptibility rocks (i.e. those with susceptibility values in the range observed here for serpentinites) reaching to the surface and extending down to maximum depths of 7.5 km. This depth is greater than the modelled depths shown by Powell (1978), but is consistent when the 3D model is sliced along the same profile line (see above). Under the outcrop of the Southern Serpentinite Belt, the 3D model shows high susceptibility rocks (i.e. those with susceptibility values in the range observed here for serpentinites) do not reach the surface (although cells with lower susceptibilities in the unconstrained model prior to applying cut-offs do approach the surface). These high-susceptibility rocks extend down maximum depths of ~6 km (Figure 5.4). This is significantly deeper than the shallow Southern Serpentinite Belt body inferred by Powell (1978), which only extends to a maximum depth of < 2 km (see Figure 1.7).

In between the outcrops of the Northern and the Southern Serpentinite Belts, the 3D model illustrates a lack of high susceptibility rocks near the surface (consistent with the mapped surface geology; BGS, 1988), but a series of mesh cells are modelled that connect across the larger anomalies associated with the serpentinite belts at depths of ~3.5 - 6.2 km, resulting in a “U-shape” to the modelled high susceptibility rocks when viewed from the west (Figure 5.5, right).

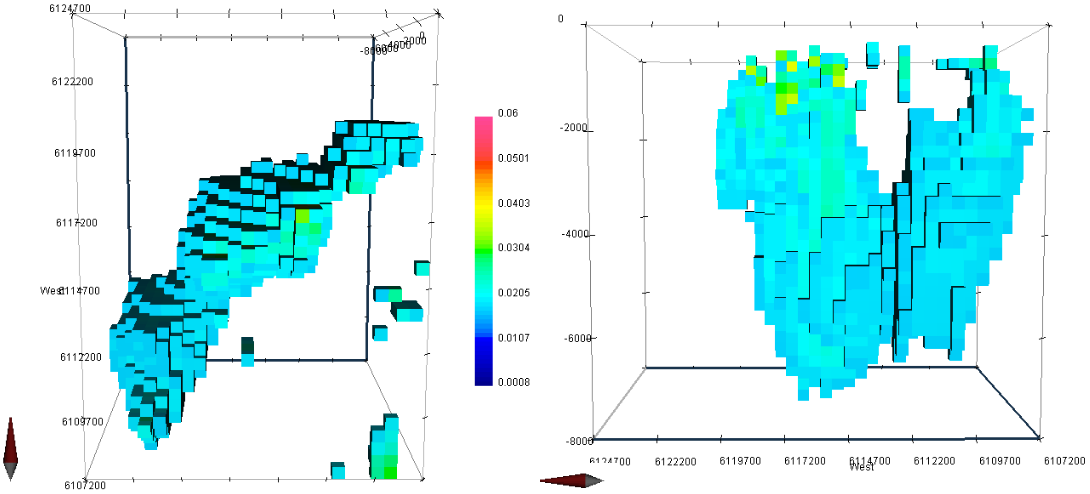

Figure 5.5. Left: A bird's eye view of the Mag3D model of the Northern and Southern Serpentinite Belts. Right: A model view demonstrating the "U-shaped connection" between the belts.

Overall, the modelled subsurface form of the high-susceptibility serpentinites suggests a structure controlled by a combination of high-angle faulting and folding. This is consistent with the BGS map of the ophiolite (BGS, 1988) which shows steep faults along the NW and SE margins of both the Northern and the Southern Serpentinite Belts. The broad strike of these faults is parallel to the Stinchar Valley and Glen App faults that are related to the Southern Uplands Fault system.

5.2.2. Modelled subsurface form of the Traboyack Formation

According to the geological map in Figure 5.6, the body marked using a red ellipse in Figure 5.7 might belong to the Traboyack Formation. The aeromagnetic anomaly map shown by Floyd and Kimbell (1995) (Figure 1.4) demonstrates a high magnetic relief over the Traboyack Formation as well as over the serpentinite belts. This is comparable to the 3D model. The susceptibility of sedimentary rocks of the Traboyack Formation reported by Floyd and Kimbell (1995) is around 4×10^{-2} SI and has the highest susceptibility value in the Tappins Group. This is comparable to the range of 2×10^{-2} to 6×10^{-2} SI in the field susceptibility readings collected for this study. The model shows the highest susceptibility ~4×10^{-2} SI for the body belonging to the Traboyack Formation

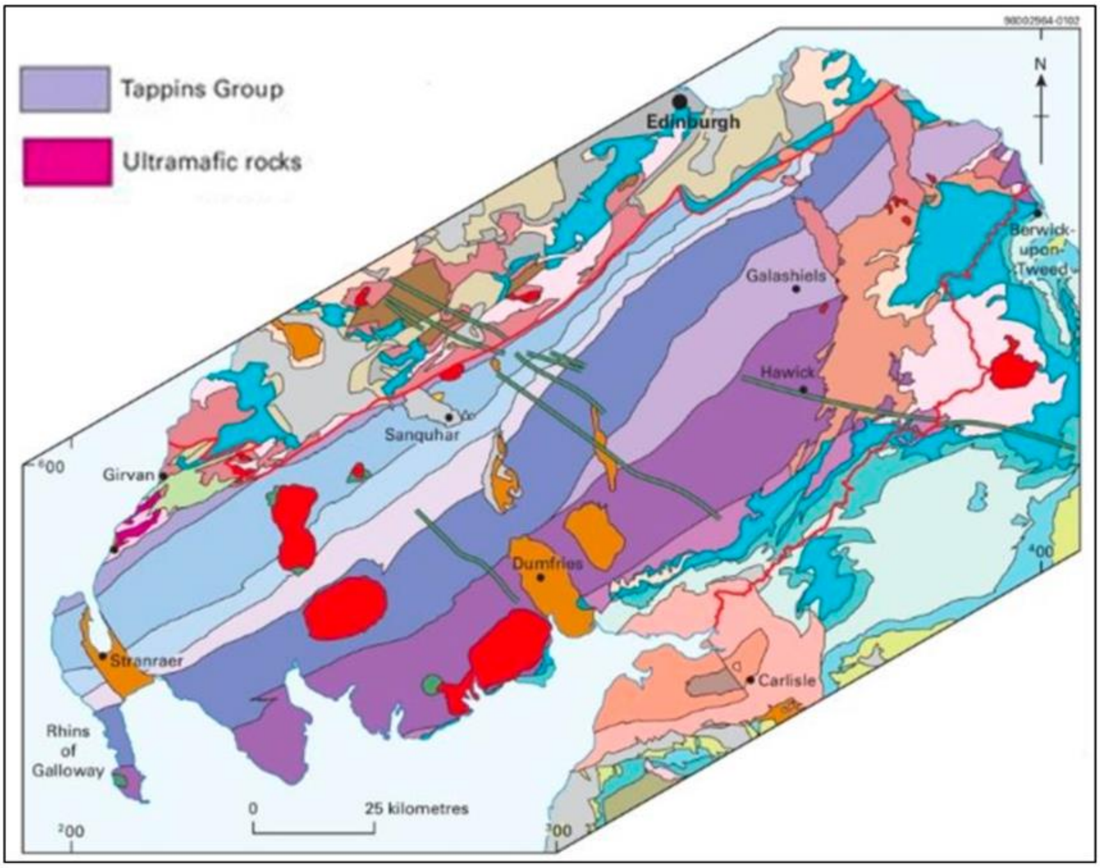

Figure 5.6. A geological map showing the ultramafic rocks (serpentinite) in the Ballantrae Complex and the Tappins Group (adapted from Stone et al., 2012).

(Figure 5.8). These results are comparable to the results found by Floyd and Kimbell (1995).

As mentioned above, the depth of high-susceptibility rocks in the Southern Serpentinite Belt reaches ~6 km. However, the 3D model shows that the high-susceptibility sediments in the Traboyack Formation extend down to maximum depths of ~2 km (Figure 5.8). This further confirms that these are unrelated, separate structures. The modelled Traboyack Formation body is narrower than the serpentinite belt and is comparable with the outcrop width of this formation shown on the BGS geological map (Stone et al., 2012).

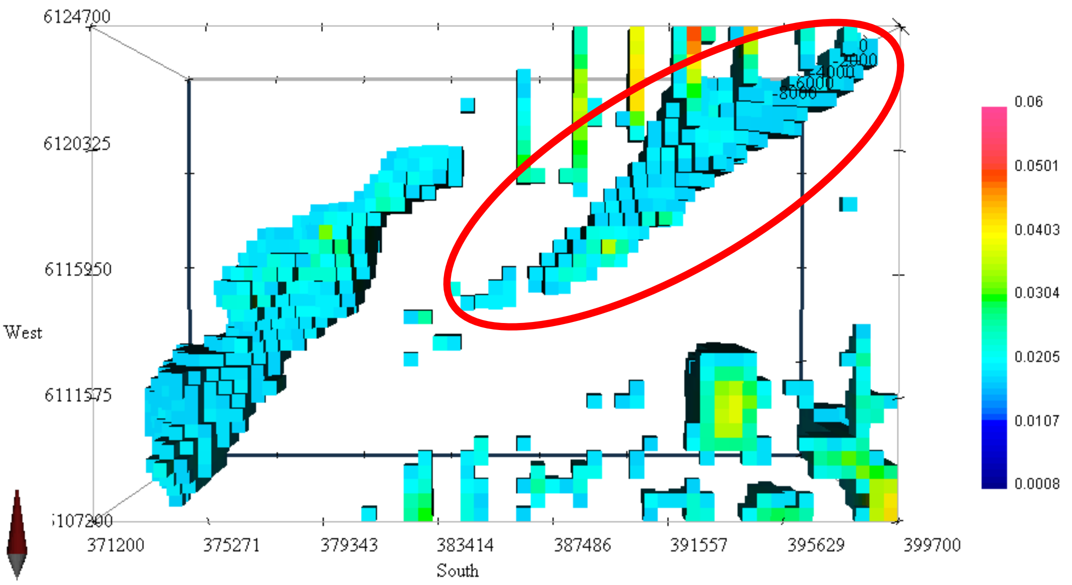

Figure 5.7. A model showing the bird's eye view of the region. The part of the model corresponding to the sedimentary rocks of the Traboyack Formation has been marked using a red ellipse.

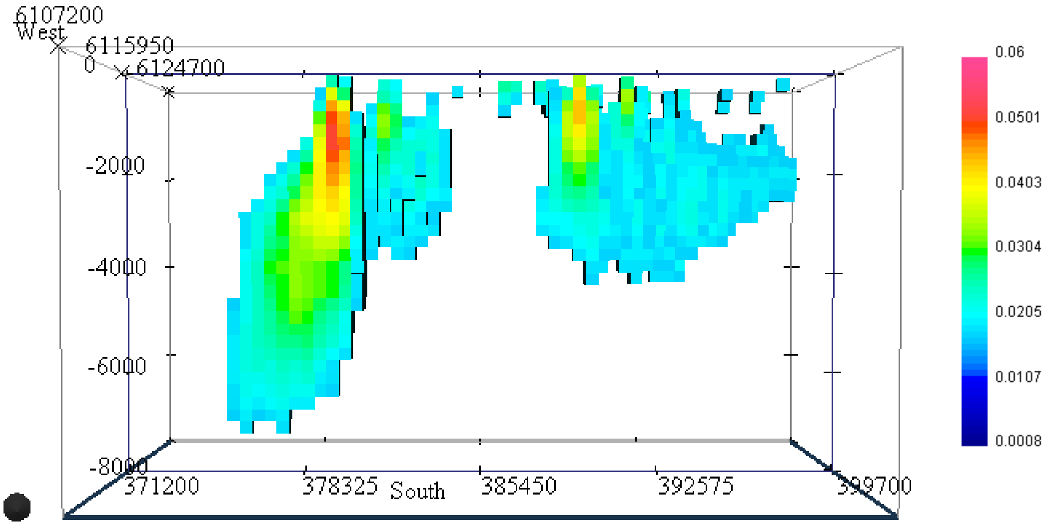

Figure 5.8. A model viewed from the south showing the high susceptibility cells and their depth.

5.3. Limitations of the modelling approaches

The 3D models of the Knocklaugh Lodge were produced by defining a mesh of 21750 cells, each of 20 m side lengths. The initial model susceptibility was assigned as $4x10^{-2}$ SI with the range of 8×10^{-3}–6×10^{-2} SI to create an optimised fit to the observed magnetic anomaly data. The 3D models of the regional aeromagnetic data were produced by defining a mesh of 71280 cells, each of 500 m side length. These were all initially assigned a susceptibility of 4×10^{-2} SI in the initial set-up and then the modelling algorithm was then allowed to adjust these susceptibilities within the range of 8×10^{-4} - 6×10^{-2} SI to produce an optimised fit to the observed aeromagnetic data. This imposes a number of limitations.

Incorporating the geological constraints on the mapped outcrop patterns of the serpentinite belts was not possible. Nonetheless, the modelled extent of the serpentinites close to the surface agrees well with the known extent of the outcrops in the field. The maximum depth extent of modelled bodies also could not be specified within Mag3D, and so the algorithm was free to assign serpentinite-like susceptibilities to cells at depths down to ~7.5 km in order to maximise the fit of the calculated and observed magnetic anomalies. However, the results from the 2D modelling carried out along the profile from Knocklaugh Lodge to the coast across the Northern Serpentinite Belt show that changing the maximum vertical extent of high susceptibility rocks between depths of 2.5 to 9.0 km makes very little difference to the fit between modelled and calculated anomalies. Hence, both the 2D and 3D models must be considered to be poorly constrained at large depths. However, it should be noted that the Mag3D model of the Northern and the Southern Serpentinite Belts anomaly suggests that rocks with susceptibilities comparable to the mean value of 4×10^{-2} SI determined in the field do not extend deeper than ~2.5 km, consistent with the results of the 2D modelling. The Mag3D modelling of the regional aeromagnetic anomaly data exhibits significant artefacts at the margins of the mesh that are not geologically significant. In particular, the aeromagnetic data are more sparse towards the southeast corner of the modelled area (Figure 4.33), resulting in the assignment of significantly high susceptibilities to cells in that corner in order to optimise a fit to these sparse data points.

5.4. The Coastal Area

The Coastal Area survey was designed to examine the effect of having low susceptibility gabbro/dolerite bodies in a host rock consisting of serpentinite. The area surveyed was entirely within the mapped extent of the Northern Serpentinite Belt.

Upward continuation aims to suppress short wavelength components originating from shallow sources in order to isolate deeper sources (see Chapter Three). In this case, upward continuation shows a long-wavelength regional gradient across the survey area from north to south (Figure 5.9). The residuals (that reflect shallow sources) show higher frequency variations that show some agreement with mapped gabbro/dolerite bodies (Figure 5.9) but there are some variations that also do not correlate with exposed geology at the surface.

A profile line A-B has been cut through the residual anomaly map using Surfer® to see whether changes in the residual field relate to outcrops of dolerite/gabbro (Figure 5.10). The results are shown in Figure 5.10 for the profile upward continued to various heights (upper lines) and the residual anomalies (lower lines). The red rectangle in this figure indicates where a gap in data coverage exists (due to presence of metal fences). The green rectangle indicates the location of an outcrop of gabbro/dolerite mapped by the BGS (1988). Finally, the grey rectangles indicate locations where gabbro/dolerite exposures were noted in the field, respectively. Some examples of these exposures can be seen in Figure 5.11.

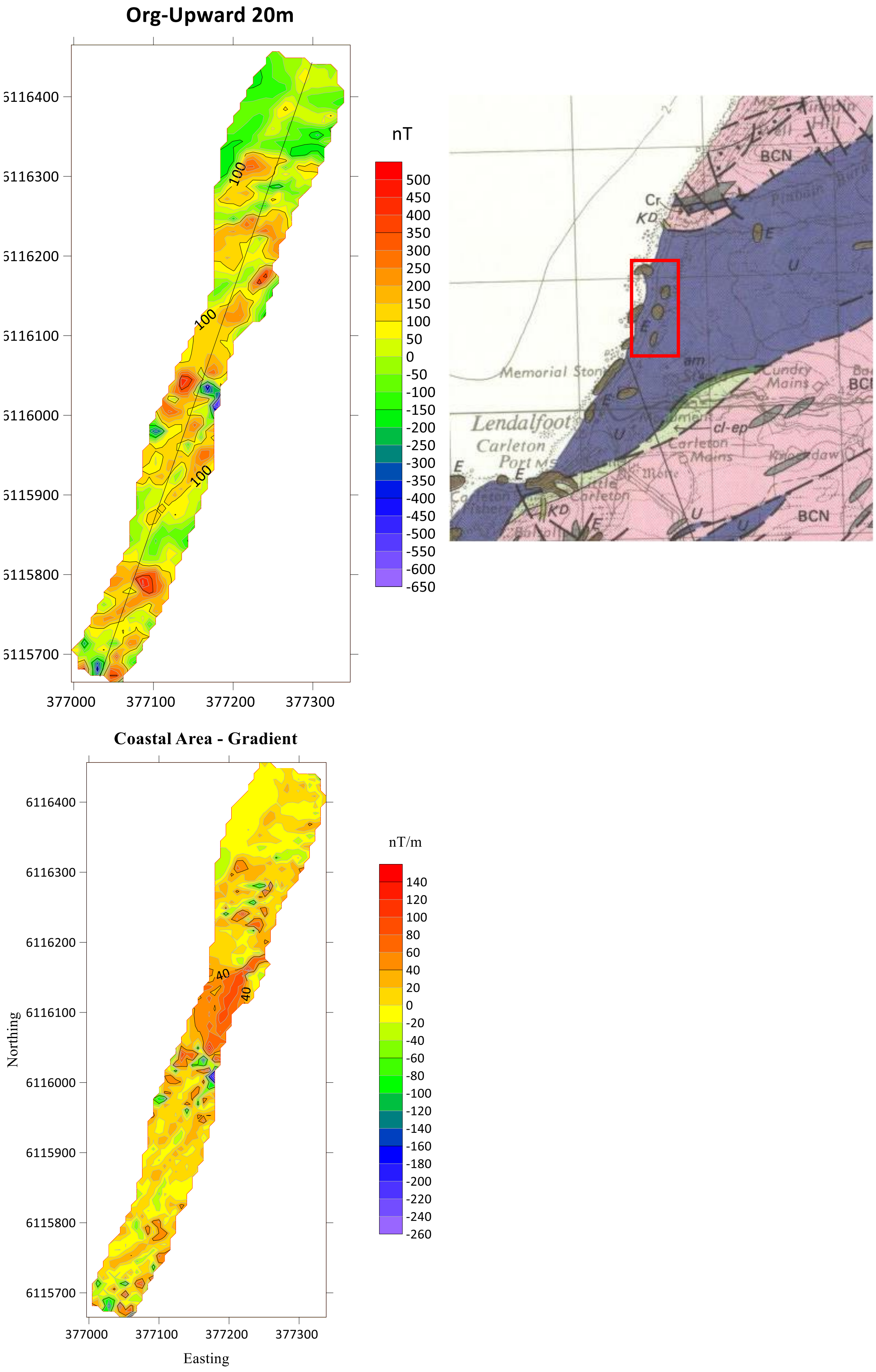

Figure 5.9. Top left: residual anomaly over the Coastal Area; top right: the BGS geological map (1988) showing the presence of gabbro/dolerite bodies in the serpentinites; bottom: gradiometer map of the Coastal Area.

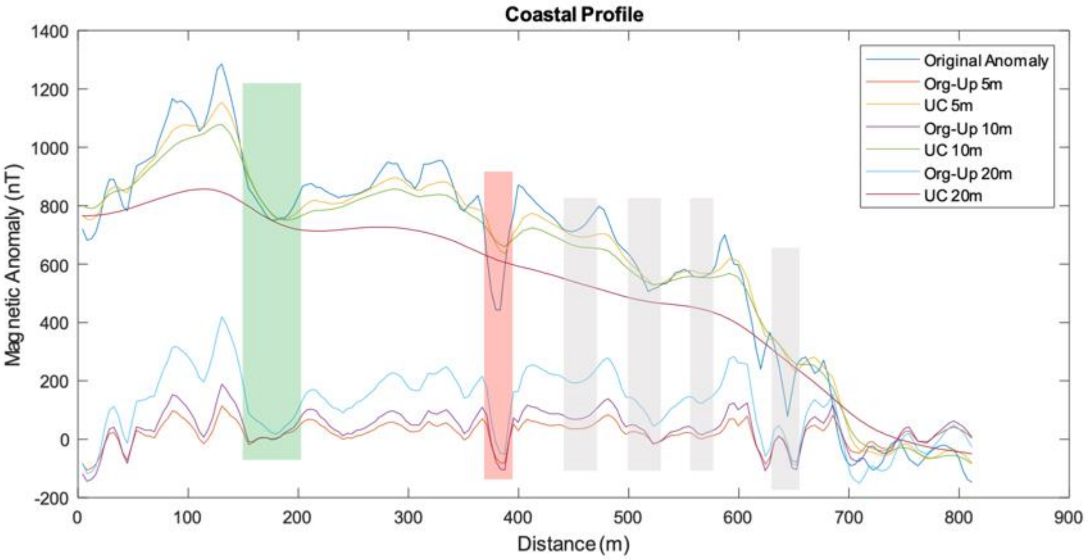

Figure 5.10. A graph showing the residual and regional anomaly changes along the A-B profile line through the Coastal Area survey. The red rectangle shows the interval where magnetic data could not be collected due to presence of metal fences; The green rectangle shows the location of a dolerite/gabbro outcrop seen on the BGS map (1988); the grey rectangles represent areas where the dolerite/gabbro exposures were observed in the field.

In each case, the location of these weakly magnetic gabbros/dolerites corresponds to a decrease in the residual field anomaly, reflecting their negative susceptibility and remanence contrast with the underlying host serpentinites. This also suggests that some of the high-frequency variability in the total field ground-level magnetic survey over the Northern Serpentinite Belt (see Figure 4.6) may arise from the presence of similar weakly magnetic gabbros within the serpentinite host, only some of which have been mapped by the BGS (1988).

The flat fields where this survey was conducted represent a raised marine terrace bounded on the inland side by a prominent paleo cliff line (Figure 5.11). Hence the surficial deposits across the survey area are likely to be covering a complex paleo-wave cut platform like that currently exposed along the rocky shoreline. It is expected, therefore, that beneath the surface there are likely to be significant variations in the depth to the serpentinite basement, reflecting paleo headlands and embayments in the fossil shoreline beneath. An illustration of this possible structure is shown in Figure 5.12. It is likely

Figure 5.11. Photograph showing sheet-like exposures of dolerite on the raised marine platform of the Coastal Area, with the paleo-cliff line visible in the background. These likely represent paleo-headlands of the ancient shoreline.

that high-frequency residual anomalies relate to paleo-geomorphological variability in this particular setting, in addition to the effects of low-susceptibility intrusions. A series of pronounced NE-SW striking features seen in the gradiometer map of Figure 5.9 runs broadly parallel to the strike of the exposed ridges of dolerite (both on the marine terrace and the modern shoreline), suggesting that more of these bodies may be present beneath the terrace and/or that the local topography of the fossil marine terrace beneath the superficial sediments has a similarly oriented structural control.

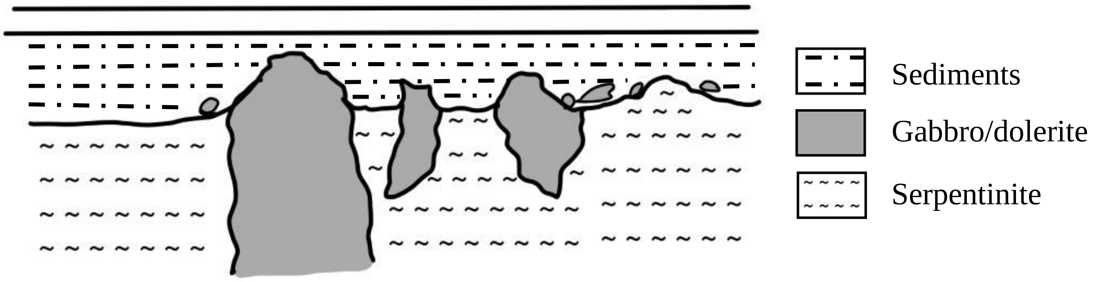

Figure 5.11. An illustration of subsurface variations in the depth of a fossil rock-shoreline beneath a raised marine terrace.

Chapter 6 - Conclusions

This study provides the first ever 3D magnetic modelling of the prominent aeromagnetic and ground-level magnetic anomalies that characterise the Girvan-Ballantrae region.

The main results of the study are:

1) A localised magnetic anomaly in the vicinity of Knocklaugh Lodge is due to a concealed, fault-bounded wedge-shaped body of serpentinite that strikes NE-SW for ~600 m and extends to a maximum depth of 590 m. The presence of this serpentinite body has been demonstrated in a borehole that penetrated its faulted SW margin (Stone, 1984), but the 3D modelling conducted here provides details of the subsurface form of this body for the first time
2) 2D modelling of a profile extending from Knocklaugh Lodge to beyond the NW side of the Northern Serpentinite Belt of the Ballantrae Complex provides evidence for a series of large, fault-bounded thrust slices of serpentinite in the subsurface, extending down to at least 2.5 km. This includes a concealed body that has not been reported previously. High-frequency variations in anomaly amplitude over the Northern Serpentinite Belt along this profile are likely to be due to the presence of gabbro intrusions with a negative susceptibility contrast compared to the serpentinites.
3) 3D modelling of data extracted from the UK National Aeromagnetic Survey (Institute of Geological Sciences, 1972, 1980) provides details of the 3D distribution of serpentinites in the subsurface for the first time. The Mag3D model suggests that their structure is controlled by a combination of high-angle faulting and folding.
4) Upward continuation of a detailed ground-level total field magnetic survey over a raised marine terrace within the outcrop of the Northern Serpentinite Belt reveals

a long-wavelength regional gradient (that cannot be modelled magnetically). Subtraction of the upward continued data from the ground-level data reveals a series of high-frequency variations in the residual field that may be related to the presence of weakly magnetic dolerite/gabbro intrusions into the host serpentinite and/or variations in the depth of overburden related to the preservation of a fossil rocky shoreline beneath the superficial deposits of the terrace.

5) More generally, it has been demonstrated that the combination of analytical methods employed here (i.e. magnetic surveying, Fourier-based upward continuation, characterisation of the bulk magnetic properties of rocks, and 2D and 3D magnetic modelling) can provide valuable information on the subsurface geometry and distribution of rocks with high magnetic susceptibilities in tectonically complex regions.

References

AGICO. (2022). *Anisoft*. Retrieved from https://www.agico.com/text/software/anisoft/anisoft.php

Araffa, S. A., Santos, F. A., & Arafa-Hamed, T. (2012). Delineating active faults by using integrated geophysical data at northeastern part of Cairo, Egypt. *NRIAG Journal of Astronomy and Geophysics*, 33-44.

Bailey, E. B., & McCallien, W. J. (1952). Ballantrae Igneous Problems: Historical Review. *Transactions of the Edinbrugh Geologocal Society, 15*, 14-38.

Beams, S. (2019, 09 03). *Ground Magnetic Survey Capabilities*. Retrieved 07 08, 2022, from Terra Search: https://terrasearch.com.au/news/ground-magnetic-survey/

BGS. (2022). *The Earth's Magnetic Field: An Overview*. Retrieved from British Geological Survey: https://geomag2.bgs.ac.uk/education/earthmag.html

Bloxam, T. W. (1980). Amphibolite contact zones, amphibolite xenoliths, and blueschists associated with serpentinite in the Girvan-Ballantrae complex, southwest Scotland. *Arch. Sci., 33*, 291-299.

Bluck, B. J., & Inghan, J. K. (1992). The Girvan–Ballantrae complex. In J. D. Lawson, & D. S. Weedon, *Geological Excursions Around Glasgow and Girvan* (pp. 301–306). Glasgow, United Kingdom: Geological Society of Glasgow.

Bullard, E. (1948). The Magnetic Field within the Earth. *Proceedings of the Royal Society of London. Series A, Mathematical and Physical Sciences, Vol. 197 No. 1051*, 433-453.

Butler, R. F. (2004). Paleomagnetism: Magnetic Domains to Geologic Terranes. (Electronic). Blackwell Scientific Publications Boston.

Cameron, I. B., Stone, P., & Smellie, J. (1986). Geology of the country around Girvan: Explanation for the 1:50 000 sheet, British Geological Survey Sheet 7, Scotland. ISBN 0 11 884418 0.

Canada, N. R. (2021). *Space weather effects on technology*. Retrieved from Government of Canada: https://www.spaceweather.gc.ca/tech/index-en.php#pip

Chen, C.-R., Yen, H.-Y., Chen, C.-H., Lee, Y., Lo, Y.-T., & Shin, T.-C. (2015). Preliminary studies on unusual magnetic diurnal variation in the Hengchun peninsula. *Terrestrial Atmospheric and Oceanic Sciences. 27*. doi:10.3319/TAO.2015.06.04.01(T)

Church, W. R., & Gayer, R. A. (1973). The Ballantrae ophiolote. *Geological Magazine, 110*, 497-592.

Cooper, G. R. (1997). FORWARD MODELLING OF MAGNETIC DATA. *Computers & Geosciences, 23 No. 10*, 1125-1129.

Earthwise. (2022, 08 02). *Ordovician Ballantrae Complex*. Retrieved from British Geological Survey: https://earthwise.bgs.ac.uk/index.php/Ordovician_Ballantrae_Complex

Ernenwein, E. G., & Hargrave, M. (2007). Archaeological Geophysics for DoD Field Use: a Guide for New and Novice Users. *ResearchGate*.

ESurveying-Softech. (2022). *Online application to convert Latitude Longitude to UTM*. Retrieved 2022, from ESurveying Softech (India) Pvt. Ltd.: https://www.esurveycad.com/online/latlong-to-utm-conversion

Floyd, J. D., & Kimbell, G. S. (1995). Magnetic and tectonostratigraphic correlation at a terrane boundary: the Tappins Group of the Southern Uplands. *Geological Magazine, 132*(5), 515-521.

Fujisaki, W., Asanuma, H., Suzuki, K., Sawaki, Y., Sakata, S., Hirata, T., . . . Windley, B. F. (2015). Ordovician ocean plate stratigraphy and thrust duplexes of the Ballantrae Complex, SW Scotland: Implications for the pelagice deposition rate and forearc accretion in the closing Iapetus Ocean. *Tectonophsics, 662*, 312-327.

GEOMETRICS. (2014). *G-857 Operation Manual.* Geometrics, Inc.

GeoSimplex. (2015). *YouTube*. Retrieved from https://www.youtube.com/watch?v=zyUVBV4jLEs

Gettings, M. (2018). In situ distributions of magnetic susceptibility in some igneous rocks. In V. B., & J. Szigethy (Eds.), *Horizons in Earth Science Research* (Vol. 18).

Institute of Geological Sciences. (1972). 1:625000 Aeromagnetic Map of Great Britain, Sheet 1, England, Scotland and Northern Ireland. London: Institute of Geological Sciences.

Institute of Geological Sciences. (1980). 1:250000 Aeromagnetic Anomaly Map, Clyde, Sheet 55" N-06" W. London: Institute of Geological Sciences.

Leggett, J. K. (1987). The Southern Uplands as an accretionary prism: the importance of analogues in reconstructing palaeogeography. *Journal of the Geological Society, 144*, 737-751. Retrieved 08 05, 2022, from https://doi.org/10.1144/gsjgs.144.5.0737

Leggett, J. K., McKerrow, W. S., & Casey, D. M. (1982). The anatomy of a Lower Palaeozoic forearc: The Southern Uplands of Scotland. In J. K. Leggett, *Trench-forearc geology* (Vol. 10, pp. 494-520). London: Geological Society. doi:10.1144/gsl.sp.1982.010.01.33

Leggett, J. K., McKerrow, W. S., & Eales, M. H. (1979). The Southern Uplands of Scotland: a Lower Palaeozoic accretionary prism. *Journal of the Geological Society*, 755-770.

Lowrie, W. (2009). *Fundamentals of Geophysics* (Second ed.). Cambridge: Cambridge University Press.

Mandal, A., & Sharma, S. (2015). Geophysical signatures of uranium mineralization and its subsurface validation at Beldih, Purulia District, West Bengal, India: A case study. *Geophysical Prospecting, 63,* 713–726.

Mattsson, H., & AB, G. (2011). *2D and 3D modelling of magnetic and resistivity data from Äspö.* Technical Report.

McElhinny, M. W., & McFadden, P. L. (1999). *Paleomagnetism : continents and oceans* (Vol. 73). Academic Press.

Morris, A. (2003). A palaeomagnetic and rock magnetic glossary. *Tectonophysics 377,* 211-228.

Morris, A. (2020). *GEOL3003 Geophysics - Modelling magnetic anomalies using Excel.*

Musset, A., & Khan, M. (2000). *Looking into the Earth: An Introduction to Geological Geophysics.* London: Cambridge University Press. doi:10.1017/CBO9780511810305

O'Driscoll, B. (2006). Magmatic Layering and Magnetic Fabrics in the Palaeogene Carlingford Later Gabbros, Co. Louth, Ireland. *Irish Journal of Earth Sciences, 24,* 43.

Oliver, G., Stone, P., & Bluck, B. (2002). The Ballantrae Complex and Southern Uplands terrane. In N. H. Trewin (Ed.), *The Geology of Scotland* (Fourth ed., pp. 167-200). London: The Geological Society.

Peach, B. N., & Horne, J. (1899). *The Silurian rocks of Britain* (Vol. I: Scotland). Memories of the Geological Survey UK.

Powell, D. W. (1978). Geology of a continental margin 3: gravity and magnetic anomaly interpretation of the Girvan-Ballantrae district. In D. R. BOWES, & B. E. LEAKE (Eds.), *Crustal evolution in northwestern Britain and adjacent regions* (Vol. 10, pp. 177-181). Geological Journal Special Issue.

Ravat, D. (2007). *Encyclopedia of Geomagnetism and Paleomagnetism.* (D. Gubbins, & E. Herrero-Bervera, Eds.) Springer Dordrecht.

Robertson, A. H. (1988). *Field guide to aspects of the Ballantrae ophiolite complex, SW Scotland.* Edinburgh: Unpublished field guide for the 'Geology and Tectonics of the Oman Region' Discussion Meeting.

Robinson, E. S., & Çoruh, C. (1988). *Basic Exploration Geophysics.* Wiley.

Spray, J. G., & Williams, G. D. (1980). The sub-ophiolite metamorphic rocks of the Ballantrae Igneous Complex, SW Scotland. *Journal of the Geological Society, 137,* 359-368.

Stone, P. (1982). *Clastic rocks within the Ballantrae complex: borehole evidence.* Institute of Geological Science.

Stone, P. (2014). A review of geological origins and relationships in the Ballantrae. *Scottish Journal of Geology, 50*, 1-25.

Stone, P., & Rushton, A. W. (2018). On the age of the Ballantrae Complex, SW Scotland. *Scottish Journal of Geology, 54,* 77-86. Retrieved 10 20, 2021, from https://doi.org/10.1144/sjg2017-012

Stone, P., & Strachan, I. (1981). A fossiliferous borehole section within the Ballantrae ophiolite. *Nature, 293,* 455-457.

Stone, P., Floyd, J. D., Barnes, R. P., & Lintern, B. C. (1987). A sequential back-arc and foreland basin thrust duplex model for the Southern Uplands of Scotland. *Journal of the Geological Society, 144*, 753-764. Retrieved 06 06, 2022, from https://doi.org/10.1144/gsjgs.144.5.0753

Stone, P., Lambert, J. L., Carruthers, R. M., & Smellie, J. L. (1984). *Concealed ultramafic bodies in the Ballantrae complex, south-west Scotland: boreholes results.* British Geological Survey.

Survey, B. G. (1988). *Geological Survey of Scotland, 1:63,360/1:50,000 geological map series-7-Girvan*. Retrieved from https://webapps.bgs.ac.uk/data/maps/maps.cfc?method=viewRecord&mapId=10759

Talwani, M. (1965). Computation with the help of a digital computer of magnetic anomalies caused by bodies of arbitrary shape. In *Geophysics* (Vol. 30, pp. 705-932). Retrieved from https://doi.org/10.1190/1.1439654

Tarling, D., & Hrouda, F. (1993). *The Magnetic Anisotropy of Rocks.* Chapman & Hall.

Thirlwall, M. F., & Bluck, B. J. (1984). Sr-Nd isotope and chemical evidence that the Ballantrae 'ophiolite', SW Scotland, is polygenetic. *Geological Society, 13,* 215-230. doi:https://doi.org/10.1144/GSL.SP.1984.013.01.18

Treloar, P. J., Bluck, B. J., Bowes, D. R., & Dudek, A. (1980). Hornblende-garnet metapyroxenite beneath serpentinite in the Ballantrae complex of SW Scotland and its bearing on the depth provenance of obducted oceanic lithosphere. *Transactions of the Royal Society of Edinburgh, 71,* 201-202.

UBC-GIF. (2013). *MAG3D.* Retrieved from Geophysical Inversion Facility: https://gif.eos.ubc.ca/software/utility_programs#mag3d

USGS. (n.d.). Retrieved from The U.S. Geological Survey: https://www.usgs.gov/media/images/earth-diagram

Webber, J. R., Brown, L. L., & Williams, M. L. (2019). Petrophysical constraints on magnetic anomalies associated with metamorphic reactions in northern Saskatchewan, Canada1. *Can. J. Earth Sci.,* 895-911.

Wiers, S. (2020). *The Arctic Ocean Palaeomagnetic Record - A Stratigraphic Approach [Doctoral thesis, Uppsala University]*. Uppsala University. Retrieved from http://uu.diva-portal.org/smash/record.jsf?pid=diva2%3A1423074&dswid=6963

Appendix

Anisotropy of Magnetic Susceptibility results

These data are presented here for completeness but are not interpreted.

In each figure, the stereonet shows the orientation of the principal axes of the AMS ellipsoid, the lower left graph shows the relationship between the anisotropy degree, P, and the mean susceptibility, Kmean, and the lower right graph shows the relationship between shape parameter, T, and the anisotropy degree, P.

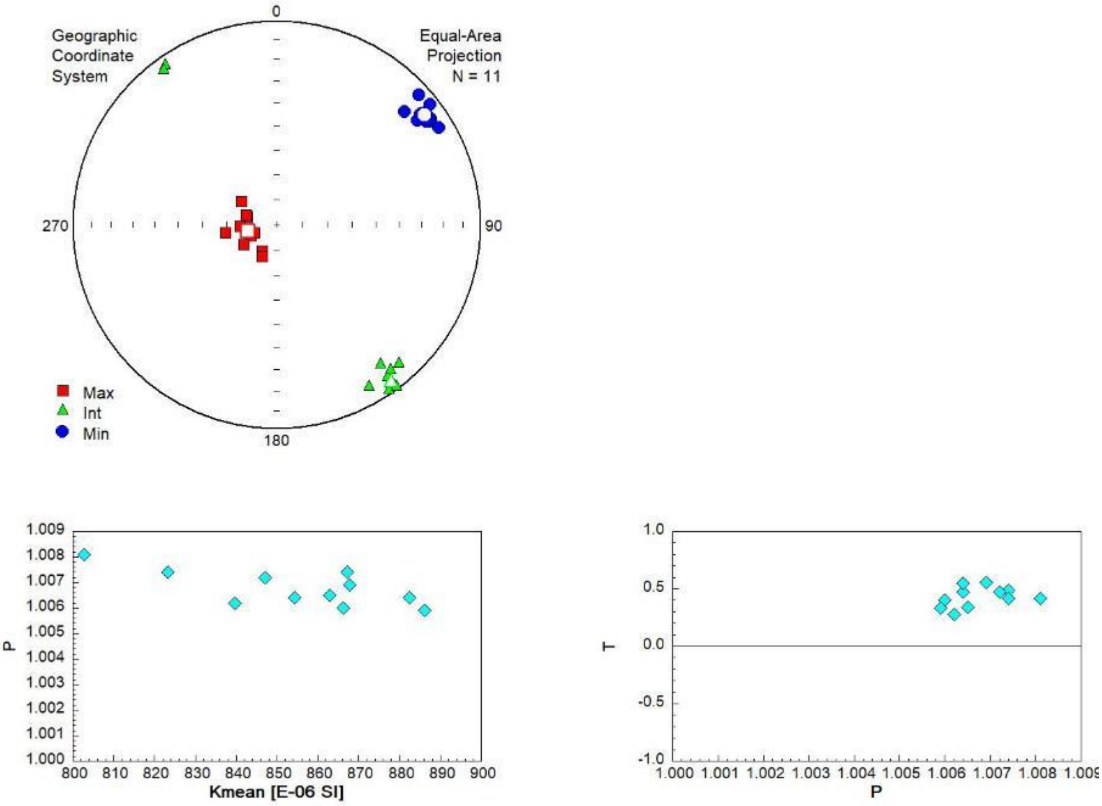

Figure A1. Basalts.

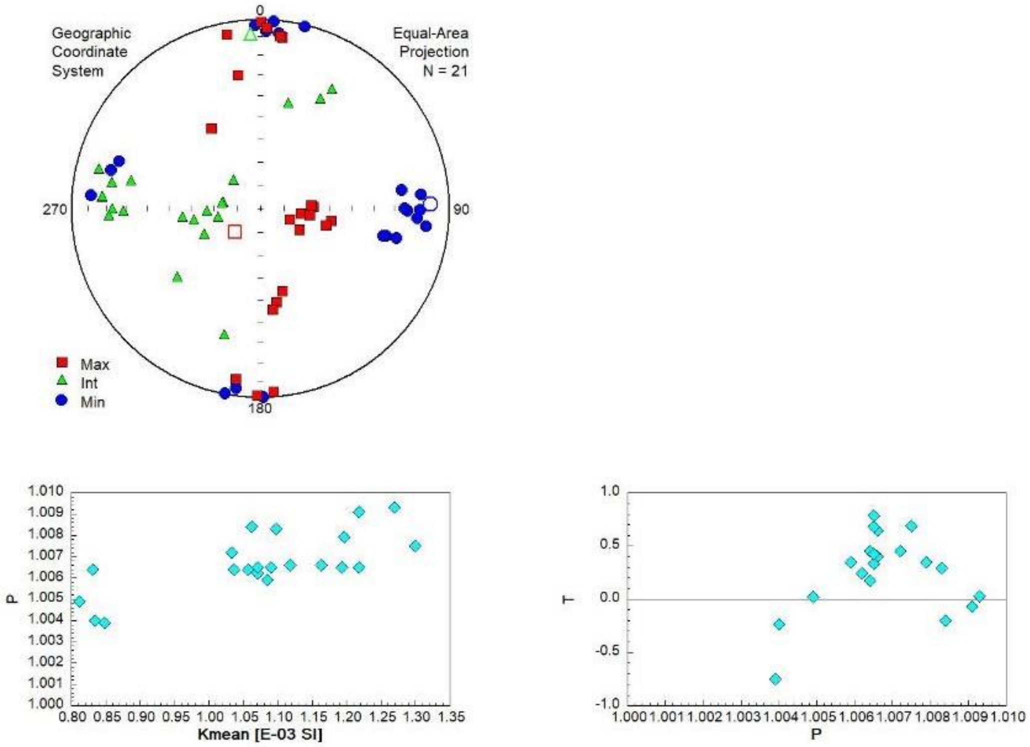

Figure A2. Dolerites.

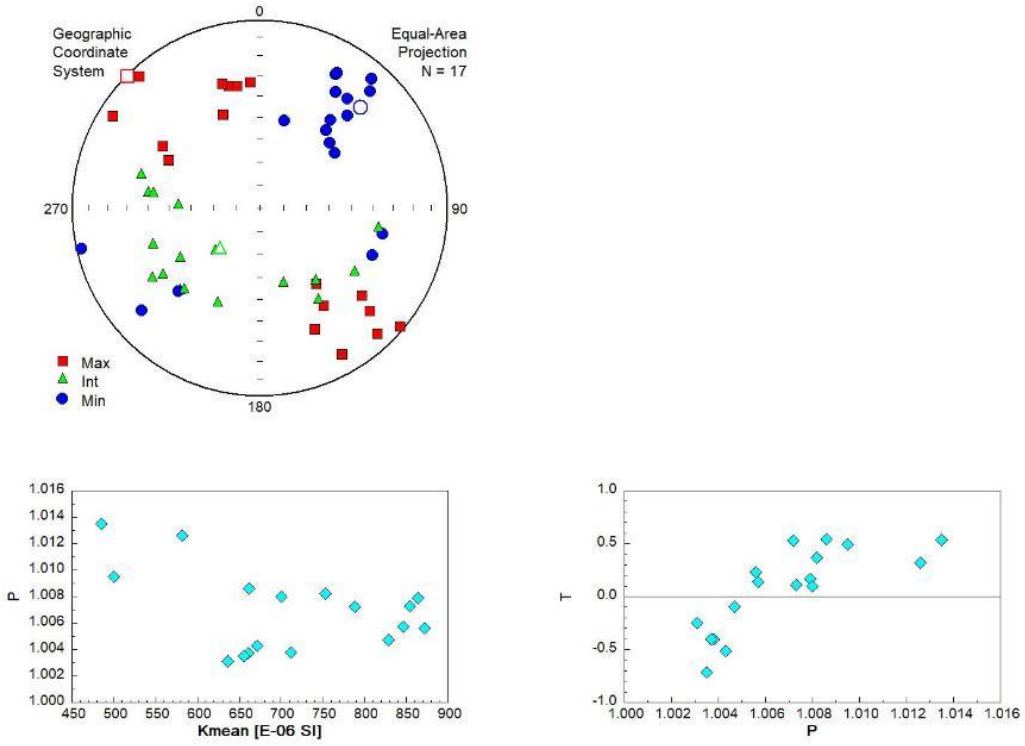

Figure A3. Gabbros.

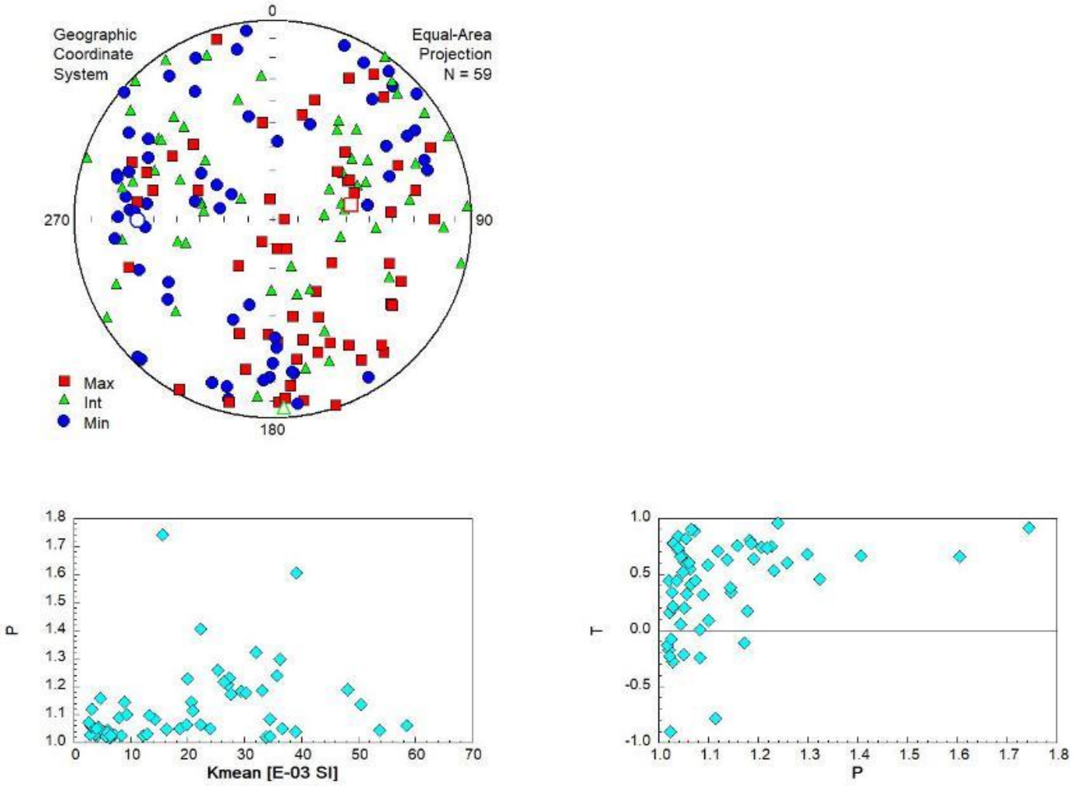

Figure A4. Serpentinites.

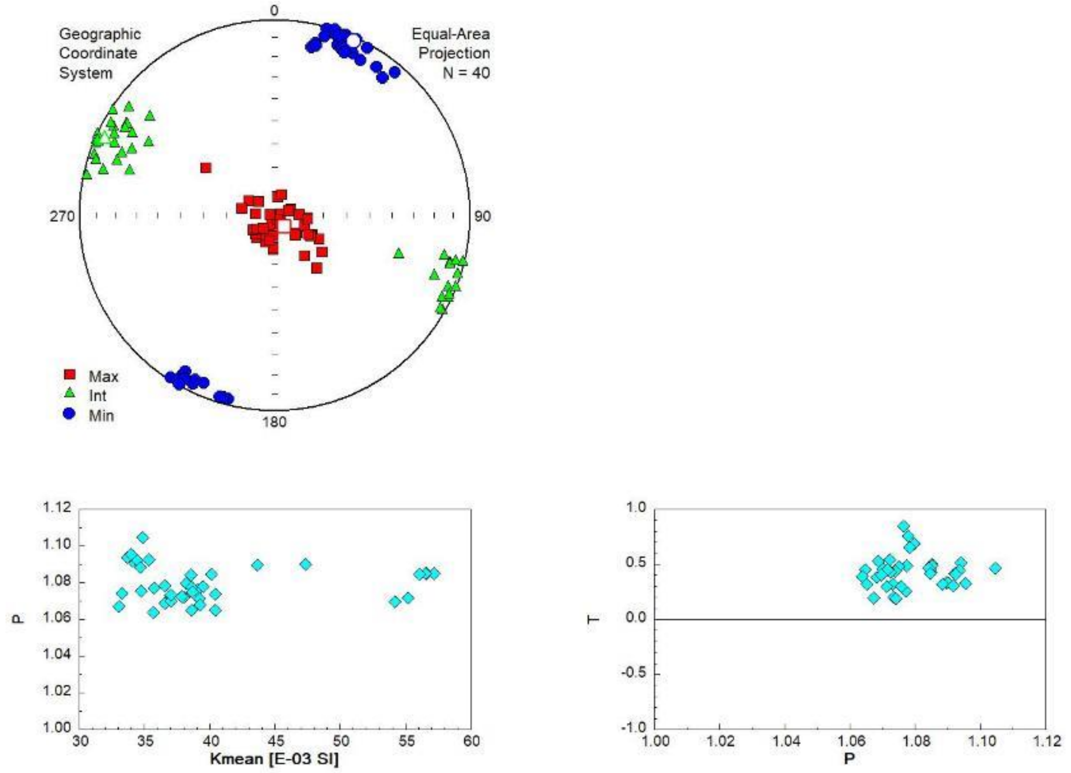

Figure A5. Traboyack Formation sediments.